THE UNIVERSITY
of EDINBURGH

This thesis has been submitted in fulfilment of the requirements for a postgraduate degree (e.g. PhD, MPhil, DClinPsychol) at the University of Edinburgh. Please note the following terms and conditions of use:

This work is protected by copyright and other intellectual property rights, which are retained by the thesis author, unless otherwise stated.
A copy can be downloaded for personal non-commercial research or study, without prior permission or charge.
This thesis cannot be reproduced or quoted extensively from without first obtaining permission in writing from the author.
The content must not be changed in any way or sold commercially in any format or medium without the formal permission of the author.
When referring to this work, full bibliographic details including the author, title, awarding institution and date of the thesis must be given.

Cerebral organoids as tools to study forebrain development: the role of Pax6

Nurfarhana Ferdaos

Thesis submitted for the degree of doctor of philosophy

The University of Edinburgh

2019

For Daniel and Rayyan

Table of Contents

Disclaimer

I (Nurfarhana Ferdaos) performed all of the experiments presented in this thesis unless otherwise clearly stated in the text. No part of this work has been or is being submitted for any other degree of qualification.

Signed:

Date:

Acknowledgements

First and foremost, I would like to thank my supervisor, John Mason for his advice and encouragement throughout my studies. Not to forget Sally Lowell for providing valuable advice on embryonic stem cell culture, and for giving me the opportunity to join her group meeting at the Scottish Centre for Regenerative Medicine (SCRM).

I also appreciate all the critical inputs and fruitful discussions from David Price, Tom Pratt and Thomas Theil during DBUG lab meetings and journal club. This group has been an inspiration.

Special thanks go to Michael Molinek, whom has helped me to derive embryonic stem (ES) cells. Some of the works presented in this thesis are not possible without his expertise, and for that I am grateful. Many thanks also to Martine Manuel for without her help, I wouldn't get the mouse blastocysts to derive ES cells.

To DBUG and team organoid lab members, know that your presence and friendship means a lot to me. I learned a lot from all of you: Idoia, Tian, Alex, Sarah, Calvin, Jonothon, Rosie, Faziela, Michela, Kai, Zrinko, Cass, Kerstin.

A special thanks also to Chandrika Rao, who has kindly helped me from the first day I joined the lab until the completion of this thesis. Thanks for your time, advice and encouragement. I wish you all the best in your future undertaking.

Last but not least, to my family and Malaysian friends for their endless support – especially to Izwan.

This thesis is not possible without all of you.

Abstract

The cerebral cortex forms the major part of the dorsal telencephalon and contains a highly diverse population of neurons that form complex neuronal networks, which is key in higher cognitive functions. Despite its complexity, recent findings have shown that this highly organised cytoarchitecture can be recapitulated spatio-temporally in a 3D in vitro model known as cerebral organoids. This provides a new platform to investigate corticogenesis in a more accessible and controlled environment. However, as mechanisms underlying the development of cerebral organoids are much less understood, the accuracy of this model as a tool in investigating cortical development remains an unanswered question.

To address this question, this study investigates the cerebral organoid system by removing *Pax6*, one of the crucial transcription factors involved in early corticogenesis. This study aims to compare phenotypes of *Pax6*$^{-/-}$ mouse cerebral organoids to the established phenotypes of *Pax6*$^{-/-}$ mouse embryonic cortices, which will provide insights to whether the roles of *Pax6* in cerebral organoids accurately match with its function in vivo. Using an established 3D culture protocol that generates robust neuroepithelial-like (NE) structures, we found that *Pax6*$^{-/-}$ cerebral organoids show precocious differentiation, with similar characteristics to *Pax6*$^{-/-}$ embryonic cortices, such as an increase of abventricular mitotic cells and alteration in the labelling index of cells in S-phase. These results suggest a consistent role for *Pax6* in cortical development in both 3D in vitro and in vivo models.

Recent studies have shown that *Pax6* controls proliferation of cortical progenitors by repressing cell cycle genes. In order to examine *Pax6* control in the cell cycle of

cerebral organoids, *Pax6* conditional knockout (cKO) embryonic stem (ES) cell lines were derived from tamoxifen-inducible *Pax6* cKO mice. This enabled the generation of cerebral organoids that can be interrogated by acute deletion of *Pax6* in the cortex-specific region.

Using a combination of cumulative EdU labelling and mosaic analysis, we found that acute deletion of *Pax6* in cerebral organoids does not cause significant changes in the total cell cycle time (Tc) of the cortical progenitors, consistent with the phenotypes of cortical progenitors in the caudo-medial region of *Pax6* cKO mice. This may also suggests that *Pax6* is cell non-autonomously required in cortical proliferation of organoids. In addition, we found that the proliferation rate of cortical progenitors in control organoids is slower than embryonic cortical progenitors.

Overall, this study indicates that cell proliferation in cerebral organoids requires *Pax6*. However, the roles of *Pax6* in cell cycle regulation in this system remain unclear, due to the complex and context-specific functions of *Pax6*.

Layman abstract

Understanding brain development is a major scientific challenge due to the highly complex nature of the tissue, which consists of a diverse population of neurons that form intricate neuronal networks. The cerebral cortex forms the outermost layer of the brain and is responsible for many higher cognitive functions, including thought and language processing.

Recent research has shown that the composition and organisation of cortical tissue can be closely reproduced in a dish using three-dimensional cell culture techniques to generate tissues which bear a remarkable resemblance to a developing brain. These structures are known as cerebral organoids, and they provide a more accessible and controlled platform in which to study brain development in the lab. However, how accurately these structures represent certain aspects of brain development is not currently known.

To explore this, this study focuses on the role of a gene called *Pax6*. *Pax6* has been identified to be crucial in early cortical development, primarily based on studies where the gene has been deleted in mice (*Pax6*$^{-/-}$*)*. The aim of this work was to compare characteristics of cerebral organoids to the established characteristics of *Pax6*$^{-/-}$ mouse embryonic cortices, which will provide insights to whether the roles of *Pax6* in cerebral organoids accurately match with its actual role in mouse embryonic forebrain. Using the cerebral organoid system, we found that *Pax6*$^{-/-}$ organoids exhibited similar defects to *Pax6*$^{-/-}$ mice, such as in cell proliferation.

Abbreviations

3D	3 Dimensional
4-OHT	4-Hydroxytamoxifen
BrdU	Bromodeoxyuridine
cKO	Conditional knock-out
CMM	Cortical maturation medium
ddH20	Double distilled water
DNA	Deoxyribonucleic acid
dNTP	Deoxyribonucleotides
E	Embryonic age (days)
ECM	Extracellular matrix
EdU	5-ethynyl-2'-deoxyuridine
ES cells	Embryonic stem cells
GF	Growth fraction
GFP	Green fluorescent protein
IKNM	Interkinetic nuclear migration
IPCs	Intermediate progenitor cells
KSR	Knock-out serum replacement
LI	Labelling index
LIF	Leukemia inhibitory factor
MEF cells	Mouse embryonic feeder cells
NE	Neuroepithelium
PBS	Phosphate buffered saline
PCR	Polymerase chain reaction
PFA	Paraformaldehyde
RG	Radial glia

rpm	Revolutions per minute
SFEBq	Serum-free embryoid bodies with quick reaggregation
Shh	Sonic hedgehog
SVZ	Subventricular zone
Tc	Total cell cycle time
Ts	Length of S-phase
VZ	Ventricular zone
RCE	Rosa26 CAG-EGFP

CHAPTER 1: INTRODUCTION

1.1 Forebrain development

The forebrain confers many of the unique and higher cognitive functions of humans, which are rooted in its complex neuronal network. Dysregulation during developmental processes could cause intellectual disabilities and neurodevelopmental disorders (Reiner et al., 2016; Tan and Shi, 2013). The principles of forebrain development are highly conserved, and therefore many studies have used animal models, such as mice to unravel the mechanisms by which development of this complex organ proceeds. Therefore, this chapter focuses on mouse embryonic forebrain development.

Following neural induction, the neural plate folds and forms a neural tube, an apico-basally polarised epithelium, which is organised around a lumen, the primordial ventricle (Lancaster and Knoblich, 2014). Subsequently, morphogen gradients such as Wnt and Sonic hedgehog (Shh) shape the rostro-caudal and dorso-ventral axes of the neuroepithelium during gastrulation (Figure 1.1, Levine and Brivanlou, 2007).

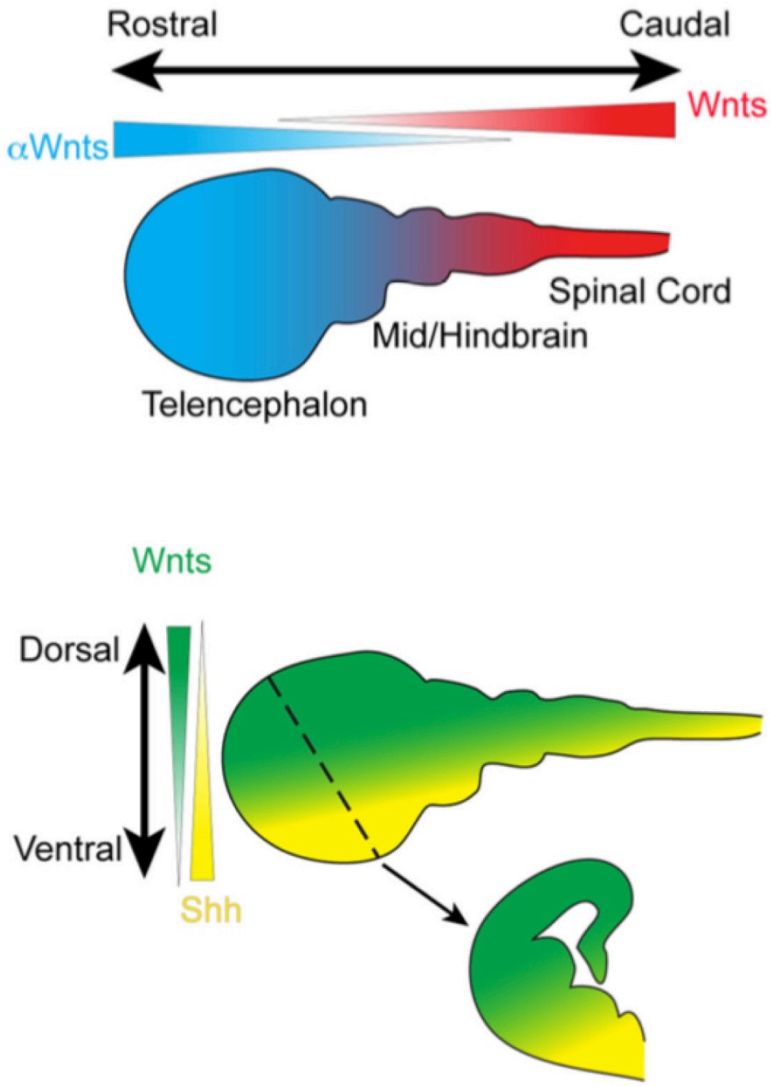

Figure 1.1 Regionalisation of the embryonic forebrain. Morphogen gradients such as Wnt and Shh regionalise the rostro-caudal and dorso-ventral axis respectively (Petros et al., 2011).

The forebrain emerges from the most rostral part of the neural plate and further subdivides into telencephalon and diencephalon, which can be distinguished by the expression of molecular marker *Foxg1* that marks the prospective telencephalon, but is absent in diencephalon (Danesin and Houart, 2012; Wilson and Houart, 2004).

Both of these forebrain subdivisions have reciprocal connections, as the diencephalon (thalamus) receives sensory information, which is relayed to the telencephalon (cerebral cortex) to be processed, and the feedback is subsequently transmitted back to the thalamus, forming a thalamo-cortico-thalamic loop (Antón-Bolaños et al., 2018). These interactions are fundamental to forebrain function, which is partly regulated by the complex neuronal networks in the cerebral cortex. These neuronal networks are built upon the interaction of two major types of cortical neurons: glutamatergic excitatory neurons and GABAergic inhibitory neurons, with the former type comprising the major part of the circuits.

The balance between these two classes of neurons is fundamental for cortical function, as disturbance could lead to cognitive dysfunction, causing various neurodevelopmental disorders such as autism (Choi et al., 2016; Geschwind and Levitt, 2007). Interestingly, these two major types of neurons are born in different parts of the telencephalon, as the dorsal telencephalic region generates glutamatergic excitatory neurons that migrate radially to the cortical plate and the ventral telencephalic region generates GABAergic inhibitory neurons that migrate tangentially to the cerebral cortex, forming complex neuronal circuits (Gelman and Marín, 2010).

1.1.1 Building blocks of cortical development

The cerebral cortex is the major and most complex part of dorsal telencephalon, consisting of a heterogeneous population of neurons that are spatio-temporally organised into six cortical layers according to their birth-date (Gaspard and Vanderhaeghen, 2011). This complex cytoarchitecture started as a simple pseudostratified neuroepithelium (NE) with apico-basal polarity, radially organised around lumen, the primordial ventricle (Suzuki and Vanderhaeghen, 2015).

Cortical progenitors are the basic unit of the developing cortex, which is also the basis of neuronal diversity. There are two major types of cortical progenitors, namely apical and basal progenitors, which can be distinguished based on their cellular characteristics and expression of specific molecular markers (Figure 1.2, Manuel et al., 2015).

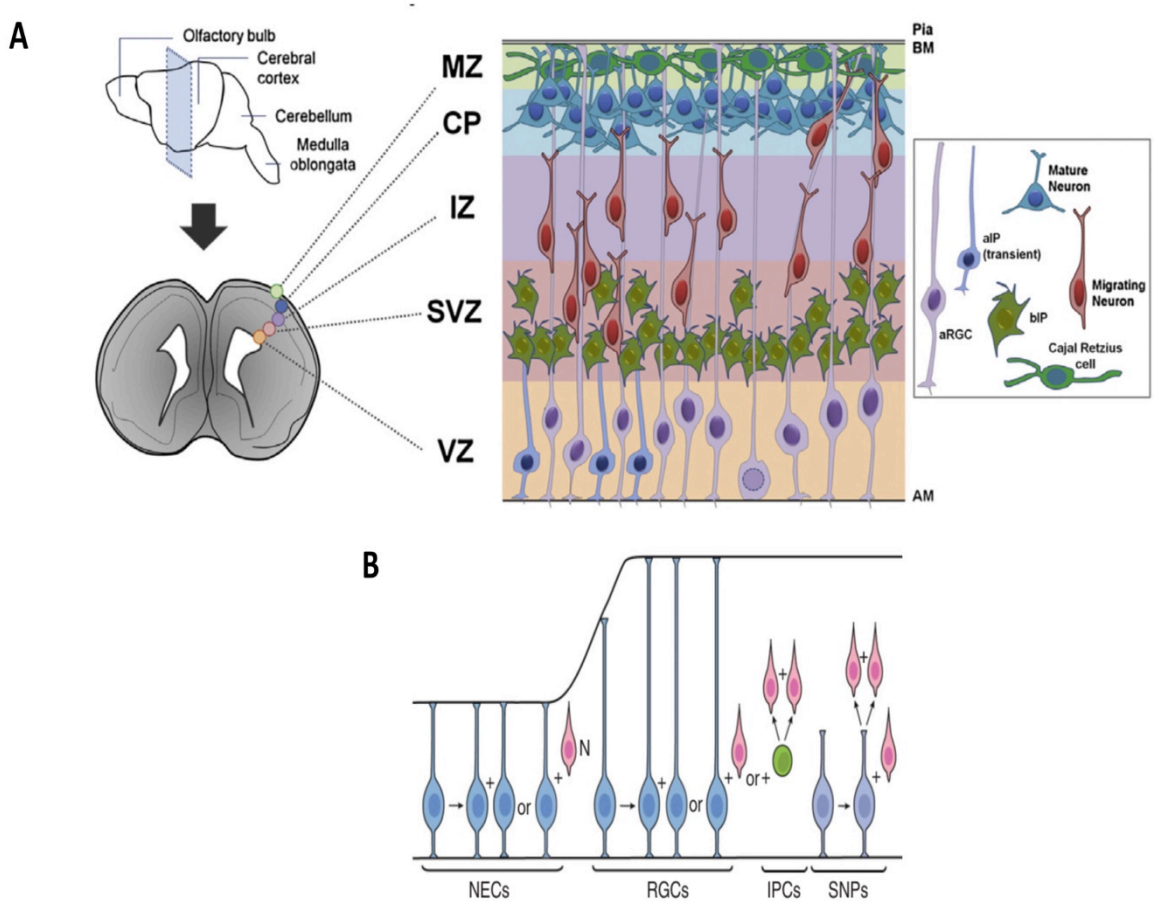

Figure 1.2 The complex and organised cytoarchitecture of the cerebral cortex. (A) Cortical progenitors such as apical and basal progenitors organised into VZ and SVZ, respectively. (B) These cortical progenitors give rise to diverse cortical neurons by undergoing symmetrical and asymmetrical cell division (Romero et al., 2018).

For example, apical progenitors such as NE and radial glia (RG) cells are cells that reside and divide at the apical side of the cortex (next to the ventricles), forming the ventricular zone (VZ). These cells are also characterised by the expression of neural progenitor markers, such as *Sox2* and *Pax6* (Azzarelli et al., 2015). Prior to neurogenesis, NE cells divide symmetrically to generate a progenitor pool, and as mouse neurogenesis commences around E10.5, these cells transform into RG cells; identified with an apical, as well as a basal process that spans the width of the cortex, which acts as a scaffold for migrating neurons. Apart from symmetric cell division to maintain the progenitor pool, RG cells can also divide asymmetrically to generate basal progenitors (Noctor et al., 2004).

Basal progenitors are intermediate progenitors (IPCs) that reside at the basal side of the cortex, forming the subventricular zone (SVZ). They are characterised by the lack of an apical process, expression of the transcription factor *Tbr2*, and mainly divide symmetrically, giving rise to neurons (Taverna et al., 2014). Cortical neurons are arranged in six layers in an inside-out fashion, with early-born neurons form the deep layers (VI-V) and the late-born neurons form the upper layers (III and II) of the cortex. Layer I is formed the earliest (E10), populated by Cajal-Retzius cells, which have migrated from outer regions of the pallium.

How these progenitors could give rise to an intricate but organised structure with diverse cortical neurons lies partly in their genetic control, as demonstrated from studies using genetically modified mice. These studies show the molecular basis of cortical development, with various transcription factors implicated, including *Pax6.*

1.1.2 *Pax6*: a key transcription factor in cortical development

Pax6 is a highly evolutionarily conserved transcription factor, which belongs to the Paired-box (Pax) gene family, and it encodes for two DNA-binding domains, the paired domain and a homeodomain (Osumi et al., 2008). During development, *Pax6* is expressed in a highly dynamic pattern, including in the forebrain, eye, spinal cord, olfactory system and pancreas (Ypsilanti and Rubenstein, 2016). Mutation of *Pax6* is implicated in aniridia, a congenital human condition characterised by absence of the iris, a condition which is homologous to the small eye (Sey) mouse; a mutant mice model with a point mutation in the *Pax6* gene that results in *Pax6* loss of function – also known as $Pax6^{-/-}$ mice (Georgala et al., 2011; Hill et al., 1991). Apart from the absence of iris and nasal structures, $Pax6^{-/-}$ mice die at birth with a plethora of telencephalic defects, such as proliferation, neurogenesis, patterning and neuronal migration defects (Georgala et al., 2011; Quinn et al., 2007; Estivill-Torrus et al., 2002; Stoykova et al., 2000; Simpson et al., 2009).

During telencephalic development in the mouse, expression of *Pax6* starts from E8.0 in a spatio-temporally controlled manner (Osumi et al., 2008). It is specifically expressed in the dorsal part of telencephalon, forming a pallial-subpallial boundary, separating the dorsal (pallium) and ventral (subpallium) telencephalic regions (Zaki et al., 2003). During early corticogenesis, *Pax6* is expressed in a gradient pattern, with high levels rostro-laterally and low levels caudo-medially, and it becomes more uniform in late corticogenesis (Figure 1.3, Manuel et al., 2015).

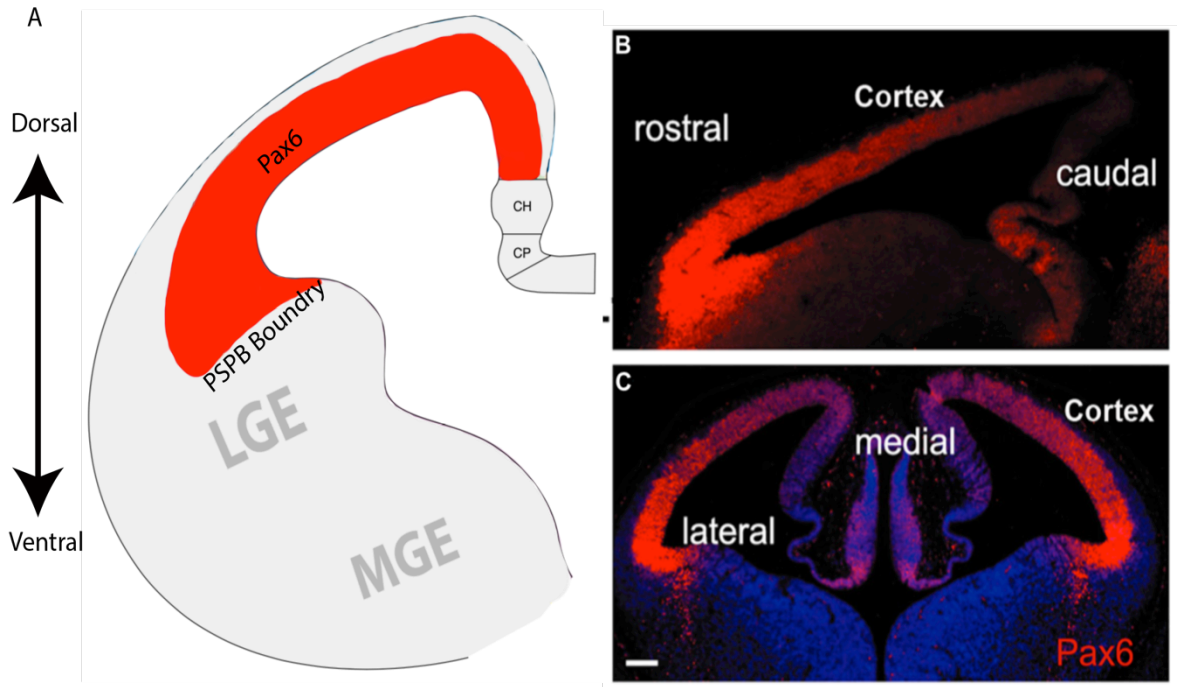

Figure 1.3 Expression pattern of *Pax6* in the telencephalon. (A) *Pax6* is expressed in the dorsal part of telencephalon, forming a sharp pallial-subpallial (PSPB) boundary between the dorsal and ventral telencephalon. (B, C) Expression of *Pax6* follows a gradient pattern, with high rostro-laterally and low caudo-medially (Manuel et al., 2015).

Recent studies demonstrate that the roles of *Pax6* in cortical development may be partly due to *Pax6* control in the proliferation of cortical progenitors (Mi et al., 2018; Georgala et al., 2011; Manuel et al., 2006; Estivill-Torrus et al., 2002).

1.1.3 *Pax6* regulates proliferation of cortical progenitors

During cortical development, expression of *Pax6* is restricted to the apical cortical progenitors, such as NE and RG cells in the VZ (Manuel et al., 2015). As neurogenesis commences, RG cells divide asymmetrically, giving rise to either an apical progenitor, which maintains *Pax6* expression, or to a basal progenitor, as *Pax6* is downregulated and *Tbr2* is upregulated (Englund et al., 2005). This indicates the requirement of *Pax6* in maintaining the balance of cortical progenitor proliferation, which is fundamental for proper cortical development.

The role of *Pax6* in cortical progenitor proliferation is well-established, and was mainly discovered using *Pax6* loss-of-function mice ($Pax6^{-/-}$) and cortex-specific *Pax6* conditional knock-out mice (cKO). The former is a classic *Pax6* mutant mouse model with constitutive loss of *Pax6*; therefore *Pax6* is lost in all types of tissues at all times, resulting in cumulative defects that might not be specific to *Pax6*. Embryos from this model die at birth, and the roles of *Pax6* can therefore only be studied during the embryonic stage. The latter is a *Pax6* conditional mutant mouse model, which enables acute *Pax6* deletion in a specific region. This control allows the determination of the direct effects of *Pax6* at a specific time and region (in this case, the cortex); therefore embryos of this model survive beyond birth and the post-natal roles of *Pax6* can also be studied.

During early cortical development, constitutive loss of *Pax6* results in an increase in the BrdU labelling index (LI) of the cortical progenitors, suggesting that either the cells are proliferating more rapidly or that the length of S-phase increased as a proportion of the overall cell cycle length (Warren et al., 1999). Estivill-Torrus et al., later quantified the cell cycle kinetics of these *Pax6*$^{-/-}$ cortical progenitors at different stages of corticogenesis and found that constitutive loss of *Pax6* at E10.5 and E12.5 caused a decrease in the total cell cycle time (Tc), which suggests rapid cell proliferation. This leads to precocious differentiation, demonstrated by the increase of post-mitotic cells expressing *Tuj1* (Estivill-Torrus et al., 2002). However increased Tc at E15.5 suggests that constitutive loss of *Pax6* at later stage of corticogenesis results in slower cell proliferation. The distinct effects of the loss of *Pax6* at different developmental stages suggest the role of *Pax6*'s in cortical progenitor proliferation is context-dependent.

Interestingly, using the same mouse model, another study found no significant change in the Tc of E12.5 *Pax6*$^{-/-}$ cortical progenitors – which is in contrast to the previous findings (Quinn et al., 2007). This could be due to the different technique used to calculate the Tc; Estivill-Torrus et al used cumulative BrdU labelling, whereas Quinn et al used BrdU-IddU double-labelling to label cells undergoing S-phase. In the former technique, the Tc is extrapolated from the plotted graph following the protocol described by Nowakowski et al., 1998, and the latter technique calculates the Tc based on cells leaving the cell cycle, known as the Q-fraction (Martynoga et al., 2005).

Nevertheless, a more recent study has reassessed the Tc of E12.5 *Pax6*$^{-/-}$ mice, taking into account the expression gradient of *Pax6*, which is high rostro-laterally and low caudo-medially (Mi et al., 2013). This study revealed that loss of *Pax6* only affected cortical progenitors in rostro-lateral region, with their Tc significantly decreased, compared to control. Similar findings also have been reported in *Pax6* cKO mice, suggesting that *Pax6* repressive control in cortical progenitor proliferation is regulated spatio-temporally. Further evidence shows that this is partly due to *Pax6* control on cell cycle genes, as acute deletion of *Pax6* causes upregulation of cell cycle genes, particularly *Cdk6*, which causes a shortening in G1 phase, causing a rapid cell proliferation (Mi et al., 2013; Mi et al., 2018).

Although animal models are useful in providing a comprehensive understanding of the roles of *Pax6 in* forebrain development, many cellular processes as well as tissue morphogenesis occur simultaneously in utero, which complicates the examination of these dynamic interactions (Heemskerk and Warmflash, 2016). For example, due to the coordination of extrinsic and intrinsic factors in forebrain development, it is difficult to perturb this dynamic system separately without affecting other processes. Therefore, an alternative system with a more accessible and controlled environment is necessary to unravel the molecular mechanisms of *Pax6* control in forebrain development.

1.2 Cerebral Organoids: A three-dimensional embryonic stem cell model for cortical development

ES cells are pluripotent cells, which are able to give rise to any cell types of the three primary germ layers, including into neuroectodermal cells. Classic neural differentiation can be performed either via direct differentiation in adherent monolayer culture (2D), or via the traditional 3D culture system, which is through the formation of embryoid bodies (Tropepe et al., 2001). Embryoid bodies (EBs) are multicellular aggregates consisting of cells representative of all the primary germ layers (Valamehr et al., 2008). Therefore, EBs are very heterogeneous, and lack distinct spatial structures (Simunovic and Brivanlou, 2017). The formation of EBs is required as an intermediate stage of the classic lineage-specific differentiation protocols (Bain et al., 1995; Bibel et al., 2004). However, subsequent study has shown that the formation of EBs is dispensable, as efficient neural induction can be achieved through the culture of ES cells in minimal, serum-free medium (Ying et al., 2003). Therefore, in the absence of external signalling molecules, ES cells adopt neural fate – supporting the default model of neural induction (Muñoz-Sanjuán and Brivanlou, 2002)

Recent progress using 2D neural differentiation techniques have demonstrated the formation of neural rosettes, a group of neural precursor cells in rosette conformation (Gaspard et al., 2008). Although the neural rosettes recapitulate spatio-temporal patterns characteristic of the cerebral cortex, they lack cell-cell or cell-basement membrane interactions, due to their attachment to plastic surfaces. This is in contrast

to the endogenous biological system and therefore might compromise the accuracy of the 2D model (Hwang et al., 2008; Van den Ameele et al., 2014).

The advent of 3D culture systems has paved the path towards the establishment of cerebral organoids. Cerebral organoids are neural-like tissues grown from pluripotent stem cells in a 3D in vitro culture, with remarkable resemblance to embryonic cortex (Lancaster et al., 2013; Qian et al., 2016; Renner et al., 2017). They generate more heterogeneous and mature neuronal populations with more complex organisation, therefore more closely resembles the cerebral cortex (Eiraku et al., 2008; Nasu et al., 2012). Their ability to recapitulate cellular complexity and organisation of early corticogenesis in vitro offers unprecedented accessibility to unravel the dynamics and molecular mechanisms underlying forebrain development. This exciting feature means more sophisticated techniques could be applied in cerebral organoids to track its development in real-time, as well as multiple genetic modifications using CRISPR/Cas9 to understand complex genetic interactions in cortical development, which can be done relatively easy in vitro.

Given their ability to recapitulate early cortical development with great cyto-architectural detail, cerebral organoids have emerged as a new, highly promising tool to model the cerebral cortex in vitro. As this 3D model can be established from human and mouse ES cells with species-specific characteristics (Eiraku et al., 2008; Lancaster et al., 2017), cerebral organoids provide access to human cortical-like tissues that would otherwise be limited in availability and hampered by ethical considerations.

However, as cerebral organoids follow species-specific developmental time, it takes a longer time to grow human cerebral organoids compared to mouse cerebral organoids. Therefore, generating human cerebral organoids is time-consuming and costly; hence mouse cerebral organoids could be considered to be more advantageous, especially for optimisation and exploration studies. Furthermore, much of our knowledge in cortical development is derived from mouse models, thus enable us to compare them to cerebral organoid system following genetic manipulation. Therefore, this study focuses on cerebral organoids derived from mouse ES cells.

1.2.1 Serum-free embryoid bodies with quick reaggregation (SFEBq) protocol

One of the earliest described techniques for producing cerebral organoids is the serum-free embryoid bodies with quick reaggregation (SFEBq) protocol, a technique that follows the key concepts of telencephalic development (Figure 1.4, Eiraku et al., 2008; Seto and Eiraku, 2018).

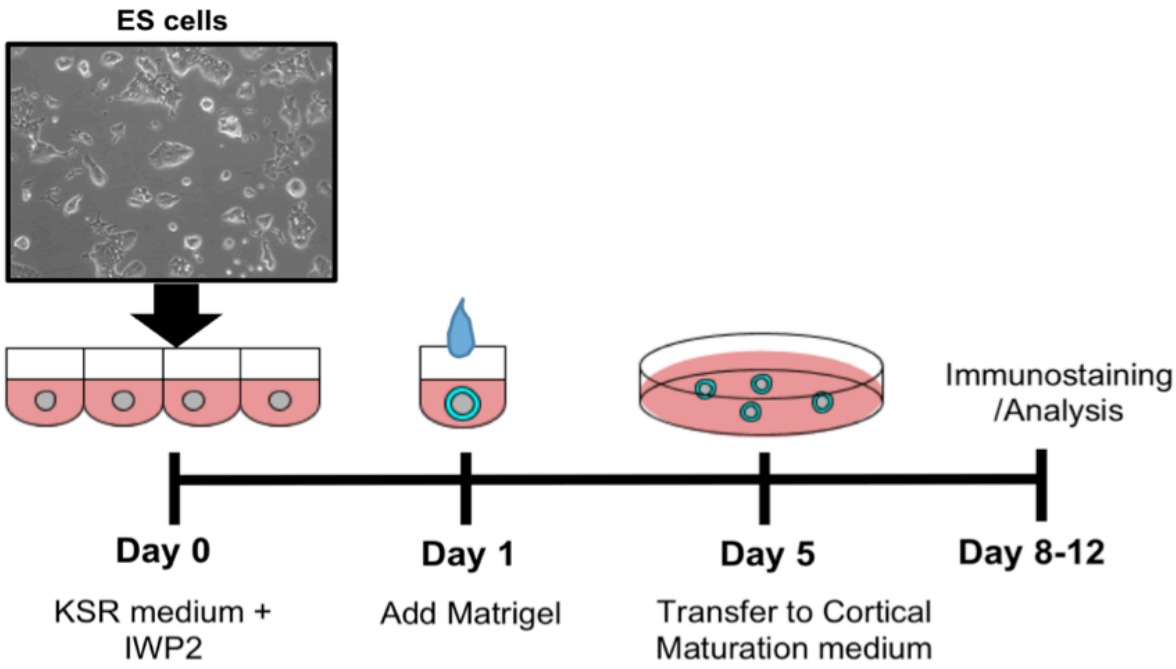

Figure 1.4 Scheme illustrating the main stages of the SFEBq protocol for generating mouse cerebral organoids.

In this technique, an optimised number of aggregated cells are cultured in a serum-free medium. A controlled number of starting ES cells is essential, as local cell-cell interaction influences differentiation potential, as well as cell specification (Valamehr et al., 2008). The cells were cultured in a serum-free medium, as serum contains highly variable and poorly defined components that triggers spontaneous differentiation of ES cells (Ying et al., 2003). Furthermore, serum-free medium triggers the intrinsic, default pathway, promoting neural induction (Watanabe et al., 2005). Among various serum-free media, Knock-out Serum Replacement (KSR) medium has been shown to better support cell growth in suspension, and induce telencephalic differentiation efficiently without concurrent induction of mesodermal and endodermal tissues (Watanabe et al., 2005). In addition, the medium is supplemented with external signalling molecules, such as IWP2 (a Wnt inhibitor) to protect the cells from caudalising signals (Wnt), thus directing them toward telencephalic specification. This is consistent with the principles of telencephalic development in vivo that highlight the influence of morphogens in region specification. Following neural induction, the aggregates form NE structures that rely on structural support provided by the extracellular matrix (ECM), which forms the basement membrane (Nasu et al., 2012).

This method was later refined by replacing KSR with a defined chemical medium, for a more stable culture. This is due to variation when different lots of KSR supplement are used that could affect cortical differentiation efficiency. However, studies have shown that organoid batch variation persists even within the same lot of KSR - suggesting other contributing factors to batch variation, which are likely intrinsic (Lancaster et al., 2017; Renner et al., 2017).

Nevertheless, this system is highly versatile, as regions of the forebrain can be specified by modulating external signalling molecules. For example, the cells are directed towards telencephalic fate by inhibiting caudalising signals such as Wnt, and ventral telencephalic fate can also be induced by controlling the addition of Shh (Nasu et al., 2012).

1.2.2 Cortical development in mouse cerebral organoids

Using the SFEBq method, mouse ES cells can form cerebral organoids that recapitulate embryonic cortical development. Around day three of culture, the cells self-organise into neuroepithelium-like (NE) structures surrounding lumen. This tissue demonstrates apico-basal polarity, characterised by the expression of apical markers such as N-cadherin, aPKC and ZO-1 on the apical side of the tissue, and laminin on the basal side (Figure 1.5A, Eiraku et al., 2008; Nasu et al., 2012). By day eight, the NE structures express one of the earliest telencephalic markers, *Foxg1* (Figure 1.5B) and show remarkable resemblance to embryonic cerebral cortex as they consist of cells expressing cortical progenitor markers, arranged in the correct pattern as they do in vivo.

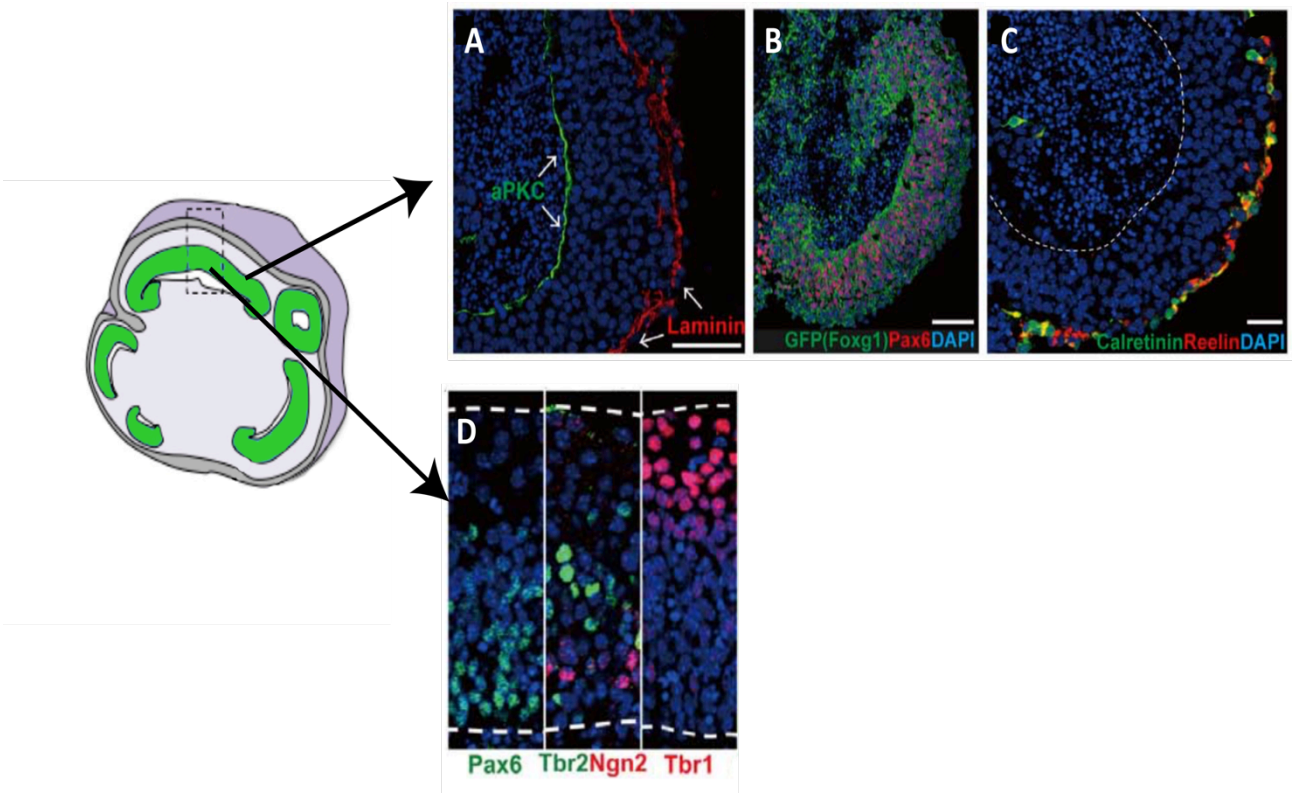

Figure 1.5 Characteristics of mouse cerebral organoids. (A) A cross-section of NE show its expression of aPKC and laminin, suggesting apico-basal polarity (B) expression of *Foxg1*, a telencephalic marker (C) expression of reelin and Calretinin, characteristic of Cajal-Retzius cells (D) and cells expressing key cortical markers (*Pax6, Tbr2, Tbr1*) in the correct apico-basal pattern (Nasu et al., 2012).

For instance, cells of the outermost part of the NE express *reelin*, a molecular marker of Cajal-Retzius cells, which form the first layer of cortical plate (Figure 1.5C). There are also cells expressing apical progenitor marker, *Pax6* at the apical side of NE, forming a layer resembling the ventricular zone (VZ). On top of this layer, there are cells expressing *Tbr2*, a marker characteristic of basal progenitor cells, which form another layer resembling subventricular zone (SVZ). This is followed by the formation of neuronal cells expressing *Tbr1*, an early marker of deep layer neurons. Furthermore, functional analysis by live imaging shows that apical progenitors of organoids (*Pax6*+) move in an apico-basal direction, characteristic of interkinetic nuclear migration (IKNM), a hallmark of cortical development (Nasu et al., 2012).

Therefore, at day eight, cerebral organoids form polarised NE structures containing cells expressing key cortical progenitor markers, organised in the same spatial arrangement as embryonic cerebral cortex (Nasu et al., 2012). This demonstrates the existence of a cell-intrinsic programme for early cortical development.

1.2.3 Limitations of cerebral organoids

Despite the remarkable resemblance of cerebral organoids to the embryonic cerebral cortex, it should be noted that the later stages of cortical development are not reproduced accurately in organoids, because the neurons fail to recapitulate the inside-out arrangement cortical layers (Nasu et al., 2012). For example, at day 12, more cortical cell types are detected in the NE, such as cells expressing *Tbr1* and *Ctip2*, characteristic of early cortical plate, as well as *Cux1*+ and *Brn2*+ cells, characteristic of neurons of late cortical plate (Nasu et al., 2012). Although these cells

were born in the correct temporal order, as well as forming multiple layers characteristic of early and late cortical plate, their lamination is not in the correct inside-out pattern, and separation between them is rudimentary (Nasu et al., 2012)

These limitations might be due to many factors, such as the limited supply of nutrients and oxygen to the core of the organoids (which leads to apoptosis and a necrotic centre), the absence of vascularization, and the lack of other supporting cells such as microglia. Ultimately, there is a limited understanding of mechanisms of organoid development, which might limit the accuracy or application of this model as a tool to investigate forebrain development. A comparison between in vitro and in vivo models, both in control and mutant conditions may fill the gap in our understanding of the extent of this model, which leads to the aim of this study.

1.3 Aim of thesis

Despite rapid development in the organoid field, very few studies have reported the use of mouse cerebral organoids, and little is known about the molecular machinery of this 3D in vitro system. Our current comprehensive understanding in mouse corticogenesis, together with the widely characterised roles of *Pax6* in normal forebrain development, as well as thorough descriptions of *Pax6* mutant mouse phenotypes, provides a basis to understand how accurately mouse cortical development and *Pax6* function can be recapitulated in mouse cerebral organoids. Furthermore, our understanding of the extent of this 3D model as a tool for investigating forebrain development remains fragmentary.

Therefore, this study aims to determine whether cerebral organoids can be used as a valid model to study mouse forebrain development. We hypothesised that if cerebral organoids develop using the same mechanisms as mouse cortical development, the effects of loss of *Pax6* in vivo can be reproduced in this 3D system. Therefore, this will be addressed by comparing normal and mutant $Pax6^{-/-}$ mouse cerebral organoids to the established characteristics of their in vivo counterparts. First, a 3D protocol based on the SFEBq method was established and the robustness of the method to generate *Foxg1*+ NE structures was demonstrated. Then, the characteristics of organoids under normal conditions were analysed and used as a baseline in the analysis of $Pax6^{-/-}$ cerebral organoids.

Once the phenotypes of $Pax6^{-/-}$ cerebral organoids were identified, the cell cycle kinetics of cortical progenitors of cerebral organoids in a normal and *Pax6* conditional

knock-out (cKO) condition was compared to the cortical progenitors of *Pax6* cKO mice. To address this, new lines of ES cells from *Pax6* cKO cerebral organoids were established and characterised. This model enables acute *Pax6* deletion in a cortex-specific region, thus provides a direct examination of *Pax6* on cortical proliferation.

CHAPTER 2: MATERIALS AND METHODS

2.1 Propagation and maintenance of embryonic stem cells

Mouse embryonic stem (ES) cells lines; Foxg1::Venus line with *Foxg1* reporter (formerly known as Bf1::Venus, Eiraku et al., 2008) and an established *Pax6*$^{-/-}$ ES cell line (Quinn et al., 2010), were cultured in a standard ES medium, GMEM (BHK-21) basal medium supplemented with 1 mM Sodium Pyruvate, 2 mM Glutamax, 1x non-essential amino acid, 0.1 mM β-mercaptoethanol, 10% fetal calf serum (FCS) and 1:1000 Leukemia Inhibitory Factor (LIF). The cells were incubated at 37°C in 5% CO_2. All cell culture reagents were obtained from Invitrogen, Thermoscientific, unless otherwise stated.

Newly established ES cell lines; *Emx1-Cre ER*^{T2}*; Pax6*$^{fl/fl}$*; RCE* and *Emx1-CreER*^{T2}*; Pax6*$^{+/fl}$*; RCE* ES cells (described in detail in section 2.10) were maintained in the same medium supplemented with 0.5 μM PD 0325901 (Axon medchem).

Cultures were maintained in T25 flask (Corning) coated with 0.1% gelatin. Porcine gelatin (1%) was prepared by dissolving 1 g gelatin (Sigma) in 100 ml 1 x PBS (Phosphate buffer saline) on a hotplate on medium setting. Prior to use, 0.1% gelatin was prepared by diluting 5 ml of 1% gelatin in 45 ml PBS.

Every other day the cells were passaged by trypsinisation with Tryple (trypsin replacement). Prior to trypsinisation, medium was aspirated and the cells were washed twice with PBS, followed by addition of 1 ml Tryple into T25 flask. After cells

detached, 9 ml fresh medium was added and the cells were further disassociated by gentle trituration. The cell suspension was split in 1:10, where 1ml of the cell suspension was pipetted into a new flask, and 4 ml of fresh medium was added.

Cells were cryopreserved by preparing cell suspension, followed by centrifugation at 250 x g for 5 minutes. The supernatant was discarded and the cell pellet was resuspended in 1 ml freezing medium, which is the standard ES medium supplemented with additional 10% FCS and 10% DMSO. The cells were transferred into a cryovial, slowly frozen at -80°C overnight and transferred to liquid nitrogen tank for long-term storage. To revive the cryopreserved cells, they were thawed in waterbath (37°C) and resuspended in 9 ml medium, followed by centrifugation at 250 x g for 5 minutes. The supernatant was decanted and the cell pellet was resuspended in a fresh ES medium before plated in a gelatin-coated flask. Medium was changed the day after.

2.2 Derivation of *Pax6* conditional knock-out embryonic stem cells

ES cell lines were established following a published protocol (Czechanski et al., 2014). They were derived from blastocysts obtained from the parental cross of a male mouse carrying *Emx1-CreER*^{T2} allele (Kessaris et al., 2006), green fluorescent protein (GFP) reporter allele (Sousa et al., 2009) and homozygous for a conditional (floxed) *Pax6*^{fl} allele (Simpson et al., 2009), with a female mouse heterozygous for *Pax6*^{fl} allele. Animal work procedures were performed following the guidelines of the UK

Animals (Scientific Procedures) Act 1986 and Edinburgh's University Animal Ethics Committee.

A day prior to blastocyst collection, four-well plates (Falcon) were coated with 0.1% gelatin (Sigma) and inactivated mouse embryonic feeder (MEF) cells (Invitrogen). MEF cells were cultured in MEF medium containing DMEM-high glucose with 10% FCS, 2 mM Glutamax and 1% penicillin-streptomycin. The next day, the feeder cells were washed with PBS and the medium was changed to serum-free (2i/LIF) medium.

At day 3.5 post-coitum, the uterus of the pregnant mouse was removed and cleaned of fat. Both uterine horns were then flushed with M2 medium (Millipore) using a 5 ml syringe attached with 27-G needle, into a petri dish. Subsequently, the flushed blastocysts were collected using a mouth pipette and washed in several drops of M2 and finally plated on a 4-well plate coated with MEF, in serum-free medium. The embryos were left undisturbed for 48 hours in the incubator at 37°C, 5% CO_2.

After 48 hours, the blastocysts were checked to determine whether they had hatched and attached to the plates. The medium was then changed every other day and the outgrowths were monitored daily. Prominent outgrowth was then treated with 100 µl of 0.05% trypsin and disaggregated vigorously using a mouth pipette. Then, defined trypsin inhibitor was added to deactivate the trypsin and the cells were transferred into new 4-well plates coated with MEF, in serum-free medium. The cells were now recorded as passage one and incubated at 37°C, 5% CO_2. After formation of ES colonies, they were subcultured with Accutase and gradually maintained in feeder-free plates.

2.3 Characterisation of Pax6 cKO embryonic stem cell lines

2.3.1 Genotyping

ES cells carrying *Emx1-CreER*^{T2}, *RCE* and homozygous for the *Pax6*^{fl} allele were genotyped by PCR (Mi et al., 2013a). Briefly, DNA was prepared from ES cells, collected at confluency. Cells were lysed with 75 µl lysis buffer (25mM NaOH, 0.2 mM EDTA) at 95°C for 30 minutes and rested on ice for 5 minutes. Then, 75 µl neutralizing buffer (40 mM Tris-HCL) was added to stop the reaction and ready to use for PCR to detect allele of interest. 1.5 µl of the DNA was amplified with 0.5 mM primer mix in a standard 25 µl PCR reaction (0.5 mM DNTP mix, 1x PCR buffer, 5U/µl Taq DNA polymerase (Promega). The size of the PCR products (195 bp were homozygous for the floxed *Pax6* allele, and 156 bp were heterozygotes) determined using electrophoresis on a 2% gel.

2.3.2 Immunocytochemistry

Cells were fixed with 4% PFA for 10 – 20 min at room temperature. Fixative was washed off with PBS for 10 minutes, three times. Cells were permeabilized in blocking buffer for 30 minutes at room temperature, followed by incubation with primary antibodies at 4°C, overnight. The next day, cells were washed with PBS for 5 minutes at room temperature, three times. Secondary antibodies were then added and left at room temperature for one hour. Finally, cells were counterstained with DAPI and mounted in Vectashield Hardset (Vectorlabs).

2.3.3 Karyotyping

Cells were passaged the day before in 10 ml medium, in a T25 flask. Approximately 18 hours after the passage, 100 µl colcemid (final concentration:100 ng/mL) was added to the flask. After 2-2.5 hours, culture medium from the flask was collected in a 15ml centrifuge tube and the cells were detached using TrypLE. A cell suspension was prepared using the previously collected old culture medium and centrifuged at 800 rpm for 8 minutes. Supernatant was then decanted, leaving the cell pellet in 1 ml residual medium. Next, 9 ml of 0.075M KCL was added slowly to swell the cells while the tube was vortexed at low speed and then incubated at 37°C for 20-25 minutes.

The cells were then fixed with Carnoy's fixative (3:1 ratio of methanol:glacial acetic acid) by adding the fixative gradually, whilst the tube was vortexed. Firstly, three drops of fixative was added and the fixative was discarded as the cells were centrifuged at 800 rpm for 8 minutes. The steps were repeated with 3 ml, 2 ml and 1 ml of fixative. Finally, the cells were resuspended by vortexing in a few drops of fixative. Finally, 40-50 µl of the cell suspension was dropped on to superfrost slides, and left on the bench to air-dry. Vectashield hard set with DAPI was then dropped to the slides to stain the chromosomes, and a coverslip was applied. The slides were imaged at 40x magnification and at least 20 chromosome spreads were analyzed by counting the total number of chromosomes. The percentage of metaphase spreads with more than 60% of 40 chromosomes was counted as normal.

2.3.4 Mycoplasma test

Mycoplasma testing was performed by tissue culture services at the Scottish Centre for Regenerative Medicine using Mycoalert mycoplasma testing kit (Lonza).

2.4 Cerebral organoid culture

Cerebral organoids were generated from the aforementioned mouse ES cells, using a modified SFEBq protocol. Instead of using chemically defined medium as described in the SFEBq protocol, this study used neural induction medium known as knockout serum replacement (KSR) medium in the beginning of cerebral organoids culture. ES cells were disassociated into single cells and resuspended in KSR medium, containing GMEM (BHK-21) medium supplemented with 10% KSR, 1 mM Sodium pyruvate, 0.1 mM non-essential amino acid, 0.1 mM β –mercaptoethanol and 2.5 μM IWP2 (Sigma). A total of 5000 cells were plated into each well of U-shaped 96 well plates (Sumitomo Bakelite), and this was counted as day zero. Following overnight culture, the cells formed an aggregate and were embedded with 200 μg/ml Matrigel (Corning), then incubated at 37°C, 5% CO_2. Prior to use, Matrigel was thawed on ice for at least 1 hour, and kept on ice during usage.

On day five, a maximum of 16 organoids were transferred into 50 mm bacterial-grade petri dishes (Fisher scientific) in 10 ml cortical maturation medium (CMM), containing DMEM/F-12 medium supplemented with 1x N2 and 1x Glutamax. Medium was changed every other day by removing half of the medium and replenished with an equal volume of fresh CMM.

2.5 Preparation of cerebral organoids for histology

Organoids were collected and transferred into 12 well plates (Greiner) using a 1 ml plastic Pasteur pipette. They were washed twice with PBS and fixed with 4% paraformaldehyde (PFA) for 15-20 minutes, at room temperature on a shaking platform. Finally, the organoids were rinsed with 1 x PBS for 10 minutes, and the washes were repeated twice. The organoids were stored at 4°C in PBS until further use.

Organoids were then cryoprotected by immersing them in 30% sucrose at 4°C, on a rocking platform, overnight. Then, the sucrose was replaced with embedding medium (50:50 mixture of 30% sucrose:OCT medium) and left at 4°C, on a rocking platform for one hour. Organoids were then transferred into embedding mould and left undisturbed for 5-10 minutes, to allow them to settle to the bottom of the mould. The remaining embedding medium was removed using p200 pipette and the organoids were arranged to the middle of the mould. The mould was then placed on a piece of dry ice to fix its position, and was quickly filled with the embedding medium. Finally, organoids in the mould were frozen in dry ice and cryosectioned at 10 μm, in a frozen microtome chamber (SakuraTek). Cryosections were collected on superfrost slides and stored at -20°C.

2.6 Immunohistochemistry

Cryosection slides were brought to room temperature at least 30 minutes prior immunostaining and then washed with PBS for 20 minutes, three times. If required,

antigen retrieval step was performed by resting the slides in 10 mM citrate buffer for 5 minutes, followed by heating with microwave for 20 minutes, starting at high power. The buffer was checked every five minutes and the power was changed to medium/low when the citrate buffer was boiling. Then, the slides were left at room temperature (approximately 20 minutes) before being washed with 1x PBS, once. Next, the slides were incubated in blocking buffer for two hours and then incubated with primary antibody overnight, at 4°C. Primary antibodies were diluted in 10% donkey serum (the concentration used can be seen in table 1).

Table 1. Primary antibodies used

Antibodies	Host	Dilution	Source	Catalog No.	Antigen retrieval	Blocking buffer
GFP	Chicken	1:1000	Abcam	ab13970	No	20% donkey serum in PBS
GFP	Goat	1:400	Abcam	ab6673	Yes	
Pax6	Rabbit	1:400	Biolegend	901301	No	
Tbr2	Rabbit	1:200	Abcam	ab183991	No	
Tbr1	Rabbit	1:200	Abcam	ab31940	No	
N-Cadherin	Mouse IgG1	1:400	BD Bioscience	610920	Yes	
Sox2	Rabbit	1:200	Abcam	ab92494	No	
Tuj1	Mouse IgG2a	1:400	Biolegend	801201	No	
Ki67	Rabbit	1:200	Abcam	ab15580	No	
Oct-4	Rabbit	1:100	abcam	ab181557	No	3% donkey serum and 0.1% TritonX-100 in PBS
Nanog	Rat IgG2a	1:1000	eBioscience	14-5761-80	No	
Pax6	Mouse	neat	A gift from Prof. V van Heyningen		No/amplify with streptavidin	20% goat serum in PBS

On the second day, the slides were washed three times in PBS, 10 minutes each, followed by incubation in secondary antibodies (1:200), diluted in 10% donkey serum in PBS, at room temperature.

If amplification with streptavidin was required, sections were incubated with species-specific biotin-conjugated secondary antibodies (goat anti-mouse IgG) instead, for 2 hours at room temperature. Subsequently, streptavidin-conjugated fluorescent probe (1:200) was added to the slides, 30 minutes at room temperature.

Finally, the slides were stained in DAPI diluted in PBS (1:10 000), followed by three times washes in PBS, 10 minutes each and finally mounted with VectaShield hard set (Vectorlabs) to preserve fluorescence.

2.7 Fluorescent In Situ Hybridisation

Expression of *Emx1* was examined by fluorescent *in situ* hybridsation, following protocol as described (Caballero et al., 2014).

2.7.1 Preparation of DIG-labeled probe

Plasmid encoding *Emx1* sequence (Simeone et al., 1992) was grown and purified following instructions of Midiprep kit (Qiagen). 10 μg of the plasmid was then digested with BamHI restriction enzyme at 37°C for 1 hour.

The size of the digested plasmid was then checked by agarose gel electrophoresis (1%) at 75V for 1 hour. The linearized plasmid was then purified using a gel extraction kit (Qiagen) and the concentration was determined by nanodrop. The cut and cleaned plasmid (3 µg) was then labeled with DIG label mix nucleotides (Roche) with T7 polymerase and incubated at 37°C for 2 hours. The labeled probe was then precipitated overnight at -20°C with 4M LiCl (0.1 vol) and 100% ice-cold ethanol (2.5vol). Finally, the probe was pelleted at 12000 x g at 4°C for 20 minutes and the supernatant was decanted prior to resuspending it in 25 µl RNase-free water.

2.7.2 Hybridisation procedure

Cryosection slides were warmed to room temperature for up to 30 minutes. A humidified box was prepared by lining with tissues soaked in 50% formamide, 0.5x salt (10x, prepared as in section 2.7.3.5) and ddH_2O topped up to 80 ml. The box was then warmed in a 70°C incubator. *Emx1* probe was diluted in hybridization buffer (1:1000) and denatured at 95°C for 10 minutes, followed by incubation on ice for 5 minutes. The probe was then added to the slides and incubated in the humidified box at 70°C, overnight.

Next day, the slides were washed with wash buffer (pre-warmed) at 70°C for 15 minutes and the washes were repeated twice, 30 minutes each. Then the slides were washed with TNT buffer (pH 7.5) twice, 30 minutes each. Finally, cryosections were blocked with TNB buffer prior to incubation with sheep anti DIG-POD (1:1000) in TNB buffer at 4°C, overnight.

On the third day, the slides were washed with TNT buffer (pH 7.5), three times, 5 minutes each. Biotin-tyramide (1:200) was then added to the slides at room temperature, for 10 minutes. The slides were washed with TNT buffer (pH 7.5), three times, 5 minutes each and Avidin-Biotin Complex solution (Vector labs) was added to the slides at room temperature for 30 minutes. The slides were washed with TNT buffer (pH 7.5), three times, 5 minutes each and Cy3 (1:200) was added to the slides at room temperature for 10 minutes. Then the slides were washed with TNT buffer (pH 7.5), three times, 5 minutes each and counterstained with DAPI. Finally, the slides were mounted with VectaShield Hardset.

2.7.3 Preparation of solutions

2.7.3.1 Hybridisation solution

The following reagents were mixed and stored at -20°C.

Final concentration		Volume (ml)
10%	10 x salt	2
10%	Dextran sulfate 50%	2
1%	100 x Denhardts	0.2
1 mg/ml	50 mg/ml tRNA	0.4
50%	Deionized formamide	10
	ddH_2O	5.4
TOTAL		20

2.7.3.2 Wash buffer

Final concentration		Volume (ml)
50%	Formamide	150
1x	20x SSC	15
0.1%	Tween 20	0.3
	ddH_2O	135
TOTAL		300

2.7.3.3 TNB buffer

Final concentration		Volume (ml)
10%	1 M Tris-HCL pH 7.5	0.5
3%	5 M NaCl	0.15
5mg/ml	Blocking reagent	25mg
	ddH_2O	4.35
TOTAL		5

2.7.3.4 TNT pH 7.5

Final concentration		Volume (ml)
10%	1 M Tris-HCL pH 7.5	100
3%	5 M NaCl	30
0.25%	Tween 20	2.5
	ddH_2O	867.50
TOTAL		1000

2.7.3.5 10x salt

Following reagents were mixed and autoclaved.

Tris-HCL	11.2g
NaCl	91.2g
Tris Base	1.1g
$NaH_2PO_4.2H_2O$ (MW 156)	6.2g
NaH_2PO_4 (MW 177)	5.7g
0.5M EDTA	80ml
ddH_2O	Top up to 800ml

2.7.3.6 20x SSC

Following reagents were mixed, pH adjusted to 5 and autoclaved.

NaCl	175.3g
Sodium citrate	88.2g
ddH_2O	Top up to 800ml

2.7.3.7 Tris-HCL pH 7.5

157.6 g Tris-HCL was added into 1L ddH2O, pH adjusted to 7.5 and autoclaved.

2.7.3.8 5 M NaCl

146.1g NaCl was added to 500 ml ddH_2O and autoclaved.

2.8 EdU labeling and detection

For measuring labeling index of EdU cells, 10 mM EdU was added to the culture medium at day eight, and collected after two hours. For cumulative EdU labeling assay, 10 mM EdU was added to culture medium at day eight, but collected after 2, 4, 6, 8 and 10 hours. The collected organoids were fixed with 4% PFA and proceeded to histology. EdU was detected during immunocytochemistry using the Click-IT

reaction, following instructions of Click-iT EdU Alexa Fluor 647 Imaging Kit (Thermo Fisher Scientific).

2.9 Data analysis

Data were analysed with Excel (Microsoft) and PRISM (Graphpad).

CHAPTER 3: *Pax6*$^{-/-}$ cerebral organoids reproduce phenotypes of *Pax6*$^{-/-}$ mice

3.1 INTRODUCTION

Pax6 is one of the best-studied transcription factors of the cerebral cortex that regulates many key cellular processes of cortical development. The roles of *Pax6* in corticogenesis have been discovered mainly from *Pax6* loss-of-function mice (*Pax6*$^{Sey/Sey}$, Hill et al., 1991), where loss of *Pax6* causes defects in cortical proliferation, differentiation, cell specification, cortical patterning and neuronal migration (Ypsilanti and Rubenstein, 2016). The well-established role of *Pax6* in cortical development provides a basis to compare and contrast its role between cerebral organoids to the in vivo system.

Although studies have shown that cerebral organoids recapitulate species-specific and unique characteristics of cortical development, the extent to which this system recapitulates developmental regulatory mechanisms of cortical development, such as *Pax6* is still unknown. Furthermore, there is a limited understanding of the mechanisms underlying organoid development, raising concerns regarding the accuracy of this system as an alternative model for forebrain development.

This chapter aims to compare phenotypes of *Pax6*$^{-/-}$ cerebral organoids to the established phenotypes of *Pax6*$^{sey/sey}$ mouse. We hypothesise that if cerebral organoids share the same regulatory mechanism by which *Pax6* controls cortical

development in the embryos, the *Pax6*$^{-/-}$ cerebral organoids would share the same phenotypes as the *Pax6*$^{sey/sey}$ mouse.

This chapter begins with the establishment of a robust 3D culture protocol that generates cerebral organoids with neuroepithelial-like (NE) structures. For this purpose, the same type of cells employed in the SFEBq protocol were used, which is the Bf1::Venus ES cells. This transgenic ES cell line was generated by fusing Venus, a mutated form of green fluorescent protein (GFP), into the *Bf1* gene locus (also known as *Foxg1*), one of the earliest telencephalic markers. Therefore, this ES cell line reports on the expression of *Foxg1*, which will enable us to assess the telencephalic differentiation efficiency of our 3D culture protocol. In SFEBq, Bf1::Venus (hereafter referred to as Foxg1::Venus) ES cells demonstrate a highly reproducible formation of NE structures with efficient differentiation of cells expressing *Foxg1* (Eiraku et al., 2008). Hence, by using the same starting ES cell line, we anticipate similar or better outcomes with our 3D culture protocol.

Next, we applied the 3D culture protocol to generate mutant cerebral organoids from an established *Pax6*$^{-/-}$ ES cell line derived from *Pax6*$^{SeyEd/SeyEd}$ blastocysts (hereafter referred to as *Pax6*$^{-/-}$, Quinn et al., 2010). This cell line has been demonstrated to have stable neural differentiation, which is not affected by the loss of *Pax6*. For example, early neural differentiation of these cells into embryoid bodies (EBs) showed comparable proportions of progenitors and neuronal cells, to the control (Quinn et al., 2010). Furthermore, they contributed well in chimaeras, thus are capable of contributing to cortical tissue in vivo. Therefore, we expect that these mutant lines can successfully form cerebral organoids.

3.2 RESULTS

3.2.1 Establishment of a robust 3D culture protocol

Building on the SFEBq protocol with few modifications, we have successfully established a 3D culture method that generates cerebral organoids with robust neuroepithelial-like (NE) structures (Figure 1.4).

Firstly, ES cells were cultured in a KSR medium supplemented with IWP2, a Wnt inhibitor, to drive the cells towards cortical differentiation (Watanabe et al., 2005). Twenty-four hours after plating, the ES cells formed an aggregate (Figure 3.1A), at which point Matrigel was added. We then observed protruding structures on the next day, followed by the formation of bright and translucent radial structures known as NE structures (indicated by arrowheads) from day 3-4 of culture (Figure 3.1B-D). This observation is similar to the findings of the SFEBq method (Nasu et al., 2012).

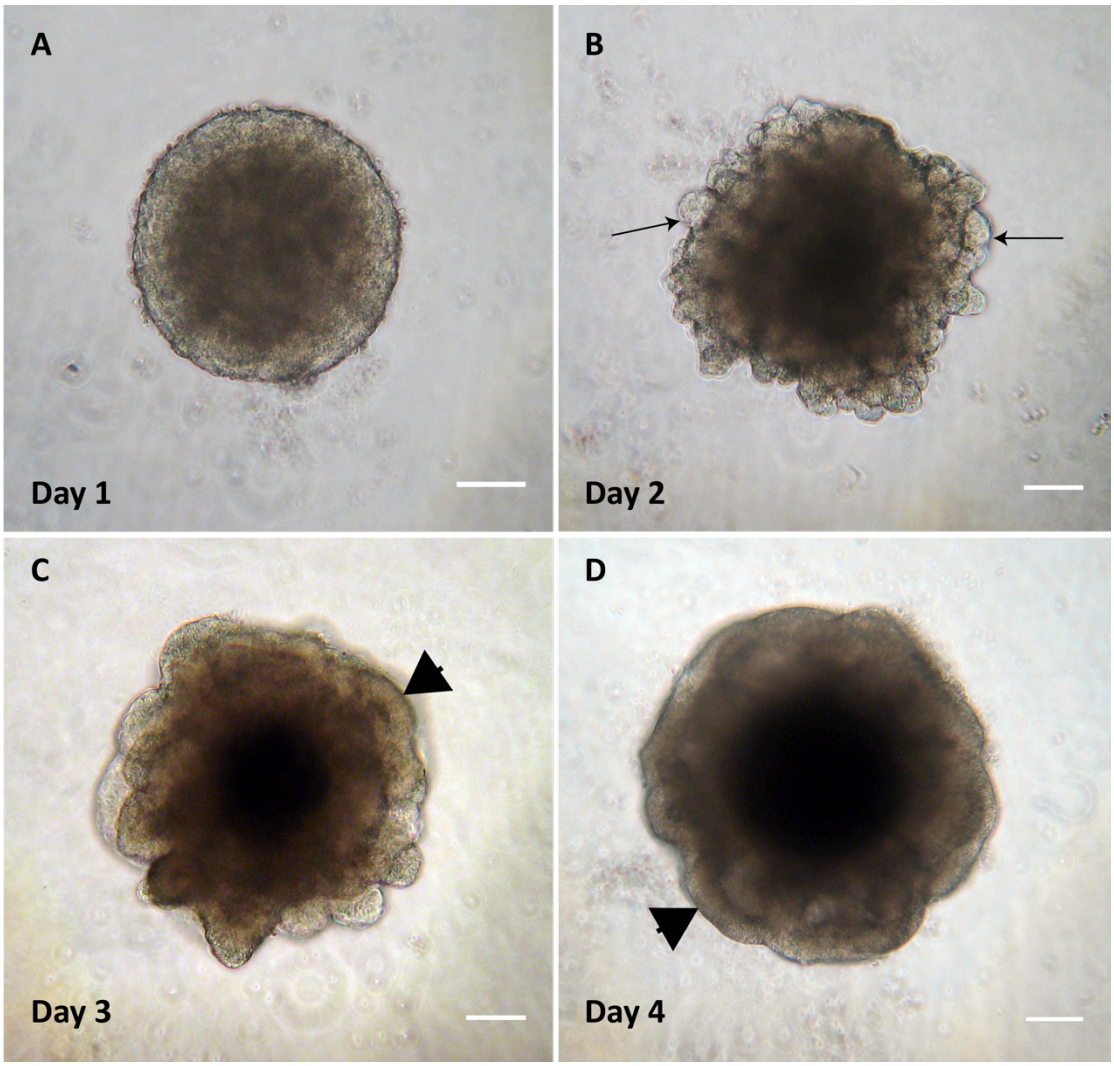

Figure 3.1 Early development of cerebral organoids. (A) Formation of spherical aggregates with smooth edges at day one (B) Aggregates lose the smooth edges and show protruding structures at day two, indicated by arrows. (C,D) NE-like structures start to form at day 3-4, indicated by arrowheads. Scale bars: 100 µm.

To examine the types of cells and tissues present, day eight cerebral organoids were sectioned and stained with various markers; starting with N-cadherin, a neuroepithelial marker that marks the apical side of neuroepithelium. Day eight organoids correspond to an early stage of corticogenesis; approximately E11.5-E12.5 in vivo. This estimation is based on the approximate equivalence of ES cells to E4.5 blastocysts (Boroviak et al., 2014). At this stage, we found that there were multiple NE structures in our organoids, and they were identified by the presence of lumen. These NE structures expressed N-cadherin on the apical surface, which is next to the lumen (Figure 3.2). This demonstrates the apico-basal polarity of these structures, consistent with previous findings (Eiraku et al., 2008; Nasu et al., 2012).

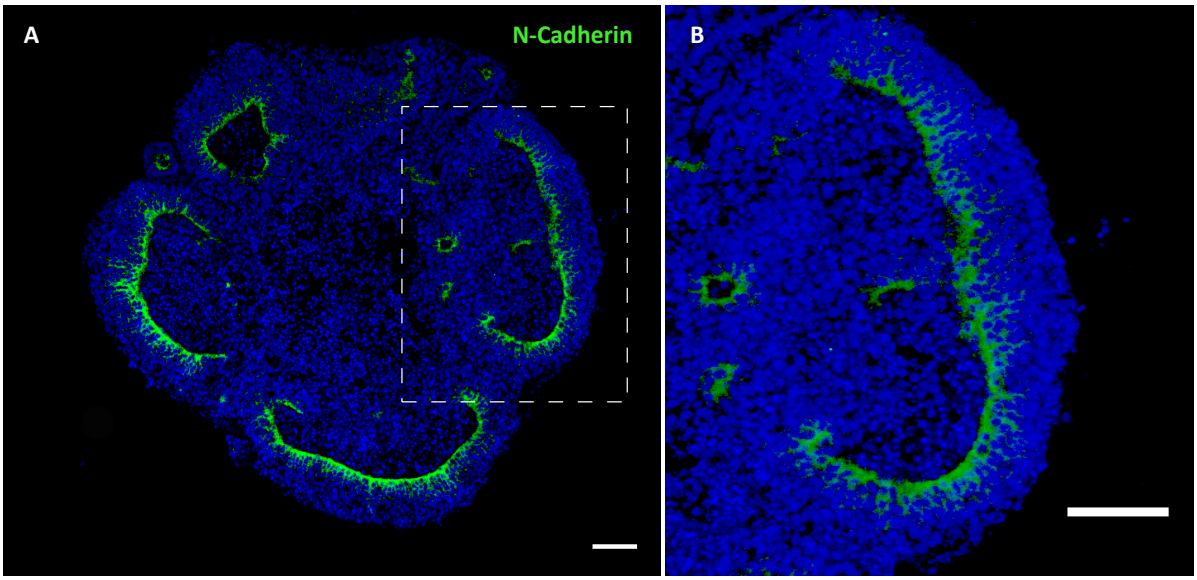

Figure 3.2 Cerebral organoids showed formation of polarised NE structures. (A) NE structures expressed N-cadherin on their apical surface (B) Higher magnification of the boxed area in panel A, showing clear polarised structure. Scale bars: 100 μm.

A previous study has reported that the SFEBq method is highly reproducible, with more than 95% of the organoids forming NE structures (Eiraku et al., 2008). To assess the reproducibility of our 3D culture protocol, NE structures of day eight organoids were examined in histological sections and image analysis was performed using Image J. Firstly, NE structures were delineated using the freehand selection tool; NE structures were defined by tissues with lumen structures, therefore analysis was restricted on this selection criterion. We then determined the proportion of NE area (excluding the lumen) from the total area of the organoid. We found that organoids from all three batches formed NE structures, and on average these structures cover 38% of the organoids total area (Figure 3.3).

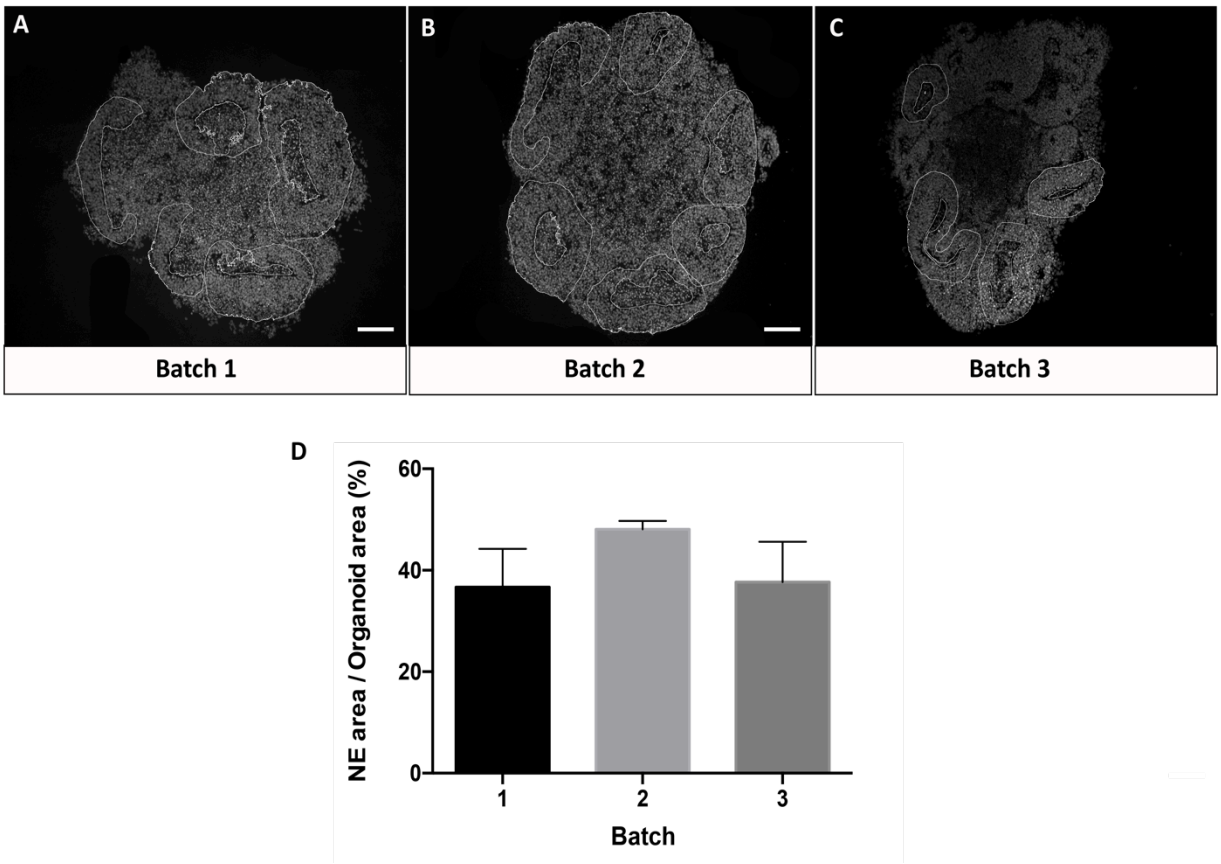

Figure 3.3 Quantitative analysis of the proportion of NE area in organoids. (A-C) Representative images of cerebral organoids delineated with NE from batch 1 – 3. (D) Mean proportion of NE area (± standard error of the mean) of 5 organoids from 3 independent batches, (One-way ANOVA, $p<0.05$, n.s., not significant).

It is also reported that organoids generated using SFEBq method show an efficient telencephalic induction (65-75%), based on *Foxg1* expression (Eiraku et al., 2008). This percentage was derived by flow cytometry, which requires cell disassociation, and therefore compromising the spatial information of organoids. To retain the spatial information of the 3D-organoids, we used histological sections to determine the expression of *Foxg1* in the NE structures, followed by image analysis using ImageJ. Day 8 cerebral organoids derived from Foxg1::Venus ES cells were immunostained with GFP to detect the expression of Venus, and the proportion of NE area expressing Venus (excluding lumen) from the total area of NE in blue (DAPI) was measured. We found that on average, 50% of the NE area expressed *Foxg1* (Figure 3.4).

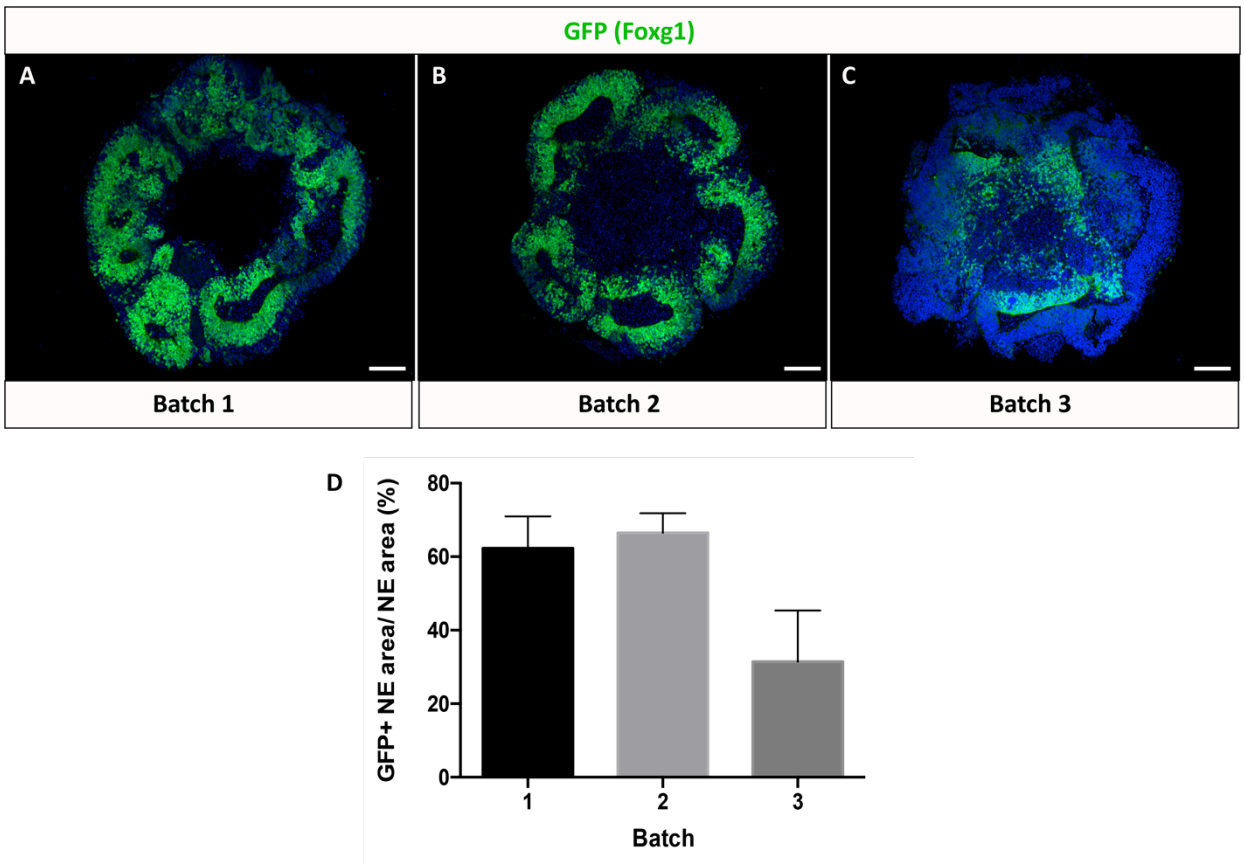

Figure 3.4 Quantitative analysis of the NE area expressing Venus (Foxg1) (A-C) Representative images of cerebral organoids labelled with GFP (*Foxg1*) from batch 1 – 3. (D) Mean proportion of GFP-positive area in the NE structures (±standard error of the mean) of 5 organoids from 3 independent batches (One-way ANOVA, $p<0.05$, n.s., not significant).

3.2.1 Cerebral organoids recapitulate embryonic cerebral cortical cytoarchitecture

Prior to neurogenesis, the mouse cerebral cortex mainly consists of neuroepithelial (NE) cells that divide symmetrically, maintaining the neural stem cell pool (Noctor et al., 2004). As neurogenesis commences (~E10.5), NE cells transform into progenitor cells known as radial glial (RG) cells, which mainly divide symmetrically during early neurogenesis. As neurogenesis progresses, RG cells also divide asymmetrically, giving rise to basal progenitors or neurons (Greig et al., 2013). These cells subsequently form progenitor and neuronal layers in an apico-basal organisation (Taverna et al., 2014).

To examine whether NE structures of cerebral organoids form organised progenitor and neuronal layers, cerebral organoids from early to late stage of development (day 5, 8, 10 and 12) were labelled with the neural stem cell/progenitor marker, *Sox2,* and the post-mitotic neuronal marker, *Tuj1*.

At day five, the NE structures consisted of a homogenous population of cells expressing *Sox2*, with very few neurons detected (Figure 3.5A). More neurons were identified on day eight, surrounding the basal side of the NE and forming a thin layer (Figure 3.5B). However, these layers were difficult to delineate during later stages of organoid development (day 10, 12), as the progenitors and neuronal cells mixed with each other and lost their organisation (Figure 3.5C,D). This was consistent in every batch of differentiation, suggesting that the spatial organisation of progenitors and

neuronal layers can be observed at day 8 of organoid development, but not at later stages.

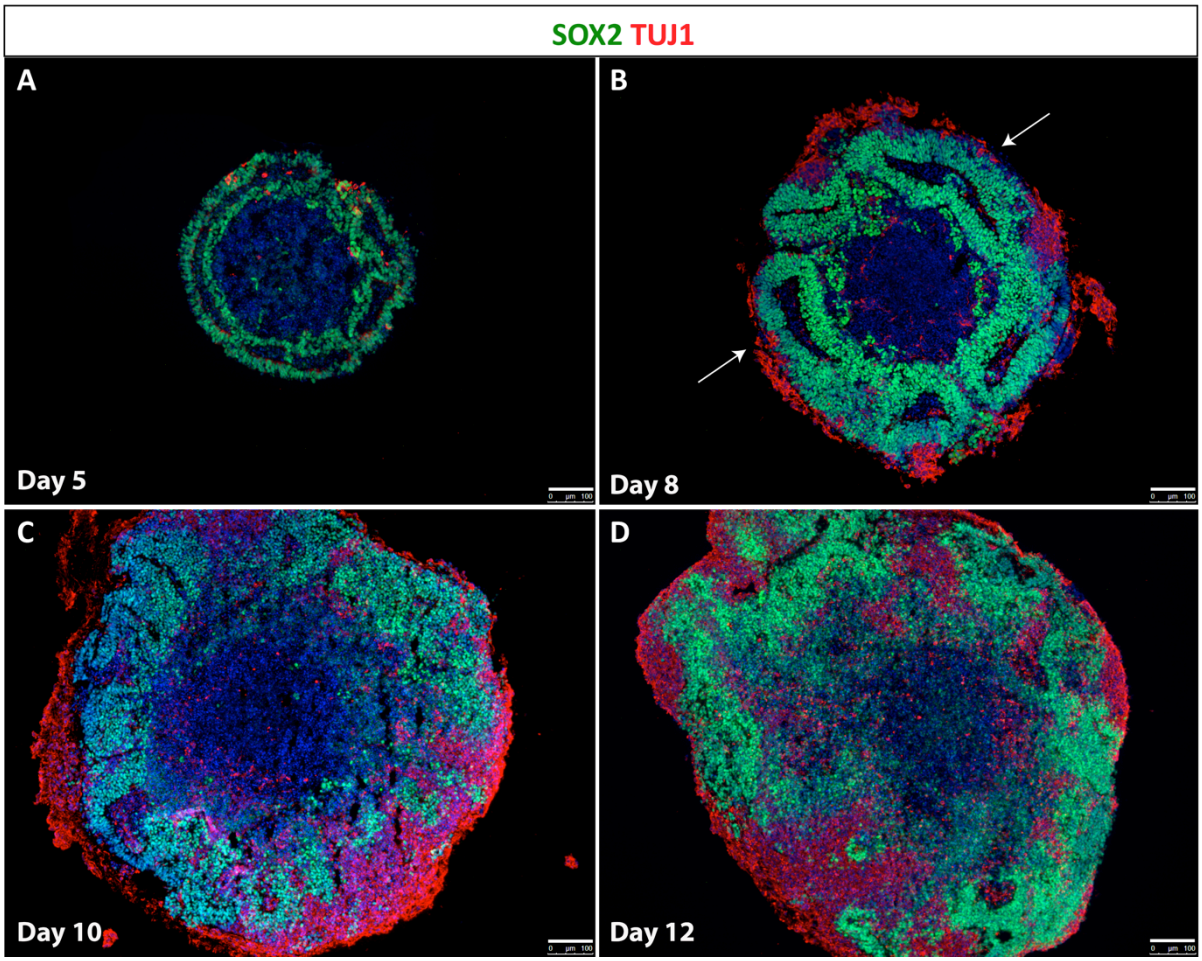

Figure 3.5 Comparison between progenitor *(Sox2+)* and neuronal *(Tuj1+)* layers in day 5, 8, 10 and 12 cerebral organoids. (A) NE formed a single layer of Sox2+ progenitor cells at day five. (B) More neuronal cells appeared at day eight, forming neuronal layer on top of the progenitor layer. (C-D) Progenitor and neuronal layers were poorly organised at day 10. (D) Layers were lost by day 12. Scale bar: 100 µm.

Regional identities in the cerebral cortex can be identified either by their morphological structures, which is guided by developmental axes, or by the expression of specific molecular markers. As cerebral organoids lack developmental axes, a combination of molecular markers is important to determine the identity of NE structures (Renner et al., 2017). To examine the cortical identity of NE structures, day eight cerebral organoids were stained with a combination of molecular markers expressed in the cortex such as *Pax6, Tbr2, Tbr1*, and *Emx1*. We found that the NE structures expressed all four cortical markers in the correct arrangement (Figure 3.6).

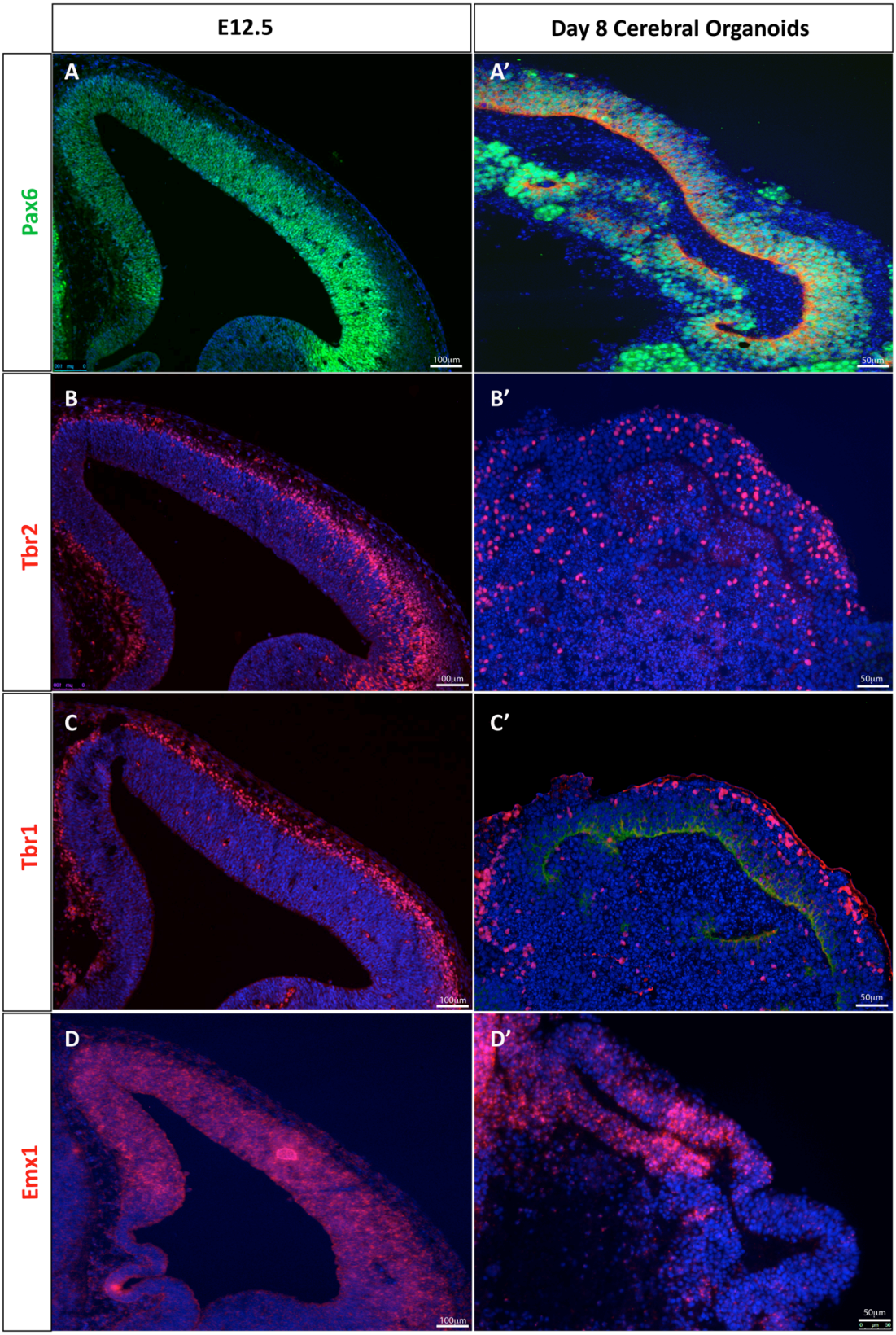
E12.5
Day 8 Cerebral Organoids
Pax6
Tbr2
Tbr1
Emx1
A
A'
B
B'
C
C'
D
D'
100µm
50µm

Figure 3.6 NE structures of cerebral organoids mimic cortical cytoarchitecture of the E12.5 cerebral cortex. (A, A') *Pax6* is expressed by cells located at the apical surface, followed by (B, B') cells expressing *Tbr2*, which forms an intermediate layer. (C, C') *Tbr1* is expressed by cells on top of the intermediate layer, characteristic of early born neurons, and (D, D') *Emx1* is expressed throughout the cortex. Scale bar A,B,C,D: 100 μm; A',B',C',D': 50 μm. Images of E12.5 mouse brain obtained with permission (Fitzgerald, 2016).

Taken together, the established 3D protocol shows generation of cerebral organoids with reproducible formation of NE structures and efficient generation of cells expressing *Foxg1*. These NE-like structures demonstrate cortical-like characteristics, based on the expression of key cortical markers in the correct organisation, and therefore recapitulate cellular aspects of embryonic cerebral cortex cytoarchitecture in vivo.

3.2.3 Formation of *Pax6*$^{-/-}$ cerebral organoids in 3D culture

Establishment of a robust 3D protocol has allowed us to generate *Pax6*$^{-/-}$ cerebral organoids and to compare characteristics of their cortex-like structures to *Pax6*$^{-/-}$ mice embryonic cortex, particularly during the early stages of corticogenesis (E11.5-E12.5). This period is fundamental in proper cortical function, as the balance of proliferation and neurogenesis is tightly coordinated to generate a diverse population of neurons, which ultimately form functional neuronal output (Tan and Shi 2013). Furthermore, we have shown that spatial information is lost at later stages of organoid development (Figure 3.5) suggesting that they are likely to model early stage corticogenesis most accurately.

At day eight, *Pax6*$^{-/-}$ cerebral organoids formed polarised NE structures, identified by the expression of N-cadherin on the apical side (Figure 3.7A). Furthermore, the progenitors and neuronal cells were organised in an apico-basal order, with the progenitors lining the apical surface of NE and form progenitor layer; followed by formation of neuronal layer at the basal side (Figure 3.7B).

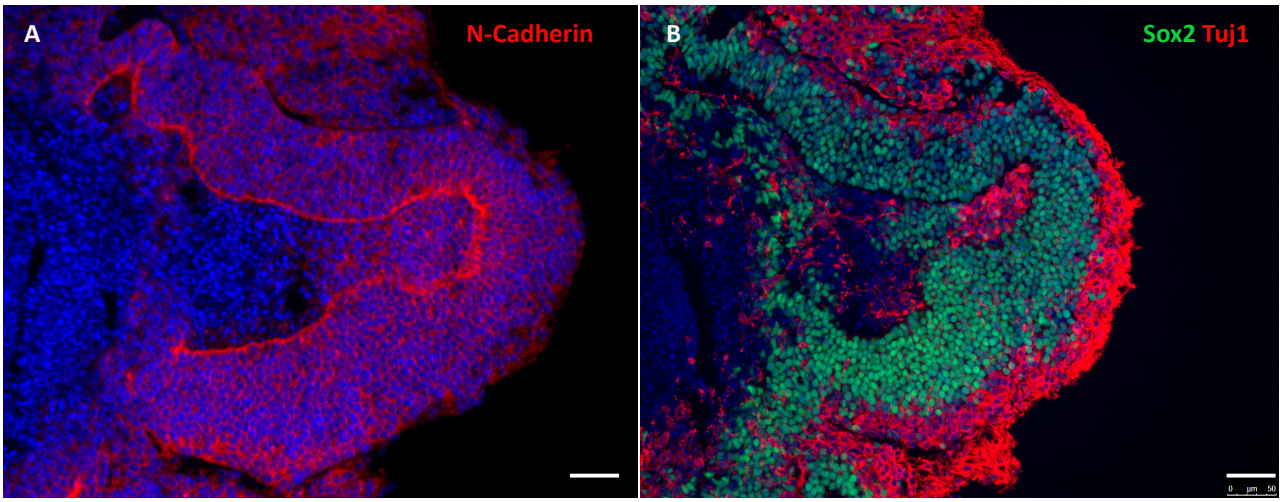

Figure 3.7 *Pax6*$^{-/-}$ cerebral organoids show polarised NE structures and an organised layer of progenitors and neuronal cells. (A) Expression of N-cadherin on the apical surface of NE (B) Formation of multiple layers of progenitor (*Sox2*+) and neuronal (*Tuj1*+) cells. Scale bar: 50 μm.

To confirm inactivation of *Pax6*, its expression was examined by labelling the organoids with *Pax6* specific antibody. Indeed, expression of *Pax6* was not detected in the organoids (Figure 3.9). As we are interested in the roles of *Pax6* in the cortical structures of cerebral organoids, cortical characteristics of the NE structures were examined by the expression of genes associated with corticogenesis, such as *Tbr2* and *Tbr1*. We found that these markers were expressed by most of the NE structures, similar to the pattern found in vivo (Figure 3.8).

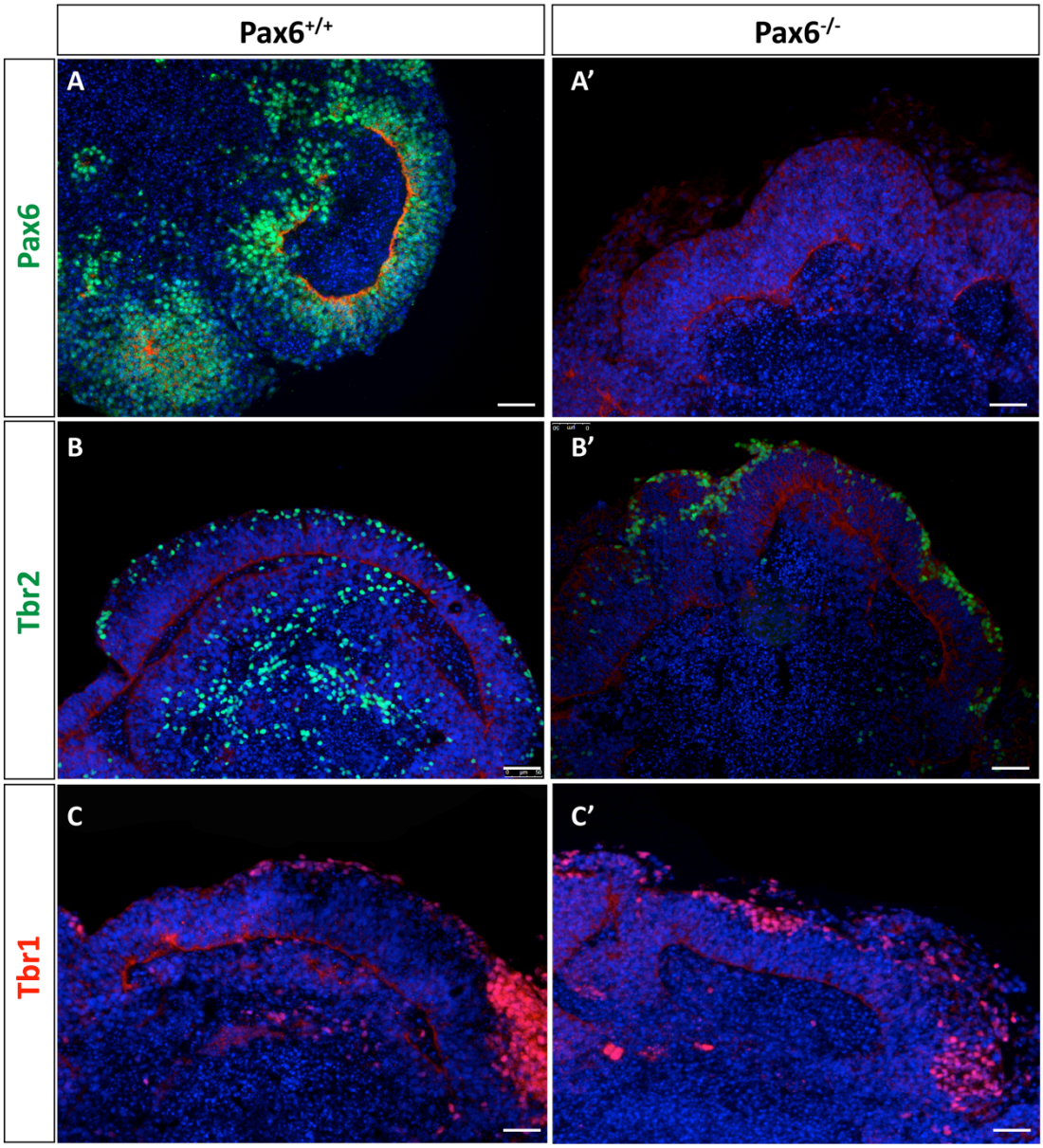

Figure 3.8 *Pax6*$^{-/-}$ cerebral organoids express genes associated with cortical development, comparable to control. (A-C) Expression of *Pax6, Tbr2, Tbr1* in the control organoids, (A') NE structures of *Pax6*$^{-/-}$ cerebral organoids lack *Pax6,* but maintain the expression of (B') *Tbr2* and (C') *Tbr1*. Scale bar; 50 μm.

3.2.4 Cortical structures of *Pax6*$^{-/-}$ cerebral organoids show an increase in mitotic cells away from the lumen

One of the features of the cerebral cortex is that radial glial (RG) cells undergo interkinetic nuclear migration (IKNM); in which the nuclei migrate in an apico-basal direction following cell cycle phases (Lee and Norden, 2013). For instance, the cells will be at the basal position during S-phase, and then move towards apical surface to enter mitosis and subsequently divide (Taverna et al., 2014). In *Pax6*$^{-/-}$ mice, there is an abnormal increase in the proportion of RG cells dividing at non-apical positions, suggesting that loss of *Pax6* affected the IKNM process (Estivill-Torrus et al., 2002).

There is evidence that cells in the cerebral organoids undergo IKNM (Nasu et al., 2012). To examine whether loss of *Pax6* affected this process and share similar cellular defects as mentioned above, both control and mutant cerebral organoids were immunostained with mitotic cell marker, phosphohistone H3 (PH3). The number of PH3+ cells located 5 or more cells away from the lumen (abventricular) were quantified, and the percentage was scored from the total number of PH3+ cells in the organoids' cortical-like structures. Our quantification revealed that the percentage of abventricular PH3+ cells at both day 8 and 9 in mutant organoids were higher than the control, with a more significant increase at day 9 (Figure 3.9). This is consistent with the findings in *Pax6*$^{-/-}$ mice that showed a more significant increase in the abventricular mitotic cells by mid-corticogenesis, suggesting a pronounced defect over developmental time (Estivill-Torrus et al., 2002).

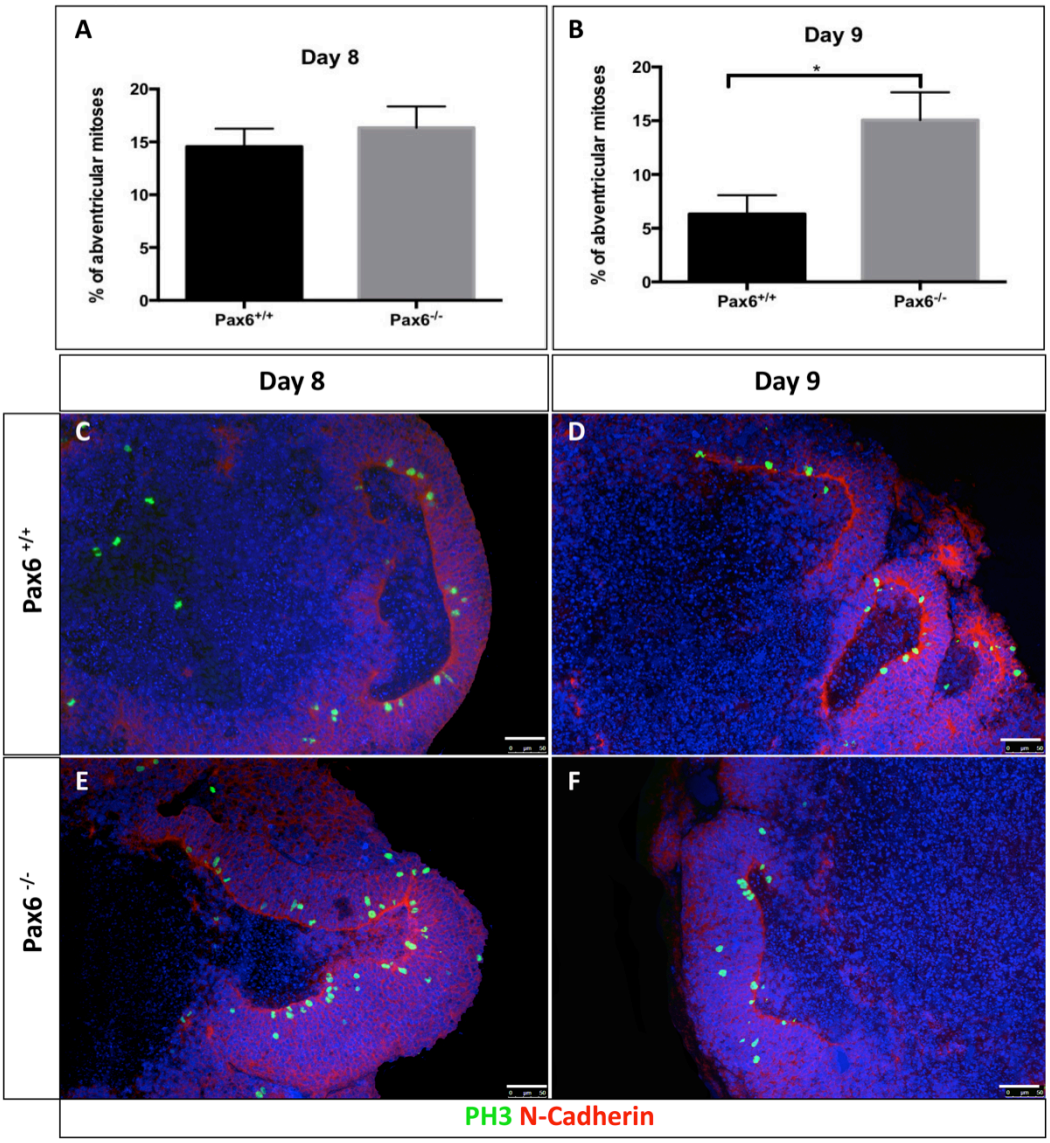

Figure 3.9 Cortical structures of *Pax6*$^{-/-}$ cerebral organoids show an increase of mitotic cells (PH3+) at abventricular position. (A) Day 8 *Pax6*$^{-/-}$ cerebral organoids show a higher percentage of PH3+ cells at abventricular position than the control, (B) Day 9 *Pax6*$^{-/-}$ cerebral organoids show a significant increase of PH3+ cells at abventricular position than control (mean ± standard error of the mean; of 10 organoids from 5 independent batches, t-test, *p<0.05). (C, D) Representative image of control cerebral organoids at day 8 and 9, (E, F) Representative image of *Pax6*$^{-/-}$ organoids at day 8 and 9. Scale bar: 50 µm.

3.2.5 Cortical structures of *Pax6*$^{-/-}$ cerebral organoids demonstrate an altered labeling index of cells in S-phase

The role of *Pax6* in cortical proliferation is well established (Estivill-Torrus et al., 2002; Mi et al., 2013). Cell proliferation analysis of *Pax6*$^{-/-}$ embryos show a higher labeling index (LI) of cells that undergo S-phase than control (Estivill-Torrus et al., 2002). In this analysis, embryos were pulsed with 5-bromo-2'-deoxyuridine (BrdU), a thymidine analogue that will incorporate into cells undergoing S-phase.

To examine the role of *Pax6* in cortical proliferation of organoids, *Pax6*$^{-/-}$ cerebral organoids were pulsed with 5-ethynyl-2'-deoxyuridine (EdU), an alternative type of thymidine analogue. We then counted the proportion of EdU+ cells in cortical-like NE (*Tbr2*+) to obtain the LI. We found that the LI of the cortical structures (*Tbr2*+) of *Pax6*$^{-/-}$ cerebral organoids was altered, with a significant decrease in the proportion of cells in S-phase compared to control, at day 9 (Figure 3.10). the altered LI suggest that Pax6 plays a role in cortical proliferation of cerebral organoids, as they do in vivo.

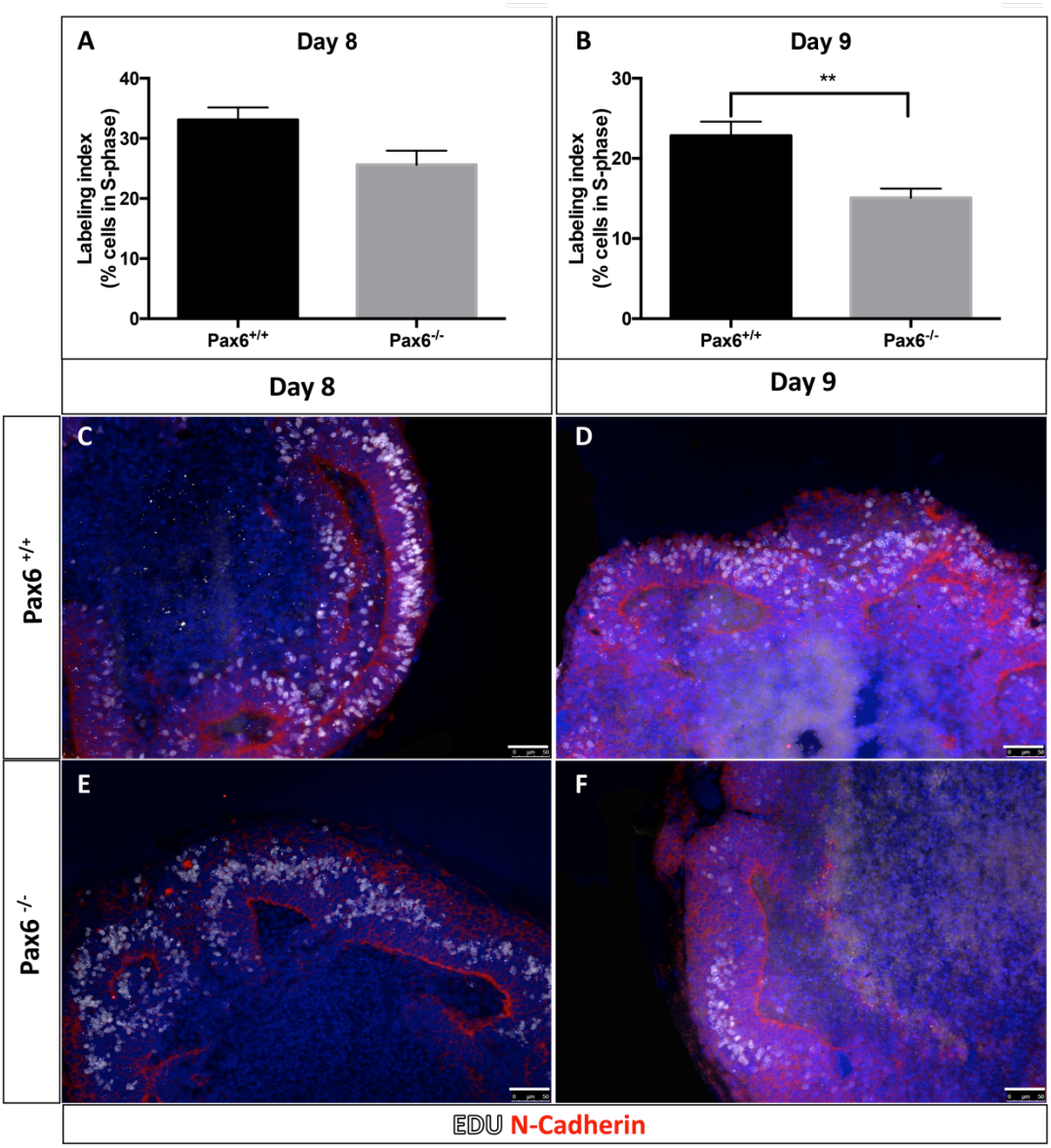

Figure 3.10 Cortical structures of *Pax6*$^{-/-}$ cerebral organoids show a decrease in the labelling index of cells in S-phase. (A) Day 8 *Pax6*$^{-/-}$ cerebral organoids show a lower percentage of cells in S-phase (EdU+) compared to control, (B) Day 9 *Pax6*$^{-/-}$ cerebral organoids show a significant decrease of cells in S-phase (EdU+) compared to control (mean ± standard error of the mean; of 10 organoids from 5 independent batches, t-test, **p<0.05). (C, D) Representative image of control cerebral organoids at day 8 and 9, (E, F) Representative image of *Pax6*$^{-/-}$ cerebral organoids at day 8 and 9. Scale bar: 50 µm.

3.2.6 *Pax6*$^{-/-}$ cerebral organoids show precocious differentiation.

Coordination of proliferation and differentiation is essential to maintain the balance of cortical progenitors and neurons, which is key to cerebral cortical function. Therefore, proliferation defects in the *Pax6*$^{-/-}$ mice consequently show precocious differentiation, as there is an increase of post-mitotic neurons during early corticogenesis (Estivill-Torrus et al., 2002; Quinn et al., 2007).

To examine whether *Pax6*$^{-/-}$ cerebral organoids share the same phenotype, progenitors and neuronal cells were labeled with *Sox2* and *Tuj1*, respectively. Compared to the control organoids (*Pax6*$^{+/+}$), areas containing neuronal cells (*Tuj1*+) in the NE structures of Pax6$^{-/-}$ cerebral organoids appeared to be expanded, and this effect is more evident over time, suggesting precocious differentiation (Figure 3.11).

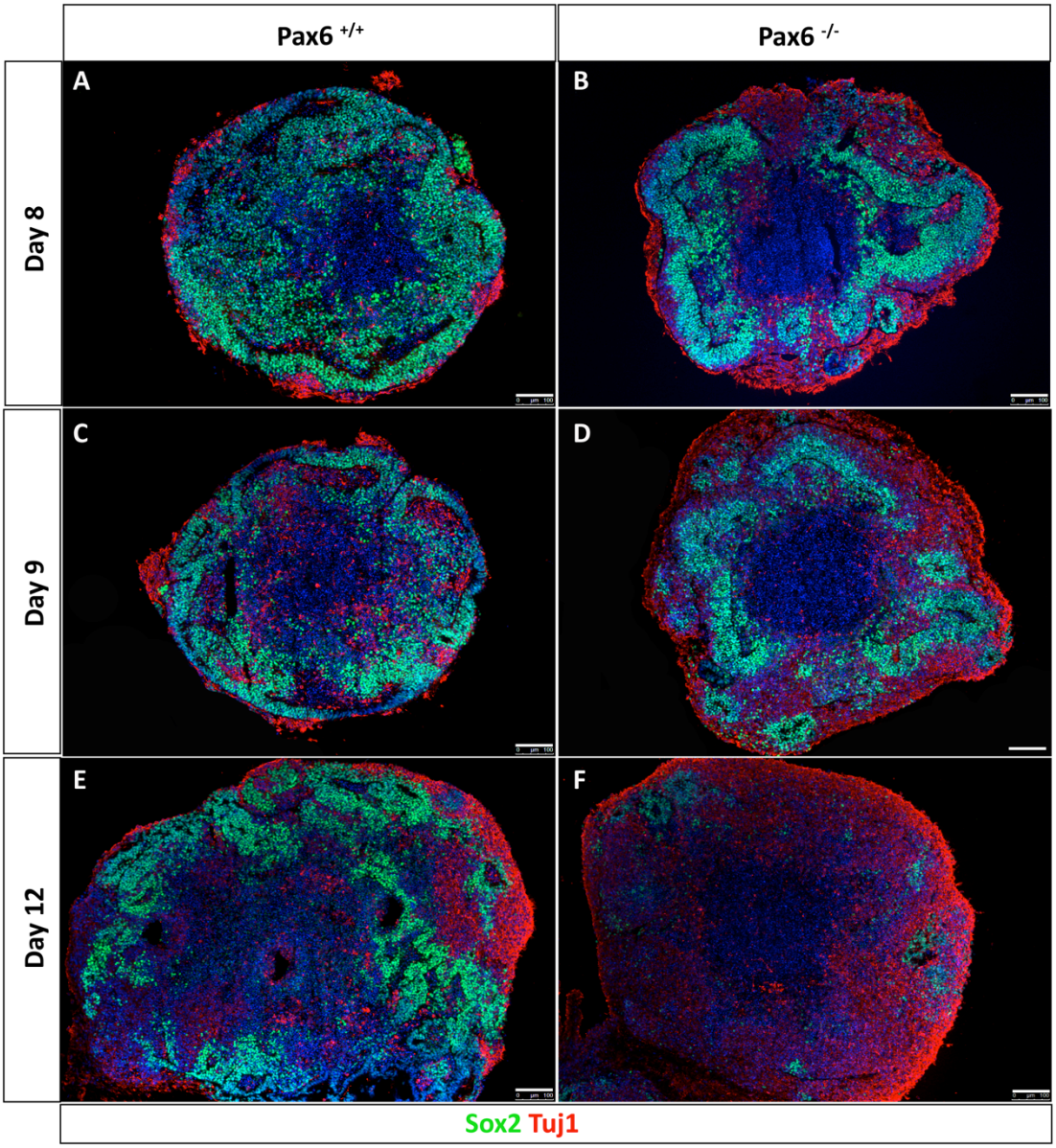

Figure 3.11 *Pax6*$^{-/-}$ cerebral organoids show a higher proportion of post-mitotic neurons than the control. (A,B) Representative images of *Pax6*$^{+/+}$ and *Pax6*$^{-/-}$ cerebral organoids labeled with Sox2 and Tuj1 at day 8 (C, D), day 9 (E, F) and day 12, respectively. Scale bar: 100 μm.

3.2.7 Cortical structures of *Pax6*$^{-/-}$ cerebral organoids show a non-significant decrease in the proportion of *Tbr2* expressing cells

The *Pax6* gene regulatory network is highly complex, with several genes directly regulated by *Pax6*, such as *Tbr2*. Established studies of *Pax6*$^{-/-}$ mice have shown that the proportion of *Tbr2* expressing cells was reduced from as early as E12.5 (Quinn et al., 2007).

To investigate this phenotype in cerebral organoids, both mutant and control organoids were labeled with Tbr2 antibody and the proportion of cells expressing *Tbr2* from the total number of cells (DAPI) of the NE structures was quantified. We found that although there is a decrease in the proportion of *Tbr2*-expressing cells in mutant cerebral organoids compared to the control at both day eight and nine, this change is not significant (Figure 3.12).

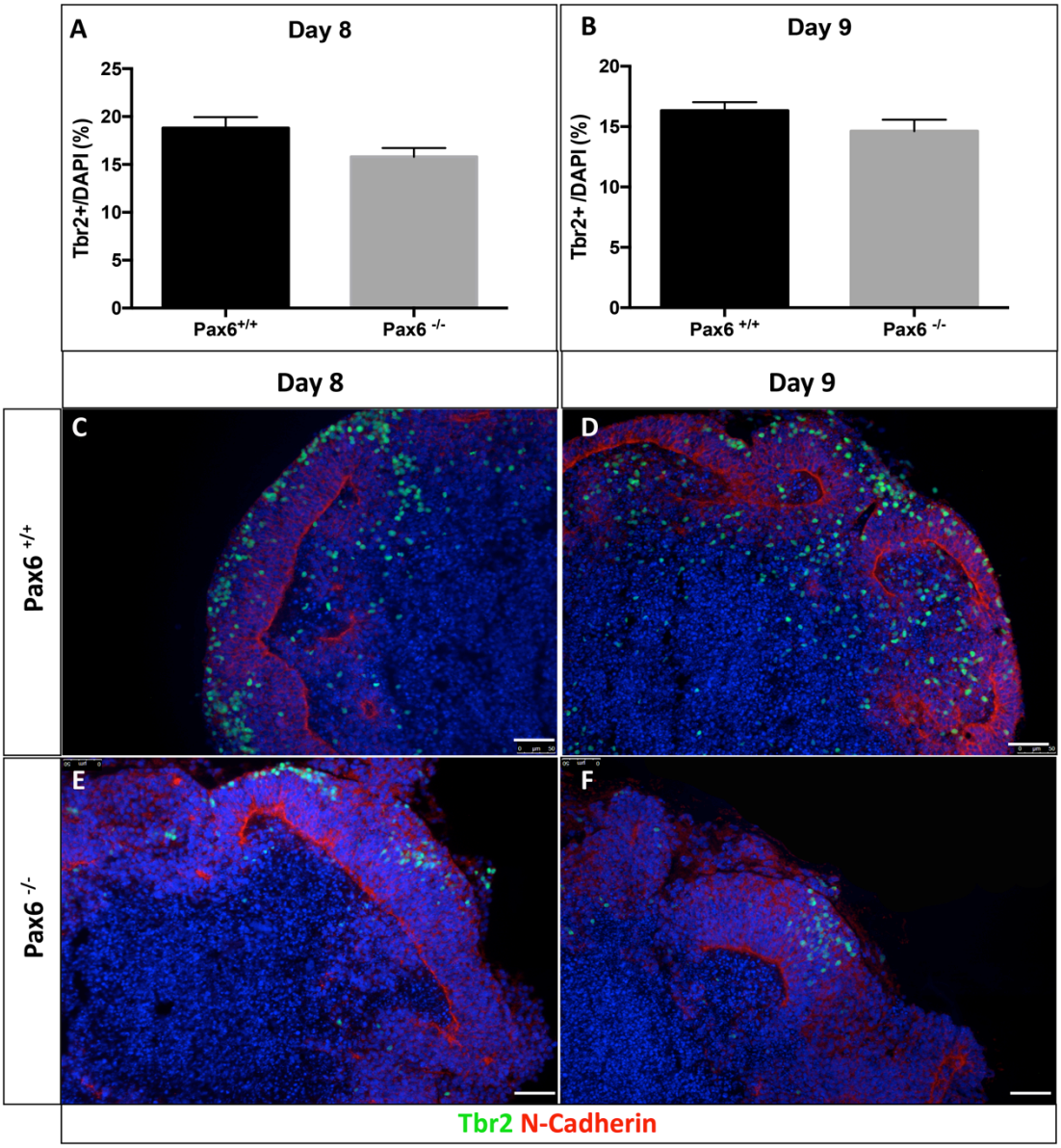

Figure 3.12 Cortical structures of *Pax6*$^{-/-}$ cerebral organoids show a decreased percentage of *Tbr2*-expressing cells. (A) Day 8 *Pax6*$^{-/-}$ cerebral organoids show a lower proportion of *Tbr2*+ cells than the control, (B) Day 9 *Pax6*$^{-/-}$ cerebral organoids show a lower proportion of *Tbr2*+ cells than the control (mean ± standard error of the mean; of 10 organoids from 5 independent batches, t-test, $p<0.05$, n.s). (C, D) Representative images of control cerebral organoids at day 8 and 9. (E, F) Representative images of *Pax6*$^{-/-}$ cerebral organoids at day 8 and 9. Scale bar: 50 μm.

3.3 DISCUSSION

Results presented in this chapter demonstrate that mouse ES cells cultured in the established 3D culture protocol can form cerebral organoids with robust NE structures expressing key cortical markers. Furthermore, this method can be used to generate mutant organoids from *Pax6*$^{-/-}$ ES cells that show similar phenotypes to the *Pax6*$^{-/-}$ mice.

The 3D culture method has allowed the emergence of patterned structures in ES cells via self-organisation. Historically, the ability of ES cells to self-organizing was discovered by Yoshiki Sasai's group in their seminal study to generate a differentiation protocol with efficient formation of telencephalic precursors (Eiraku et al., 2008). Known as the serum-free embryoid bodies with quick reaggregation (SFEBq), this method combines suspension culture and serum-free medium – two of the principles of organoid culture (3D). This condition allows more freedom for the cells to establish interactions and form an aggregate, reminiscent of embryos. Unlike embryoid bodies, aggregates from SFEBq mainly consist of neuroectodermal cells and lack other cell derivatives of the three germ layers (Watanabe et al., 2005). This may be due to the use of serum-free medium, which has been shown to allow ES cells to achieve neural induction by default mechanism (Smukler et al., 2006) – consistent with the default acquisition of rostral neural fate in vivo (Levine and Brivanlou, 2007). In addition, this protocol is relatively simple compared to other protocols, as it only uses a single signaling molecule in the medium; Wnt inhibitor (IWP2). IWP2 inhibits Wnt secretion via Porcupine (Porcn), therefore only endogenous Wnts are blocked (Chen et al., 2009). Wnt is a caudalising factor, and inhibiting this molecule

further supports formation of telencephalon, a rostral part of the brain (Suzuki and Vanderhaeghen, 2015). Indeed, supplementation with this small molecule has been shown to increase the efficiency of cortical differentiation (Nasu et al., 2012).

3.3.1 Cerebral organoids show reproducible formation of neuroepithelium structures expressing *Foxg1*

Similar to the findings of SFEBq, here we show that our 3D culture provides a permissive environment for the ES cells to make cell-cell interactions, subsequently forming an aggregate. Moreover, they can self-organise and form NE structures, characteristic of an organoid culture (Nasu et al. 2012). Most importantly, this protocol is reproducible, demonstrated by the formation NE structures in all of the cerebral organoids from different types of ES cells; Foxg1::Venus, *Pax6*$^{-/-}$ and *Pax6* conditional knock out (cKO) ES cells (chapter five).

Structural and spatial features of organoids can be analysed in whole mount, using a combination of tissue clearing techniques and advanced microscopy – such as light-sheet microscopy. However, due to the lack of developmental axes, organoid analysis requires multiple molecular markers for tissue identification, which is a limitation in whole mount analysis if there are no compatible antibodies available (Renner et al., 2017). Therefore, the organoids were analysed in histological sections, a classic approach used in analysing mouse embryos, including embryonic brain. This technique is useful in revealing the NE structures, allowing a more detailed analysis of the organoids. To minimise the underestimation of NE structures due to random 2D sections; organoids were cut in serial sections, which enables adjacent sections to be

collected on multiple slides. Around 6-8 sections can be collected in a single slide, with the first and the last two sections being smaller sizes, as they were cut from the top and bottom end of the organoids. As such, these sections usually show shorter NE structures with smaller lumens, like the neural rosettes. Therefore, sections that were cut from the middle part of organoids (sections 4-5) are usually more elaborate and suitable for analyses.

NE structures are the key feature of cerebral organoids, and also an indicator of self-organisation of ES cells in 3D culture. Interestingly, these structures are varied in shapes and size, thus making each organoid unique. Heterogeneity has been described as one of the inherent limitations of organoid culture, possibly due to their self-organising mechanism (Bredenoord et al., 2017; Quadrato et al., 2017). This heterogeneity is more evident between different batches, as demonstrated in our quantitative data (Figure 3.3). We show that between the three batches of organoids; two of them are comparable in terms of the proportion of NE (area), with 43% and 47%, respectively. This estimation seems to reflect the analysed images accurately. This data also suggests that slightly over 50% of the remaining organoids are not NE structures. These remaining areas could include lumen, cells surrounding the NE and cells at the core centre. Given the limited space and nutrients, the majority of cells in the organoids core centre do not form any particular organisation. Unlike in vivo tissue, organoids lack vascularisation, which limits diffusion of nutrients to the core, resulting in a necrotic centre (Giandomenico et al., 2018; Renner et al., 2017). On the other hand, cells surrounding NE are likely to be non-cortical cells, as several findings have reported the presence of subcortical cells in the organoids, identified by specific

molecular markers as they often lack structural pattern (Lancaster et al., 2013; Renner et al., 2017).

In addition to the reproducible formation of NE, we also show that 60-70% of the NE area expressed *Foxg1*, one of the markers that specify telencephalic region. The efficient generation of *Foxg1*+ NE structures could be the result of Wnt inhibition in our 3D culture, which drives the organoids towards more rostral-part of the brain (telencephalon). This indicates that the endogenous programme of organoids can be manipulated according to the principles of forebrain development established from animal models.

3.3.2 Corticogenesis in cerebral organoids.

The cerebral cortex consists of heterogeneous population of cortical cells that can be identified by the expression of molecular markers, as well as the position of the cells in the cortex. For example, cortical progenitors form a germinal layer at the apical side of the cortex, demarcated by the expression of *Sox2* by the progenitors. This germinal layer can be further classified into ventricular zone (VZ) and subventricular zone (SVZ), which is populated by apical progenitors *(Pax6+)* and basal progenitors *(Tbr2+).* As these progenitors differentiate, a neuronal layer forms on top of the SVZ, characterised by the expression of early neuronal marker, *Tbr1*, as well as *Tuj1*, a marker for post-mitotic neurons.

Here we show that the NE structures of organoids recapitulate characteristics of the embryonic cerebral cortex. Firstly, its epithelial and polarised nature was reflected by

the apical localisation of N-cadherin (Figure 3.3), a cell adhesion molecule which is highly expressed on the apical end of NE during early corticogenesis (Kadowaki et al., 2007). These NE structures started as a single layer of progenitor cells *(Sox2+)* at day five of culture, similar to the neural tube stage. Subsequently at day eight of culture, neuronal cells emerge, forming an extra layer that separates the progenitor and neuronal zone – similar to the early stage of neurogenesis (E11.5-E12.5). However, this organisation of progenitors and neuronal layers was progressively lost by day 10 and 12 of culture (Figure 3.6). This is not surprising, given the consensus of the limitation of organoids to model later stages of development (Camp et al., 2015; Di Lullo and Kriegstein, 2017). Therefore, day eight organoids are more organised and could recapitulate cortical cytoarchitecture. Indeed, further characterisation of day eight cerebral organoids show that they express molecular markers associated with cortical development (*Pax6, Tbr2, Tbr1*), organised in the correct pattern as observed in cerebral cortex (Figure 3.7).

Emx1 is a transcription factor expressed specifically in the cortex, which includes the cortical progenitors and neurons (Chan, 2001). Therefore, its expression is restricted to the dorsal part of the telencephalon, forming a boundary between dorsal and ventral telencephalic regions. We show that *Emx1* was also expressed in the NE of cerebral organoids, with a few of them expressing *Emx1* in an interesting pattern; where one half of the NE was *Emx1*+, and the other half was *Emx1*-, as shown in Figure 3.7D. This creates a sharp boundary between these two halves of the NE, reminiscent of the boundaries between dorsal and ventral telencephalon, in vivo. Therefore, the tissues outside of this boundary (*Emx1*-) could be cells expressing *Gsx2*, a marker for the

lateral part of ventral telencephalon. Further characterisation of the organoids with ventral telencephalic markers is thus necessary in future analyses to confirm this.

Taken together, our results suggest that the established 3D protocol successfully generate cerebral organoids containing robust telencephalic NE-like structures with cortical characteristics.

3.3.3 Roles of *Pax6* in the cortical structures of cerebral organoids

By implementing the established 3D culture method, *Pax6*$^{-/-}$ cerebral organoids were successfully generated, which enabled us to compare their characteristics to the control organoids. This has provided us with an insight into the roles of *Pax6* in cerebral organoids, and whether they correspond to the roles of *Pax6* in corticogenesis in vivo.

3.3.3.1 *Pax6* is required in proper cell cycle regulation of cortical progenitors in cerebral organoids

Cortical progenitors, particularly radial glial (RG) cells undergo cell cycle regulation that affects many aspects of cellular biological processes; such as the balance of proliferation and differentiation, as well as cell fate determination (Dehay and Kennedy, 2007). During this cycle, cells oscillate in an apico-basal direction as they undergo different phases of the cell cycle; for example, the cells undergo M-phase (mitosis) at the apical side, and then enter G1-phase as they move basally to enter S-phase at the basal side, and finally enter G2-phase as they move apically to enter M-

phase again (Kosodo et al., 2011). This synchronised movement is also referred to as interkinetic nuclear migration (IKNM), a hallmark of neurogenesis (Sauer and Walker, 1959).

IKNM has been demonstrated in cerebral organoids (Nasu et al., 2012). Interestingly, we found that there is an abnormal increase in the proportion of cells undergoing M-phase (PH3+) away from the apical side (abventricular) in the cortical NE of *Pax6*$^{-/-}$ cerebral organoids, with a more significant increase at day 9 (Figure 3.9). This phenotype is similar to the established findings in *Pax6*$^{-/-}$ embryonic cortex that showed an increase in the proportion of abventricular mitotic cells from E10.5 until E15.5, with a significant increase in the latter (Estivill-Torrus et al., 2002).

As basal progenitors divide at the basal side of the cortex, therefore co-expressing *PH3* (*Tbr2*+,*PH3*+), it is also possible that these abventricular *PH3*+ cells are basal progenitors. However, previous study has shown that the proportion of *Tbr2*+ cells are significantly reduced in *Pax6*$^{-/-}$ embryonic cortex, therefore most of the abventricular *PH3*+ cells do not express *Tbr2*, suggesting the ectopic expression of *PH3*+ (Quinn et al., 2007). Although this could also explain the ectopic expression of *PH3*+ cells in *Pax6*$^{-/-}$ cerebral organoids, future studies should further characterise these *PH3*+ cells to confirm the role of *Pax6* in IKNM of cerebral organoids.

As IKNM coordinates with the cell cycle (Kosodo et al., 2011), the increased proportion of abventricular mitotic cells could also indicate an abnormal cell proliferation. Indeed, both *Pax6*$^{-/-}$ cerebral organoids and *Pax6*$^{-/-}$ embryonic cortex show an altered labelling index of cells in S-phase. However, the altered LI between

these two models are different, as *Pax6*$^{-/-}$ embryonic cortices demonstrated a higher LI than the control, whereas *Pax6*$^{-/-}$ cerebral organoids showed a lower LI than control organoids (Estivill-Torrus et al., 2002).

To explain this discrepancy, further analysis on the cell cycle kinetics is required, as higher LI could be due to either rapid cell proliferation, or longer length of S-phase (Warren et al. 1999). This has been demonstrated in a more recent study, using a cortex-specific *Pax6* conditional knock-out (cKO) mice, which enables acute deletion of *Pax6* in cortex-specific region (Mi et al., 2013). This study revealed that following acute deletion of *Pax6,* cortical cells of rostro-lateral region cycles rapidly, with shorter G1 phase; while there is no significant change on cortical cells of caudo-medial region (Mi et al., 2018; Mi et al. 2013).

Therefore, it is intriguing whether acute deletion of *Pax6* in cerebral organoids could recapitulate the aforementioned effect in *Pax6* cKO mice, and this will be addressed in subsequent chapters. In general, it is evident that *Pax6* plays an important role in cell proliferation in both *in vivo* and 3D *in vitro* models.

Proliferation of cortical progenitors is tightly regulated to maintain the correct balance of progenitors and neuronal cells, as well as the size of the cortex (Hindley and Philpott, 2012). Therefore, changes in proliferation consequently lead to either a lag or precocious differentiation of the progenitors, which is evident in the proportion of neuronal cells. For example, it is well established that *Pax6* plays an important role in proliferation, demonstrated by the altered proportion of cells in S-phase as well as the cell cycle time, in the absence of this gene (Estivill-Torrus et al., 2002; Mi et al.,

2013; Quintana-Urzainqui et al., 2018). Consequently, a higher proportion of post-mitotic neurons was detected during early corticogenesis of *Pax6*$^{-/-}$ embryos (Estivill-Torrus et al., 2002; Quinn et al., 2007). Indeed, a similar phenotype was found in *Pax6*$^{-/-}$ cerebral organoids, suggesting the compatibility of these two systems (Figure 3.12).

3.3.3.2 Transcription factor *Tbr2* may not be regulated by *Pax6* in cerebral organoids

The pleiotropic functions of *Pax6* in telencephalic development suggest the complexity of its gene regulatory network. For example, evidence from E13.5 cortex-specific *Pax6* cKO embryos demonstrated that *Pax6* control in cell proliferation is region-specific, as changes in cell cycle kinetics were detected only in the rostro-medial region, where *Pax6* expression is the highest (Mi et al., 2013). This finding is consistent with the *Pax6* gain-of-function study, which suggests the importance of *Pax6* expression level in proper corticogenesis (Sansom et al., 2009; Georgala et al., 2011). Furthermore, a more recent study found different roles of *Pax6* in cell cycle regulation between the cortex and thalamus, possibly regulated by another transcription factor, namely *Foxg1* (Quintana-Urzainqui et al., 2018).

Tbr2 is one of the direct target genes of *Pax6*, which is downregulated in *Pax6*$^{-/-}$ embryos (Quinn et al., 2007; Sansom et al., 2009). *Tbr2* is a marker for basal progenitors, which is sequentially expressed after differentiation of apical to basal progenitors, following downregulation of *Pax6* (Englund et al., 2005). We have shown that the proportion of cells expressing *Tbr2* was also decreased in the *Pax6*$^{-/-}$

cerebral organoids, compared to control, at both day 8 and day 9 (Figure 3.13). However, this decrease was not significant. Considering the use of *Tbr2* to define the cortical region in our analysis, this result could be due to an underestimation of cortical regions, as *Tbr2* is downregulated in the absence of *Pax6* (Quinn et al., 2007). Therefore, the use of an alternative cortical marker that is not affected by the loss of *Pax6* might be a more accurate way to define the cortical region in this mutant, for example, *Emx1*.

Taken together, our results demonstrate comparable phenotypes of *Pax6*$^{-/-}$ cerebral organoids to *Pax6*$^{-/-}$ embryos. Given the caveats of the results, the following chapter will describe the establishment of cortex-specific *Pax6* cKO ES cells, which will allow us to delete *Pax6* specifically in the cortex, at a specific time. This will enable a more accurate analysis of the role of *Pax6* in cell cycle kinetics in cerebral organoids.

CHAPTER 4: Establishment of cortex-specific *Pax6* conditional knock-out embryonic stem cell lines.

4.1 INTRODUCTION

The results presented in the previous chapter demonstrated that *Pax6*$^{-/-}$ cerebral organoids reproduced similar phenotypes to E12.5 *Pax6*$^{-/-}$ embryos. This may suggest that *Pax6* in these two systems could be operating by comparable developmental regulatory mechanisms. Although the labeling index (LI) of EdU+ cells in both systems was altered, it is notable that the proportion of cells in S-phase was decreased in the mutant organoids compared to the control, which is in contrast to what has been found in vivo (Warren et al., 1999). This discrepancy could be due to constitutive loss of *Pax6*, which possibly leads to the accumulation of secondary defects that may affect cell proliferation of cerebral organoids. In fact, constitutive loss of *Pax6* is lethal to embryos, which hampers the study of the role of *Pax6* later in development (Warren et al., 1999). Additionally, the use of *Tbr2* to define cortical regions in *Pax6*$^{-/-}$ cerebral organoids may have caused an underestimation in the quantitative analysis, as *Tbr2* is downregulated in the absence of *Pax6* (Quinn et al., 2007).

In vivo, a cortex-specific *Pax6* conditional knock out (cKO) mouse model is used to circumvent the limitations of the *Pax6* constitutive loss-of-function model (*Pax6*$^{-/-}$, Mi et al., 2013). The *Pax6* cKO mouse utilises the inducible Cre-Lox recombinase system, which enables acute deletion of *Pax6* with spatio-temporal control. The *Cre* recombinase is fused with a mutated estrogen receptor (*CreER*^{T2}), which is responsive to 4-OHT, a tamoxifen metabolite (Hayashi and McMahon, 2002). Furthermore, the

CreER^{T2} is controlled by the *Emx1* promoter, driving *Cre* activity specifically in the cortex and constrains *Pax6* deletion to this region (Figure 4.1A; Kessaris et al., 2006). Therefore, in the presence of 4-OHT, *Cre* catalyses recombination of loxP sites flanking a stop sequence, which activates the downstream EGFP in the RCE:loxP allele (Figure 4.1B;Sousa et al., 2009), as well as loxP sites flanking exons 5, 5a and 6 of *Pax6* (Figure 4.1C; Simpson et al., 2009). This results in *Pax6* deletion in a cortex-specific region, which can be monitored by the expression of GFP that reports on *Emx1*-driven *Cre* activity.

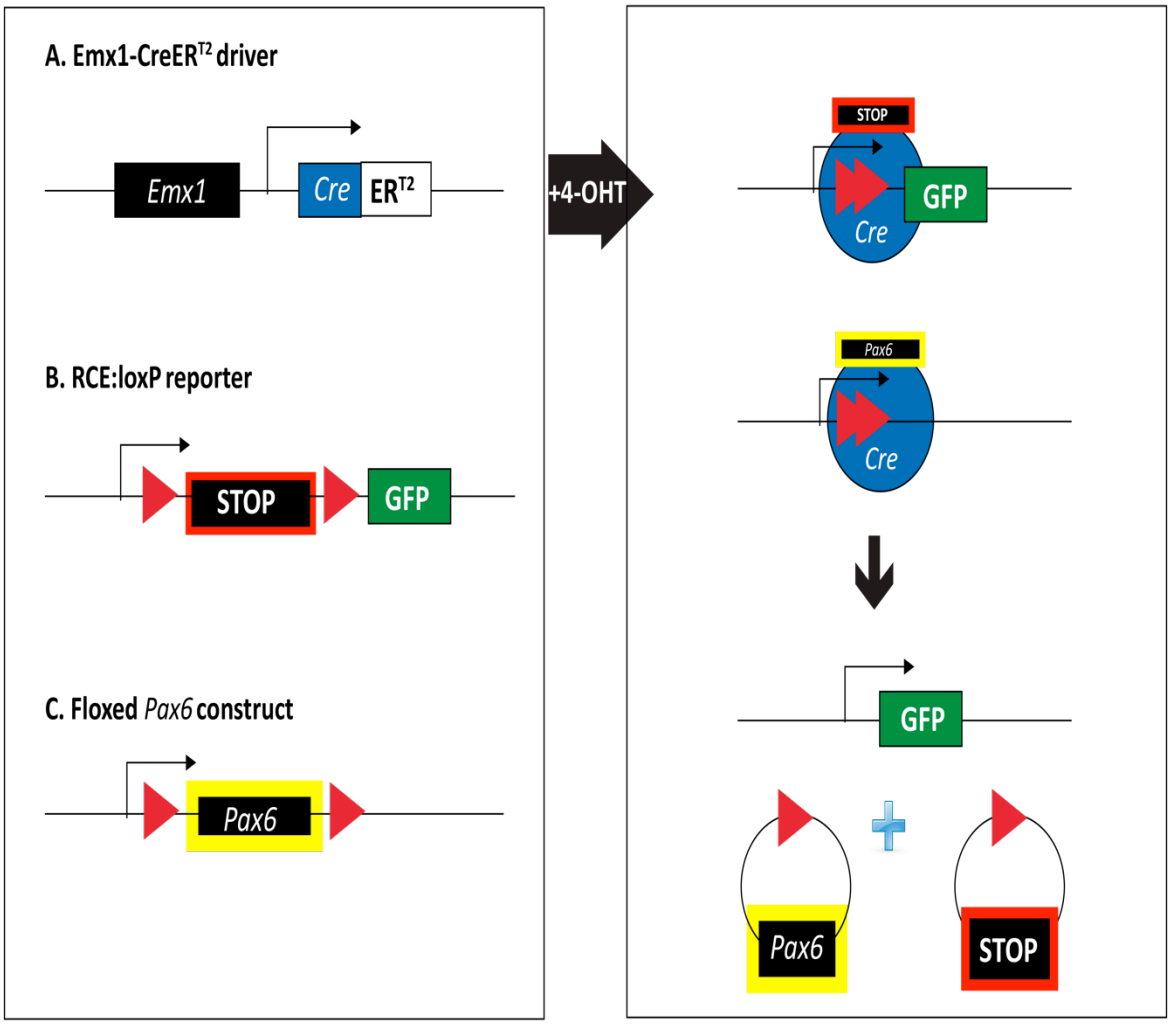

Figure 4.1 Genetic elements of the inducible, cortex-specific *Pax6* conditional knockout system. Upon treatment with 4-OHT, (A) CreER^{T2} allele is activated, which is driven by *Emx1* and the activation is reported by the (B) RCE allele, with upstream floxed STOP cassette, as well as deletion of *Pax6* sequence in the (C) Floxed *Pax6* construct.

To date, there are very few studies using conditional mutant organoids, with only one study reported in gut organoids, and none in cerebral organoids (Andersson-Rolf et al., 2017). Considering that conditional mutants are one of the important tools in neurodevelopmental studies, it is therefore imperative to explore their use in cerebral organoids.

In order to generate this conditional mutant model, this chapter aimed to derive embryonic stem (ES) cells from the cortex-specific *Pax6* conditional knock out (cKO) mouse (Mi et al., 2013). This will not only allow us to further investigate *Pax6* control in the cortex-specific region of the cerebral organoids, but also will enable us to determine the extent to which this model recapitulate the in vivo system by comparing the phenotypes of *Pax6* cKO cerebral organoids directly to the well-established phenotypes of *Pax6* cKO mice. Furthermore, this model, which contains the *Emx1*-driven *Cre* reporter, could improve the analysis of cerebral organoids by using the expression of GFP as a proxy to identify cortical neuroepithelium-like (NE) structures in the organoids – hence reducing the underestimation in quantitative analyses.

Pax6 conditional knock out (cKO) mice are maintained on a CD1 background, an outbred stock. To the best of our knowledge, derivation of ES cells from this stock has not been reported before, thus the ES cell derivation efficiency is unknown (Czechanski et al., 2014).

There are two types of medium widely used for ES cell derivation; the standard ES medium with LIF and serum, and the serum-free medium supplemented with two small molecule inhibitors, known as 2i/LIF medium. The former medium is used in the classic ES cell derivation technique, and it is quite inefficient due to the presence of poorly defined components in the serum, promoting spontaneous differentiation. Furthermore, ES derivation using this medium is limited to a very few mouse strains such as the 129 and C57B1/6 mice, also known as the permissive strains. Other strains are categorised as recalcitrant or non-permissive, as it was difficult to derive ES cells from them using this medium (Martello and Smith, 2014; Czechanski et al., 2014).

However, problems with this classic technique were resolved with the use of 2i/LIF medium, which further allows ES cell derivation from recalcitrant strains and species (Buehr et al., 2008; Nichols et al., 2009; Reinholdt et al., 2012). This serum-free medium employs two small molecule inhibitors (PD0325901 and CHIR99021), which are sufficient to maintain ES cell self-renewal as well as preventing spontaneous differentiation (Ying et al., 2003). PD0325901 inhibits cell differentiation via the MEK/Erk pathway, and CHIR99021 maintains cell proliferation via inhibition of the glycogen synthase kinase-3 pathway (GSK3). This culture condition is also known as the "ground state" condition, as it maintains ES cells in their ground state of pluripotency, equivalent to the early pre-implantation blastocyst, E3.5 (Martin Gonzalez et al., 2016).

As ES cell derivation efficiency from the cortex-specific *Pax6* cKO mouse on a CD1 background is unknown, this chapter describes establishment of the ES cells using 2i/LIF medium (hereafter referred to as 2i/LIF).

4.2 RESULTS

4.2.1 Derivation of ES cells from *Pax6* cKO mice of CD1 background

To determine whether ES cells can be derived from *Pax6* cKO mice of CD1 background, 2i/LIF medium was used and the derivation efficiency was determined by scoring the number of stable ES cell lines over the number of attached blastocyts. A total of 24 blatocysts at ~E3.5 were collected from three independent parental crossings of $Pax6^{fl/fl}$; *Emx1-CreER*^{T2}; *RCE* males with $Pax6^{+/fl}$ females, and a unique number was assigned to each batch (Table 4.1).

Table 4.1 Summary of the established ES lines.

Batch	# Collected blastocysts	# Attached blastocysts	# ES cell lines	ES cell lines ID
113	9	8	2	113.1, 113.2
114	4	3	2	114.1, 114.3
115	11	10	9	115.1-115.9

Based on Mendelian inheritance, 50% of the ES cell lines were expected to carry the *Emx1-CreER*^{T2} allele, with half of them homozygous for the floxed *Pax6* allele (*Emx1- CreER*^{T2};*Pax6*$^{fl/fl}$, 25%) and another half heterozygous for the floxed *Pax6* allele (*Emx1- CreER*^{T2};*Pax6*$^{+/fl}$, 25%).

To assist the attachment of blastocysts, mouse embryonic fibroblast (MEF) were successfully propagated one day prior to blastocyst isolation. MEFs formed matrix to assist blastocyst attachment, as well as producing growth factors for cell viability (Czechanski et al., 2014). Indeed, 88% of the isolated blastocysts were successfully attached and formed outgrowth at day seven (n=24, Figure 4.2).

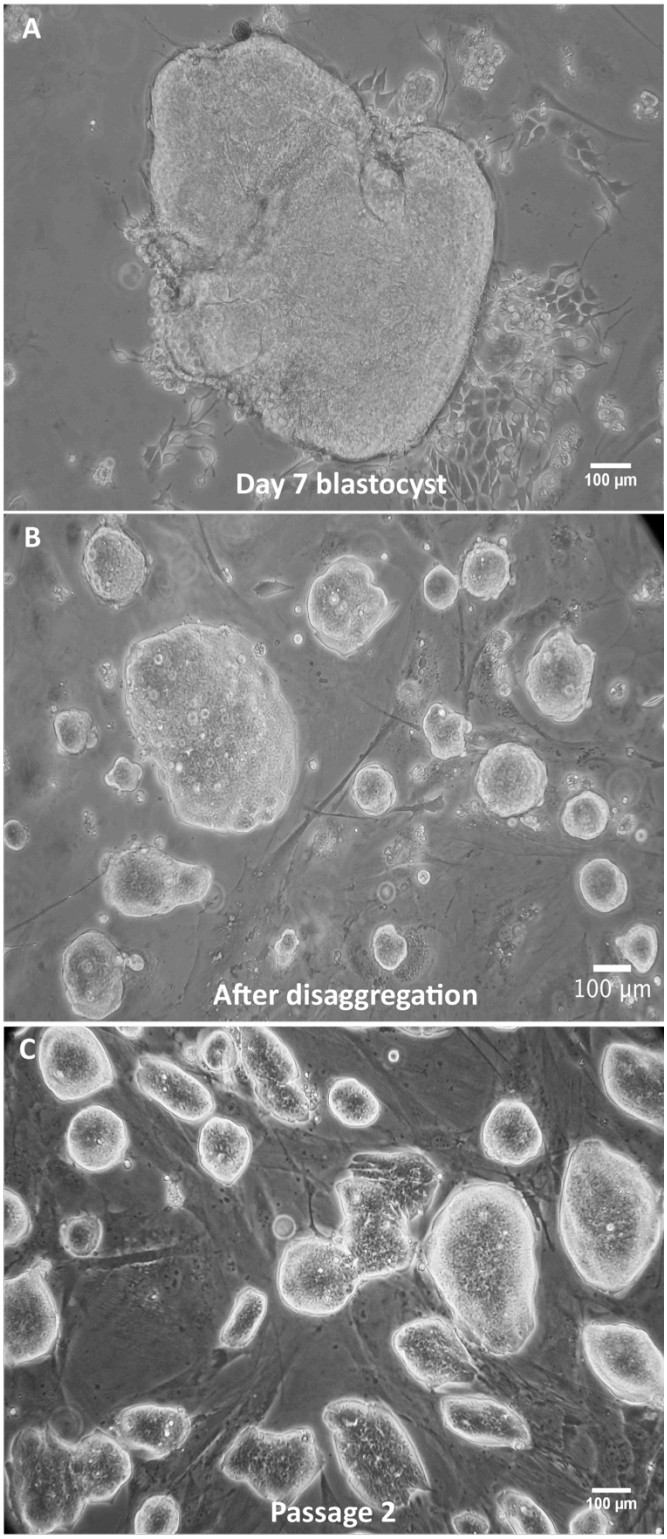

Figure 4.2 From blastocyst to ES cells. (A) Blastocyst forms an outgrowth at day seven of culture, (B) After disaggregation of the outgrowth, cell colonies formed, and later known as (C) ES cell lines, following stable growth for several passages.

Following disaggregation of the outgrowth, only 62% of the disaggregated outgrowth continued to propagate (n=21, Figure 4.2), while the remainder either failed to grow after disaggregation or became contaminated. Therefore, the ES derivation efficiency from CD1 mice was 62%, consistent with the efficiency of ES cell derivation from recalcitrant strain using 2i/LIF medium, which is around 50-70% (Czechanski et al., 2014).

Although 2i/LIF condition supports efficient derivation of ES cells, long-term maintenance of ES cells in this medium is controversial. There are emerging reports of altered epigenome, as well as chromosomal abnormalities in ES cells after prolonged culture in 2i/LIF medium (Chen et al., 2015; Choi et al., 2017). Therefore, to prevent such consequences, these cells were gradually cultured in a standard ES medium (LIF/serum), without feeder cells. The cells were incubated in a mixture of 2i/LIF: LIF/serum medium, with the ratio of LIF/serum being gradually increased in every passage, from 30%, 50%, 70% to complete LIF/serum (100%). During the transition period, changes in cell morphology were observed; from a refractile and tight colony in 2i/LIF medium to a more heterogenous population of cells; a mixture of cells with higher ratio of nuclei to cytoplasm and differentiated cells in the standard LIF/serum medium (Figure 4.3).

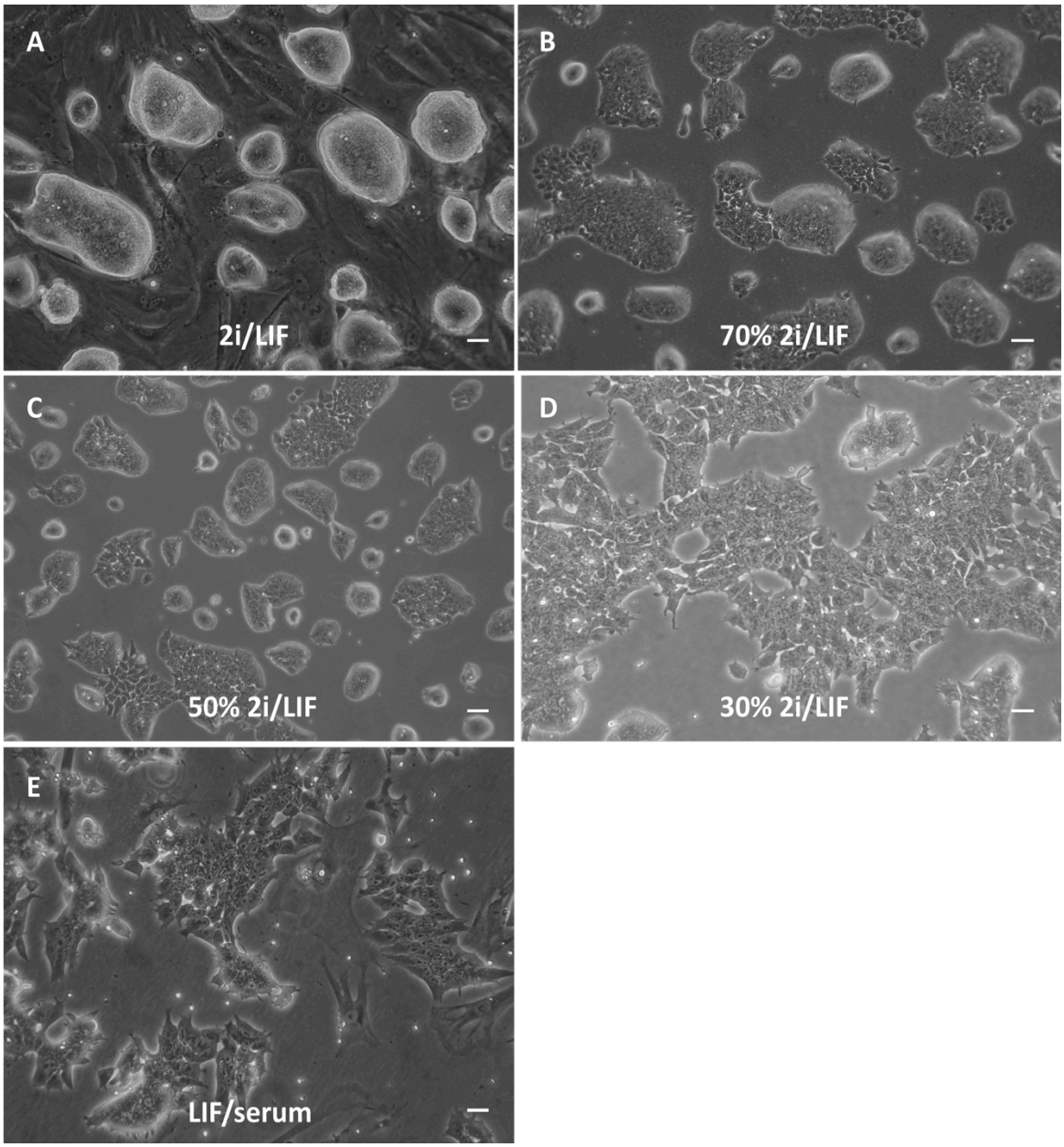

Figure 4.3 Transition of ES cells cultured in 2i/LIF to LIF/serum medium. (A) ES cell colonies cultured in 2i/LIF culture were tightly-packed and refractile, (B-D) The colonies became less refractile during the gradual increase of LIF/serum medium, (E) Heterogeneous population of cells with less tightly formed ES colonies in LIF/serum medium.

The presence of differentiated cells in LIF/serum culture might reflect the effect of serum showing inevitable spontaneous differentiation, which results in a more heterogenous culture.

4.2.2 Characterisation of the ES cell lines genotypes

Following establishment of the ES cell lines, the next step was selecting ES cells with the following genotypes: *Pax6$^{fl/fl}$; Emx1-CreER^{T2}; RCE* (experimental cells), and *Pax6$^{+/fl}$; Emx1-CreER^{T2}; RCE* (control cells). Note that the only difference between the experimental and control sample was the status of the floxed *Pax6* allele, with the former being homozygous and the latter being heterozygous for the allele.

Genotyping by PCR was performed, and cell lines with the genotypes of interest were further maintained. We found that ~50% of the established ES cell lines (113.1, 113.2, 114.1, 114.3, 115.7, 115.9) carried the *Cre* allele (n=13, Figure 4.4A), and out of these *Cre*+ cell lines (n=6), 50% of them were homozygous for the floxed *Pax6* allele (113.1, 114.1, 115.7) and another 50% were heterozygous (113.2, 114.3, 115.9). Therefore, three sets of experimental and three sets of control ES cell lines were successfully established (Figure 4.4B).

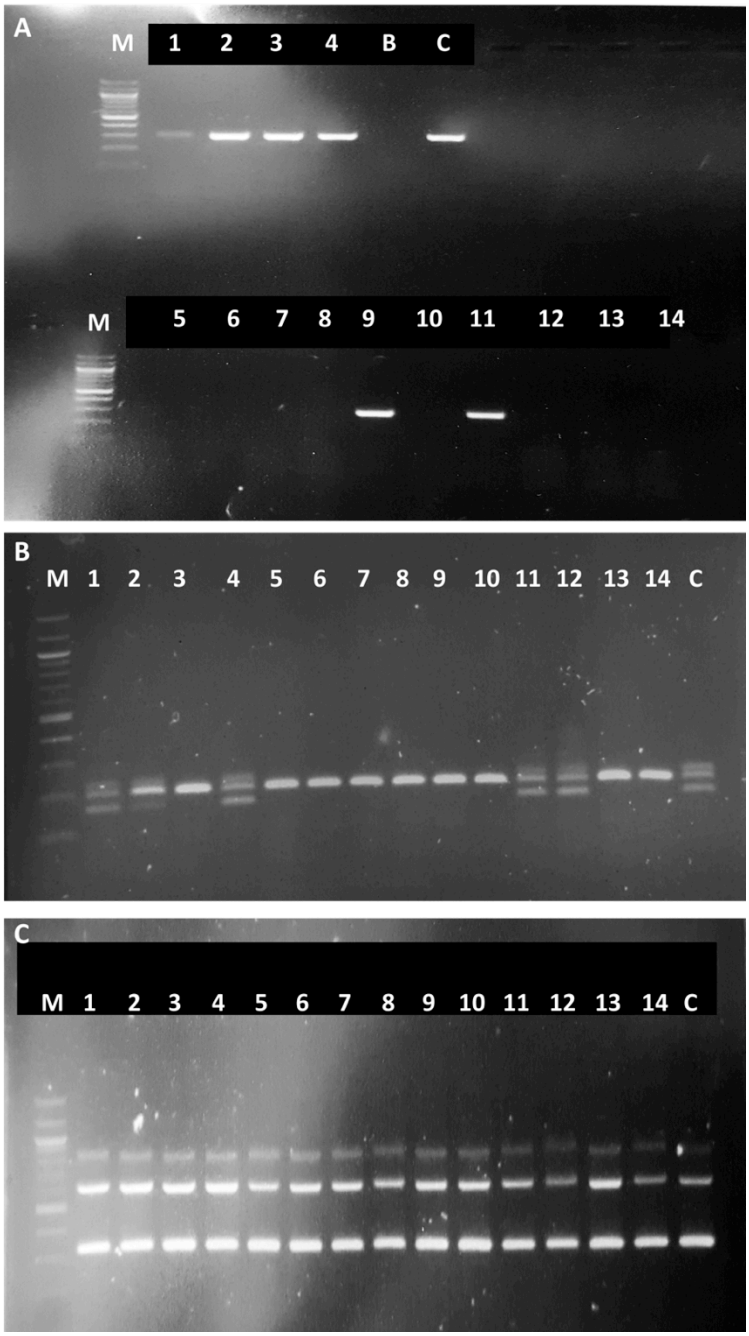

Figure 4.4 Genotypes of the ES cell lines. (A) Six of the cell lines carry the *Cre* allele. (B) Three of the *Cre*+ cell lines (113.2, 114.1, 115.7) are homozygous for the floxed *Pax6* allele, and three of the *Cre*+ cell lines (113.1, 114.3, 115.9) are homozygous for the floxed *Pax6* allele. (C) RCE allele was detected in all of the cell lines. M: 100bp, B: negative control, C: positive control, 1: 113.1, 2: 113.2, 3: 114.1, 4: 114.3, 5:115.1, 6:115.2, 7:115.4, 8:115.6, 9:115.7, 10:115.8, 11:115.9, 12:115.10, 13:115.11, 14:115.12.

To facilitate the identification of the cell lines to their genotype, these cell lines were renamed as following (Table 4.2).

Table 4.2 Summary of the established ES lines.

Batch	Blastocyst no.	Former name (ES cell lines ID)	Genotype	Simplified name
115	7	115.7	*Pax6$^{fl/fl}$; Emx1-CreER^{T2}; RCE*	cKOhom1
	9	115.9	*Pax6$^{+/fl}$; Emx1-CreER^{T2}; RCE*	cKOhet1
114	1	114.1	*Pax6$^{fl/fl}$; Emx1-CreER^{T2}; RCE*	cKOhom2
	3	114.3	*Pax6$^{+/fl}$; Emx1-CreER^{T2}; RCE*	cKOhet2
113	1	113.1	*Pax6$^{fl/fl}$; Emx1-CreER^{T2}; RCE*	cKOhom3
	2	113.2	*Pax6$^{+/fl}$; Emx1-CreER^{T2}; RCE*	cKOhet3

4.2.3 Karyotype analysis and the expression of pluripotency markers

To check chromosomal stability of the selected ES cell lines, their karyotype was assessed by counting the number of chromosomes from at least 20 metaphase spreads (Figure 4.5A). The percentage of metaphase spreads with 40 chromosomes were calculated and cell lines with the score of >60% were considered to be euploid. Quantitative analysis showed that four of the six *Cre*+ ES cell lines were karyotypically normal (Figure 4.5B).

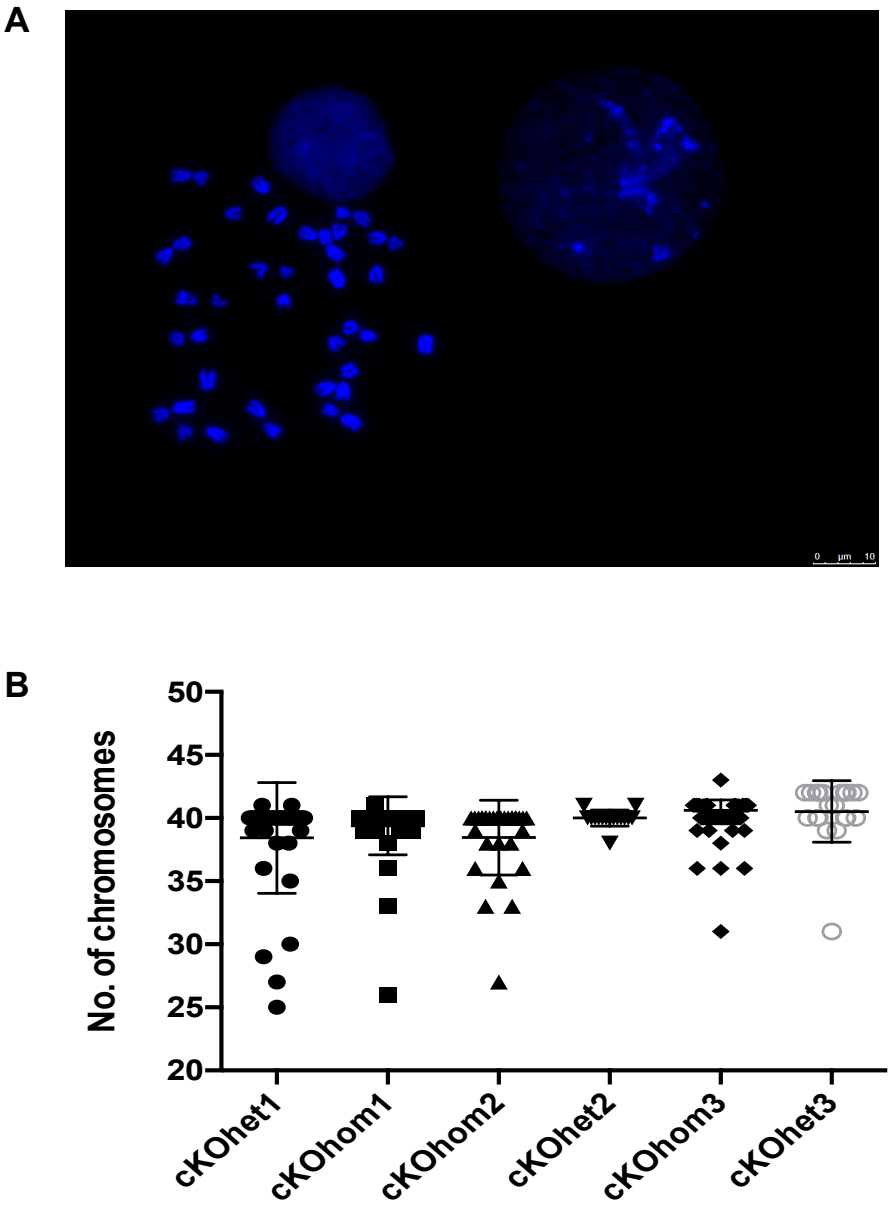

Figure 4.5 Distribution of ES cells with different number of chromosomes. (A) Representative image of metaphase spread stained with DAPI. (B) All ES cell lines showed >60% of the cells with 40 chromosomes (normal karyotype), except cKOhet3 and cKOhom3 with <60% of the cells with 40 chromosomes. Data presented as SEM, n=>10 cells from two independent experiments.

However, cKOhet3 and cKOhom3 lines show <60% normal chromosome count and therefore were abnormal (n= 3 batches). It is noted that both of these aneuploid ES cell lines were derived from the same batch (#113), and 75% of the blastocysts from this batch failed to survive in culture, mostly after outgrowth disaggregation, probably due to the instability of the cell line (Czechanski et al., 2014). Therefore, it is possible that all of the blastocysts from batch #113 were abnormal from the start, including the cKOhet3 and cKOhom3 lines. Taken together, a total of four ES cell lines with normal karyotypes were established and further characterised and maintained.

The ES cell gene regulatory network is centred on three core transcription factors, *Oct4, Sox2* and *Nanog*. *Oct4* is the master regulator of pluripotency, which is downregulated upon differentiation and often acts together with *Sox2* (Nichols and Smith, 2012). However, the mere presence of expression of these genes is insufficient to demonstrate pluripotency as it is a dynamic process characterised by heterogenous expression of *Nanog* (Silva et al., 2008; Chambers et al., 2007). Therefore, to assess pluripotency of the four karyotypically normal ES cell lines, they were stained with *Oct4 and Nanog* antibodies.

Consistent with the reported expression patterns of *Oct4* and *Nanog* in mouse ES cells, almost all of the cells in the four established ES lines expressed *Oct4*, with heterogenous expression of *Nanog*, which is evident from subpopulation of cells with high and low expression of *Nanog* (Figure 4.6).

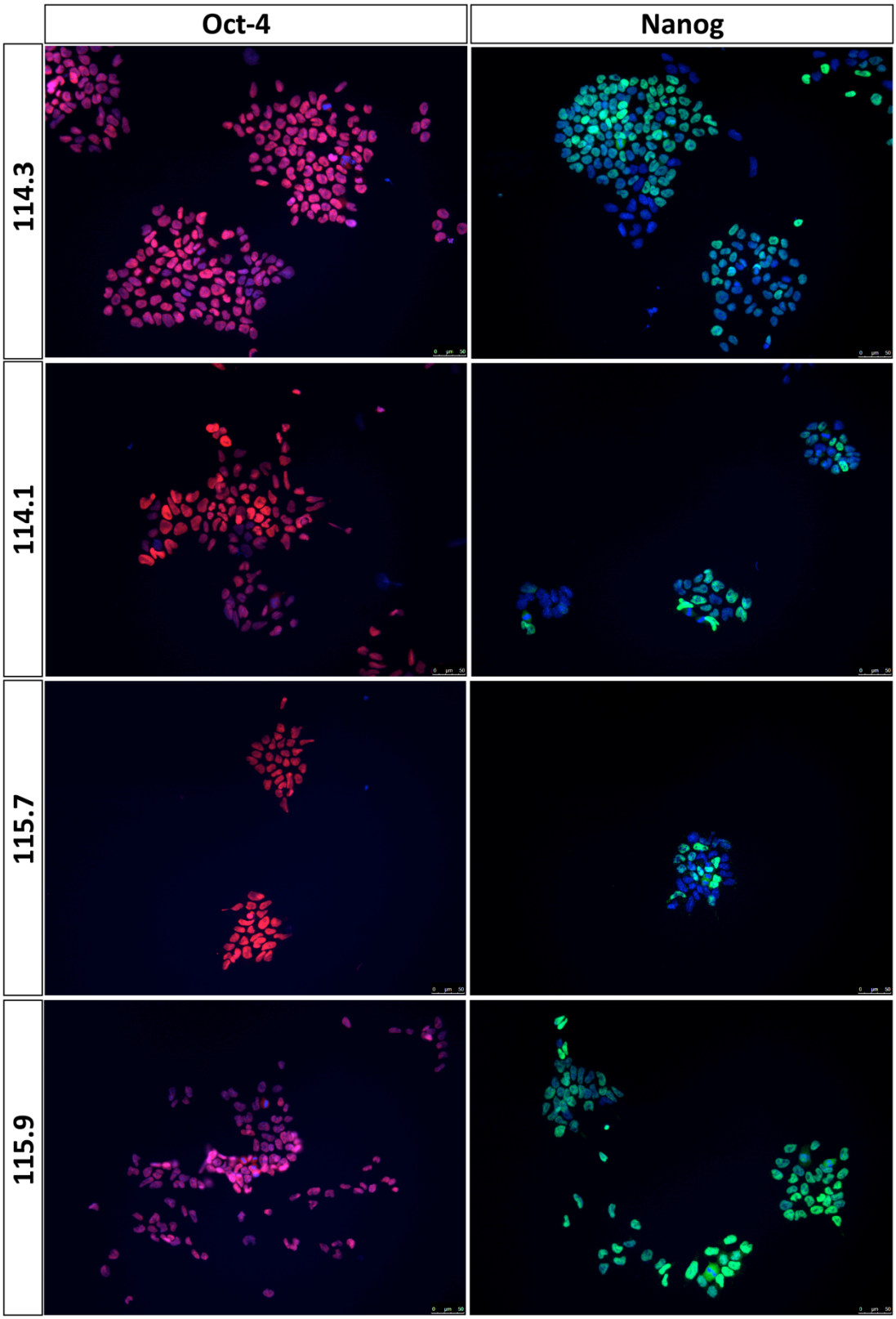

Figure 4.6 Expression of *Oct4* and *Nanog* in all of the established cell lines.

Different levels of *Nanog* are associated with pluripotency stability, as subpopulations with low *Nanog* were found to be more susceptible to differentiation (Nair et al., 2015; Kalmar et al., 2009). Nevertheless, this dynamic state of pluripotency is inevitable in ES cell culture. Therefore, based on the expression of these hallmark pluripotency markers, the established cell lines are considered pluripotent.

ES cell lines were also tested for mycoplasma contamination by the tissue culture facility at the Scottish Centre for Regenerative Medicine and were confirmed free from mycoplasma (Appendix A).

4.2.4 *Pax6* cKO ES cell lines show incomplete aggregation

As mentioned in the previous chapter, the first step in the formation of cerebral organoids is cell aggregation (Figure 3.1). An optimal aggregate can be identified by its spherical morphology, size, as well as smooth and clear edges. In contrast, a suboptimal aggregate is surrounded by visible dead cells, which were possibly differentiated cells that unable to aggregate and were therefore unable to survive in a serum-free medium. These suboptimal aggregates have fewer aggregating cells, resulting in insufficient cell-cell interaction that could affect neural induction, as well as cell fate – hence they will usually be discarded, as part of cerebral organoids quality control (Lancaster and Knoblich, 2014).

To determine the formation of optimal cerebral organoids in the established ES cell lines, equal numbers of cells (5000 cells) were aggregated following the established 3D protocol as described in chapter three and section 2.4. Then, day one aggregates

were examined for the presence of cells that were unable to aggregate. Organoids from Foxg1::Venus ES cells were used as a control, as they have been used previously in the establishment of the 3D protocol and successfully formed optimal aggregates, which ultimately showed robust formation of NE structures, as reported in the previous chapter.

Interestingly, almost all of the day one aggregates from the established ES cell lines exhibited the presence of non-aggregating cells, which has affected their size – smaller than the control (Figure 4.7 A, B, C, D).

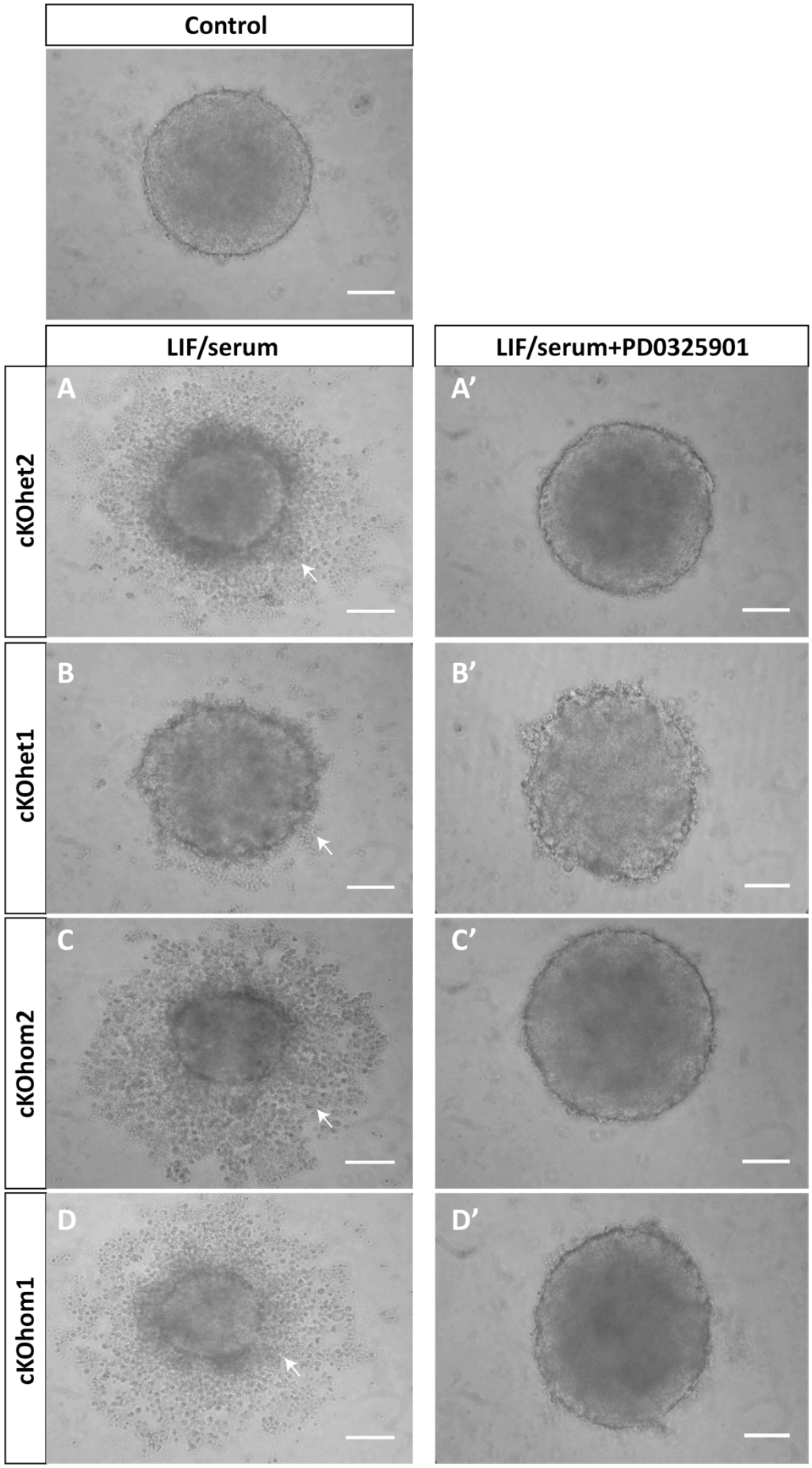
Control
LIF/serum
LIF/serum+PD0325901
cKOhet2
cKOhet1
cKOhom2
cKOhom1
A
A'
B
B'
C
C'
D
D'

Figure 4.7 Aggregation of *Pax6* cKO ES cells before and after treatment of ES cells with PD0325901. (A-D) ES cells without treatment with PD0325901 show incomplete aggregation, results in smaller aggregates compared to control. (A'-D') ES cells after treatment with PD0325901 improves aggregation, showing comparable size to control. Scale bar: 100 µm.

These non-aggregating cells could be differentiated cells that were unable to survive in the serum-free medium. This may be due to the poor ES cell culture, which contains higher proportion of differentiated cells due to spontaneous differentiation (Figure 4.8)

.

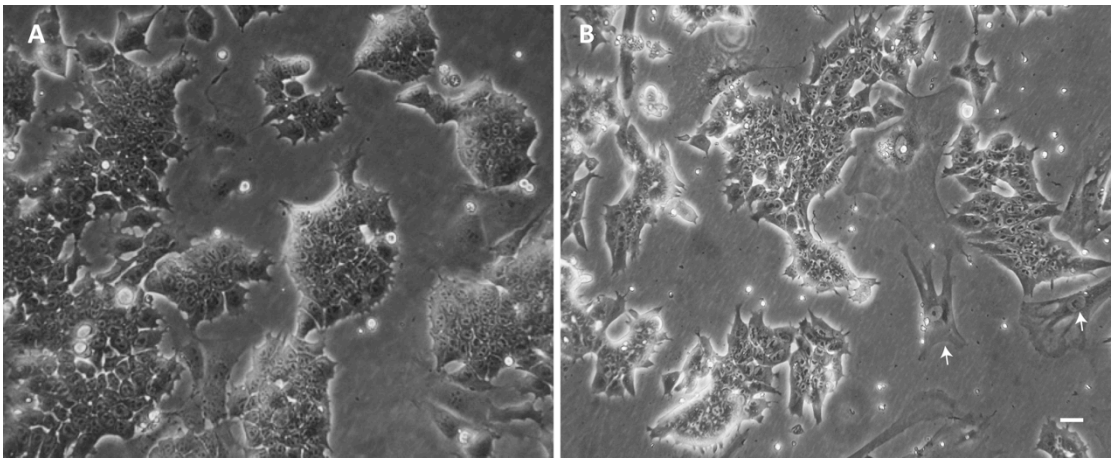

Figure 4.8 *Pax6* cKO ES cell lines are more heterogenous. (A) Control ES cell colonies (Foxg1::Venus ES cells) are more compact, with few flat/differentiated cells (B) *Pax6* cKO ES cell lines show ES colonies with less tight colonies and more heterogenous, indicated by the presence of differentiated cells with flat morphology. Scale bar: 100 µm.

Spontaneous differentiation can be triggered by the poorly defined components in serum, as well as from the activation of MEK/Erk kinase, an important pathway in cell differentiation (Martello and Smith, 2014). This pathway can be activated by FGF4, which is secreted endogenously by ES cells (Kunath et al., 2007). Evidence showed that blocking the MEK/Erk pathway in the presence of LIF is sufficient to prevent differentiation of ES cells and can rescue a deteriorating culture (Tamm et al., 2013; Ying et al., 2008; Nichols and Ying, 2006). Therefore, to reduce the proportion of differentiated cells in the established ES cell cultures, as well as to rescue the undifferentiated ones from differentiating, the ES cell lines were treated with PD0325901, a small molecule inhibitor that blocks the MEK/Erk pathway. Indeed, this treatment significantly reduced the non-aggregating cells and improved cell aggregation, evident from the size of the aggregates, which were comparable to the control (Figure 4.8 A',B',C',D').

Although inhibition of MEK/Erk pathway in a prolonged culture has been shown to compromise epigenetic stability and cause aneuploidy, a recent study found that this can be prevented with a lower concentration of PD0325901 (Di Stefano et al., 2018). Therefore, considering the effects of suppression of MEK/Erk pathway, the ES cells were treated with a reduced concentration of PD0325901 (0.5 μM), and only low passage number ES cells (<p20) were used for generation of cerebral organoids.

4.2.5 *Pax6* cKO ES cell lines form cerebral organoids in 3D culture

Following the establishment of *Pax6* cKO embryonic stem (ES) cells, their ability to form cerebral organoids with neuroepithelium-like (NE) structures expressing *Pax6* was determined. Cerebral organoids were generated using the established 3D culture protocol described in chapter three, collected at day eight of culture and cross-sectioned to examine the formation of NE structures. To ensure that these organoids expressed *Pax6* prior treatment with 4-OHT, the sections were labeled with Pax6 (apical progenitor marker) and Tuj1 (post-mitotic neuronal marker) antibodies.

Figure 4.9 shows that three out of four ES cell lines formed cerebral organoids with NE structures expressing *Pax6* and *Tuj1,* except cKOhet2 cell line (n=3). Although this suggests variability between cell lines, it also indicates the robustness of the established 3D culture protocol.

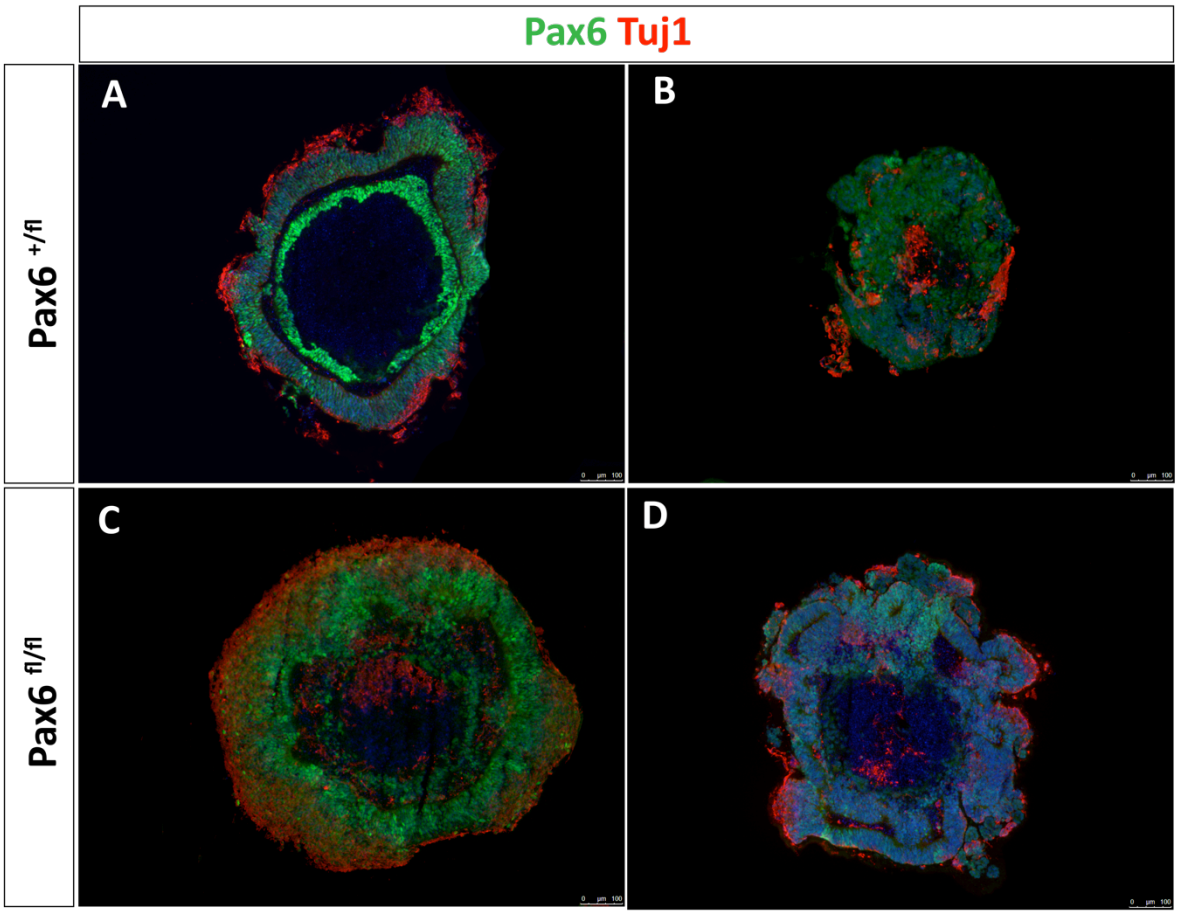

Figure 4.10 Formation of NE structures in *Pax6* cKO cerebral organoids. (A) One of the control cell lines (cKOhet1) form NE structures expressing *Pax6* and *Tuj1*, (B) while NE structures are not detected in cKOhet2 cerebral organoids. (C, D) Both of the experimental cell lines (cKOhom1 and cKOhom2) successfully form cerebral organoids with NE structures (n=3). Scale bar: 100 µm.

4.3 DISCUSSION

Embryonic stem (ES) cells are pluripotent cells derived from pre-implantation embryos and they are the building blocks of cerebral organoids. Results presented in this chapter collectively demonstrate the successful derivation of ES cells from cortex-specific *Pax6* cKO mice on a CD1 background. A total of four ES cell lines with the desired genotypes were successfully established, and they retained normal karyotypes, expressed pluripotency markers and were free from mycoplasma contamination.

4.3.1 Efficient derivation of ES cells from *Pax6* cKO mice using 2i/LIF medium

One of the ways to probe the cerebral organoid system is by acute removal of an important gene in cortical development (e.g. *Pax6*). Therefore, establishment of cortex-specific *Pax6* cKO cerebral organoids is important in this endeavour. This conditional mutant model employs the Cre-Lox recombinase system, which can be readily established by deriving ES cells from the established cortex-specific *Pax6* cKO mice (Mi et al., 2013). Phenotypes of this *Pax6* cKO mouse are well established, allowing comparison with the newly established *Pax6* cKO cerebral organoids.

The cortex-specific *Pax6* cKO mice were maintained on a CD1 background, a stock with unknown status of efficiency to derive ES cells (Czechanski et al., 2014). Derivation of ES cells was previously inefficient and limited to very few mouse strains; such as the 129 and C57B1/6 mice (Martello and Smith, 2014). However,

following the discovery of ground-state pluripotency, ES cells can be derived from any type of mouse background with 60-90% efficiency, a dramatic increase from the traditional technique using LIF/serum medium at only 30% efficiency (Czechanski et al., 2014; Nichols and Ying, 2006).

Using the "ground state" condition, we found that ES cells can be derived from CD1 mice with 62% efficiency (n=21). Although this condition has greatly facilitated ES cell derivation, prolonged culture in 2i/LIF has been reported to alter the epigenome and introduce aneuploidy (Chen et al., 2015; Choi et al., 2017). This could be due to the nature of ground state pluripotency, which is a transient stage in vivo; and prolonged culture might perturb this equilibrium (Choi et al., 2017; Weinberger et al., 2016). To prevent these complications, the ES cells were successfully maintained in the standard ES medium (LIF/serum) after gradual transition from the 2i/LIF medium.

4.3.2 Characteristics of *Pax6* cKO ES cell lines

Although both 2i/LIF and LIF/serum media are able to maintain ES cells in a pluripotent state, they support ES cells of distinct embryonic stages. Based on transcriptomic data, ES cells cultured in 2i/LIF were found to be comparable to the early stage blastocyst, whereas ES cells cultured in LIF/serum condition are reported to be equivalent to the late stage blastocyst (E4.5, Martin Gonzalez et al., 2016). Furthermore, the differences between these two types of ES cells are reflected in many other aspects, including their morphology, heterogeneity and the ability to form chimeras (Wu and Izpisua Belmonte, 2015). Indeed, we observed striking changes in the ES cell morphology and heterogeneity, during the medium transition – from a

fairly homogenous and refractile ES cell colonies in 2i/LIF medium, to a more heterogenous population of cells in the LIF/serum medium. Recognising the different states of ES cells is important, as their characteristics may affect downstream applications. For example, due to the difference in the developmental stage of the starting cell population, specific types of differentiated cells may appear at later time-points using 2i ES cells compared to LIF/serum ES cells.

Nevertheless, all four *Pax6* cKO ES cell lines cultured in LIF/serum show pluripotent characteristics, based on the expression of *Oct4* and *Nanog* (Figure 4.7). Moreover, they demonstrated the signature profile of pluripotency, which is heterogenous expression of *Nanog*, with subpopulations of *Nanog*-high and *Nanog*-low cells (Kalmar et al., 2009). A previous study using quantitative analysis showed a high correlation between heterogeneity of *Nanog* with *Oct4*, which further categorises ES cells into three subpopulations: pluripotent, lineage-primed or differentiated cells (Descalzo et al., 2012). For instance, uniform and high levels of both *Oct4* and *Nanog* indicate cells with stable pluripotency, a low level of both *Nanog* and *Oct4* indicates cells that are primed for differentiation and the absence of both *Oct4* and *Nanog* suggest the presence of differentiated cells (Torres-Padilla and Chambers, 2014). Although these genes were not analysed quantitatively in this study, heterogenous expression of *Nanog* indicates the heterogeneity of the ES cell lines at the molecular level, consistent with the heterogenous population of cells.

4.3.3 *Pax6* cKO ES cell lines require MEK/Erk inhibitor for optimum cell aggregation

Although heterogeneity is inevitable in serum-containing medium, undifferentiated cells should be predominant in a healthy culture, as a higher proportion of differentiated cells in ES cell culture could affect the generation of cerebral organoids (Lancaster and Knoblich, 2014; Eiraku and Sasai, 2012). Despite careful handling of the ES cells, generation of cerebral organoids from the established *Pax6* cKO ES cell lines revealed inefficient cell aggregation, as the majority of the cells failed to aggregate properly. This stage is important, as the number of aggregating cells may affect later stage of organoid development, such as in neural induction or cell specification (Eiraku and Sasai, 2012).

Interestingly, there is evidence that ES cells derived from recalcitrant strains are dependent on exogenous factors such as PD0325901 (MEK/Erk inhibitor) to maintain their undifferentiated state (Hanna et al., 2009). Indeed, we show that maintaining the established ES cell lines in LIF/serum supplemented with PD0325901 has dramatically improved cell aggregation. Interestingly, these cell lines also appeared to be dependent on this small molecule, as withdrawal of PD0325901 resulted in persistent cell aggregation inefficiency. PD0325901 is one of the small molecules in 2i culture that inhibits cell differentiation by blocking the MEK/Erk pathway. Its combination with serum is sufficient to reduce spontaneous differentiation, thus it is routinely used to rescue undifferentiated cells in a very heterogenous ES cell culture (Tamm et al., 2013; Ying et al., 2008). Therefore, supplementation of PD0325901 in the ES cell culture has successfully improved cell aggregation.

Although a reduced concentration of PD0325901 is safe for ES cell culture (Di Stefano et al., 2018), it is not required in standard ES medium, as supplementation with Leukaemia inhibitory factor (LIF) is sufficient to maintain the undifferentiated cells. Therefore, the requirement of PD0325901 to maintain ES cell culture suggests that the signaling pathway to maintain the undifferentiated state in these ES cell lines might be different and intrinsic to the recalcitrant strain. Moreover, since ES from recalcitrant strains can only be derived using the 2i medium but not the standard LIF/serum medium, it is plausible that these small molecules are indeed essential in maintaining ES cells, which distinguish them from the permissive strain.

4.3.4 *Pax6* cKO ES cells form cerebral organoids with NE structures

We showed that all of the established *Pax6* cKO ES cell lines successfully aggregate on day one of 3D culture. However, despite the standard condition used, only three of them form NE structures, whilst the cKOhet2 line cannot. This is despite comparable characteristics of the cKOhet2 ES cells to other cell lines, in terms of expression of pluripotency markers and normal karyotype (Figure 4.3, 4.4).

Formation of NE structures is driven by a spontaneous phenomenon known as self-organisation, governed by segregation of cells and cell fate specification (Lancaster and Knoblich, 2014). Although cKOhet2 cells are able to form aggregates, it appears that the cells were unable to sort properly and self-organise. The inability to sort out properly could be due to lack of adhesion molecules, such as N-cadherin (Detrick et

al., 1990; Fujimori et al., 1990). To confirm this, it will be important to characterise the expression of N-cadherin in cKOhet2 cerebral organoids in future studies.

Furthermore, compared to the other three lines of cerebral organoids, cKOhet2 cerebral organoids were unable to differentiate into neural progenitors (*Pax6+)* and neurons (*Tuj1+)*. This indicates that the cKOhet2 cell line failed to achieve neural specification, despite its pluripotent characteristics (Figure 4.7). Although expression of pluripotency markers is the standard test to demonstrate pluripotency, an alternative and more stringent pluripotency test via formation of chimeras might be necessary to assess whether cKOhet2 cells can truly give rise to cells of the three germ layers (Martin Gonzalez *et al.*, 2016; Morgani et al., 2017). Therefore, due to the inability of these cells to give rise to neural progenitors and neurons, a functional pluripotency assay such as formation of chimera will be useful in future studies to validate the pluripotency of cKOhet2 cell line.

Consistent with the aim of this study, this chapter demonstrates efficient derivation of ES cells from cortex-specific *Pax6* cKO mice. Although most of the isolated blastocysts were able to propagate in culture (62%), the odds of obtaining at least four karyotypically stable ES cell lines with the correct genotype was only 1/5, which requires more than 20 blastocysts to be isolated. No doubt, expertise in handling the blastocysts is therefore critical and this process was performed by a lab technician (Michael Molinek). However, if this is not available, developing the necessary technical skills could take some time. In addition, maintaining 20 ES cell lines simultaneously prior to genotyping is highly laborious.

As described above, ES cells derived from CD1 mice appeared to be dependent on inhibition of the MEK/Erk pathway. Nevertheless, they were still able to form cerebral organoids in 3D culture, which will assist us to test specific roles of *Pax6* in cortical proliferation. This aim will be covered in the subsequent chapter.

CHAPTER 5: Effects of cortex-specific, acute *Pax6* deletion on the cell cycle of cortical progenitors in cerebral organoids

5.1 INTRODUCTION

In chapter four, we established embryonic stem cell (ES) lines from *Pax6* conditional knock out (cKO) mice, which are able to form cerebral organoids in 3D culture. These ES lines enable us to probe the cerebral organoid system by acutely removing *Pax6* specifically in the cortex-specific region. Therefore, specific roles of *Pax6* in the cortical region of cerebral organoids could be accurately determined, circumventing limitations of the constitutive loss of *Pax6*.

The aim of this chapter is to determine whether *Pax6* plays a role in cortical cell proliferation following its acute loss in cerebral organoids. Although we have previously demonstrated that constitutive loss of *Pax6* altered the LI of cerebral organoids, it appeared that the alteration was in contrast to what was observed in vivo (Mi et al., 2013; Warren et al., 1999). This further suggests the cell cycle regulation underlying *Pax6* control between these two systems might be different.

In vivo, *Pax6* plays a repressive effect on the total cell cycle time (Tc) of cortical progenitors – therefore, in the absence of *Pax6*, the cell cycle is faster, which results in a shorter Tc, as well as G1 phase (Mi et al., 2018; Mi et al., 2013). To induce *Pax6* deletion in the organoid system, firstly we demonstrate optimisation of 4-OHT, a substrate of the $CreER^{T2}$ that will activate *Cre* and subsequently remove *Pax6* from

the system. We then further characterised the activated *Cre*, showing that it is specific to the region expressing the cortex-specific marker, *Emx1,* and that *Pax6* is efficiently deleted. Finally, we compared the cell cycle kinetics of *Pax6* cKO cerebral organoids to the established cell cycle kinetics of *Pax6* cKO mice.

Cell cycle parameters such as the Tc and the length of S-phase (Ts) can be calculated by several techniques, mainly by tracing cells undergoing S-phase (Nowakowski et al., 1989; Martynoga et al., 2005). During S-phase, cells undergo DNA synthesis to prepare for the next phase of the cell cycle and this process can be traced by using thymidine analogues, such as EdU or BrdU. BrdU cumulative labelling is a classic, well-established technique to calculate Ts and Tc, in which the cells were pulsed with BrdU periodically until all of the proliferating cells were labelled (Nowakowski et al., 1989).

This technique is based on several assumptions, including that all of the cells are proliferating, and that they are proliferating at the same rate. However, in the case that not all of the cells are proliferating, the calculation takes into account the proportion of proliferating cells, or the growth fraction (GF). It is also assumed that there is a linear relationship in the type of daughter cells produced, or a steady-state growth (i.e asymmetric differentiation, with half of the daughter cells continuing to proliferate and the other half differentiating). Therefore, a linear regression line can be drawn on the data plot and the GF can be determined (Figure 5.1). Equally, the slope of the linear line is GF/Tc, which is the increase in proportion of labelled cells.

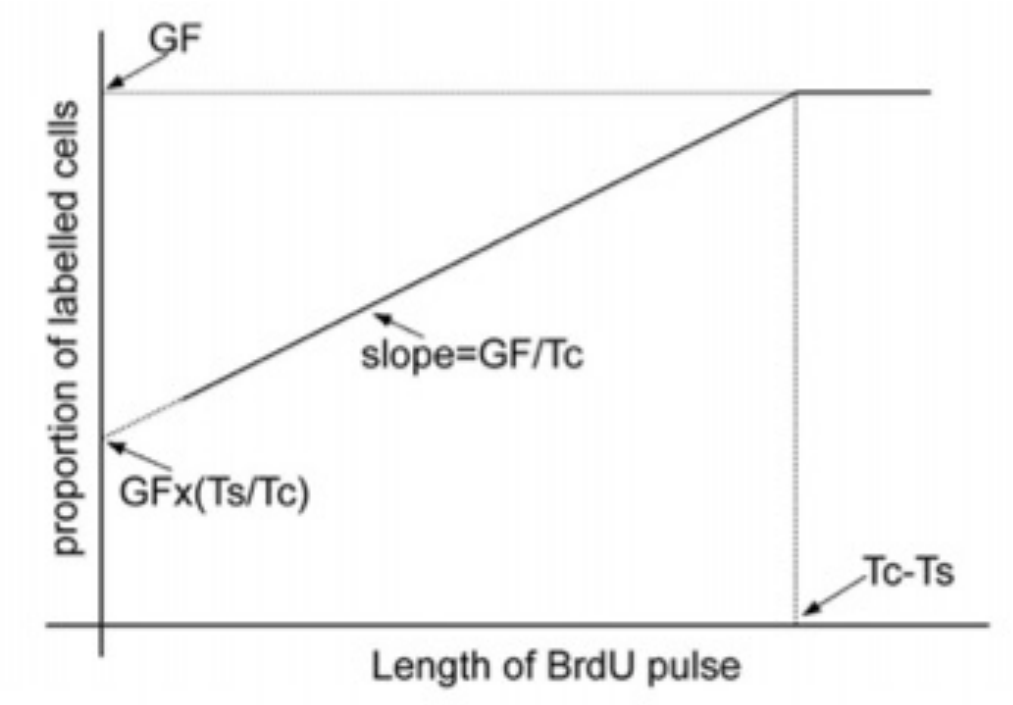

Figure 5.1 Example of graph plotted using data obtained from BrdU cumulative labelling. Calculation of Ts and Tc can be determined from the information obtained from the graph: GF, Tc-Ts, slope and the y-intercept (Estivill-Torrus et al., 2002).

The proportion of cells in S-phase can be determined from the y-intercept of the plot, as it is the proportion of cells taking up the first pulse of BrdU (Ts/Tc). Thus, information obtained from the graph (GF, GF/Tc, y-intercept and Ts/Tc) can be used to calculate the Tc and Ts.

To date, there are no published findings on cell cycle parameters for cerebral organoids derived from mouse ES cells. Therefore, exploration of these parameters is significant, as a first step to recognise the extent to which the cerebral organoid system can model the cerebral cortex at the molecular level.

5.2 RESULTS

5.2.1 Optimisation of 4-OHT treatment

To test the efficiency of *CreER*^{T2} activation in *Pax6* cKO cerebral organoids, two different concentrations of 4-OHT (1 μM and 2 μM) across three time points (24, 48, 72 hours) were compared. In this experiment, two ES cell lines were selected as representatives of each genotype, namely cKOhom1 and cKOhet1 lines. Organoids were collected at day eight and immunolabelled with GFP, which reports on *CreER*^{T2} (Figure 4.1), and the percentage of NE area expressing *CreER*^{T2} (GFP) was then quantified using ImageJ.

Quantitative analysis showed that there was a decrease in the proportion of NE area expressing GFP upon prolonged treatment of 4-OHT (Figure 5.2A). Treatment with 1 μM 4-OHT showed that the GFP+ area was ~30% after 24 hours, followed by a slight decrease at 48 hours, which further decreased to 25% at 72 hours. A similar trend was observed with the 2 μM 4-OHT treatment, as GFP+ area was 31% at 24 hours, and further decreased to ~25% at 48 hour. No data was taken at 72 hours as the NE tissues were damaged, suggestive of tamoxifen toxicity (Figure 5.2B).

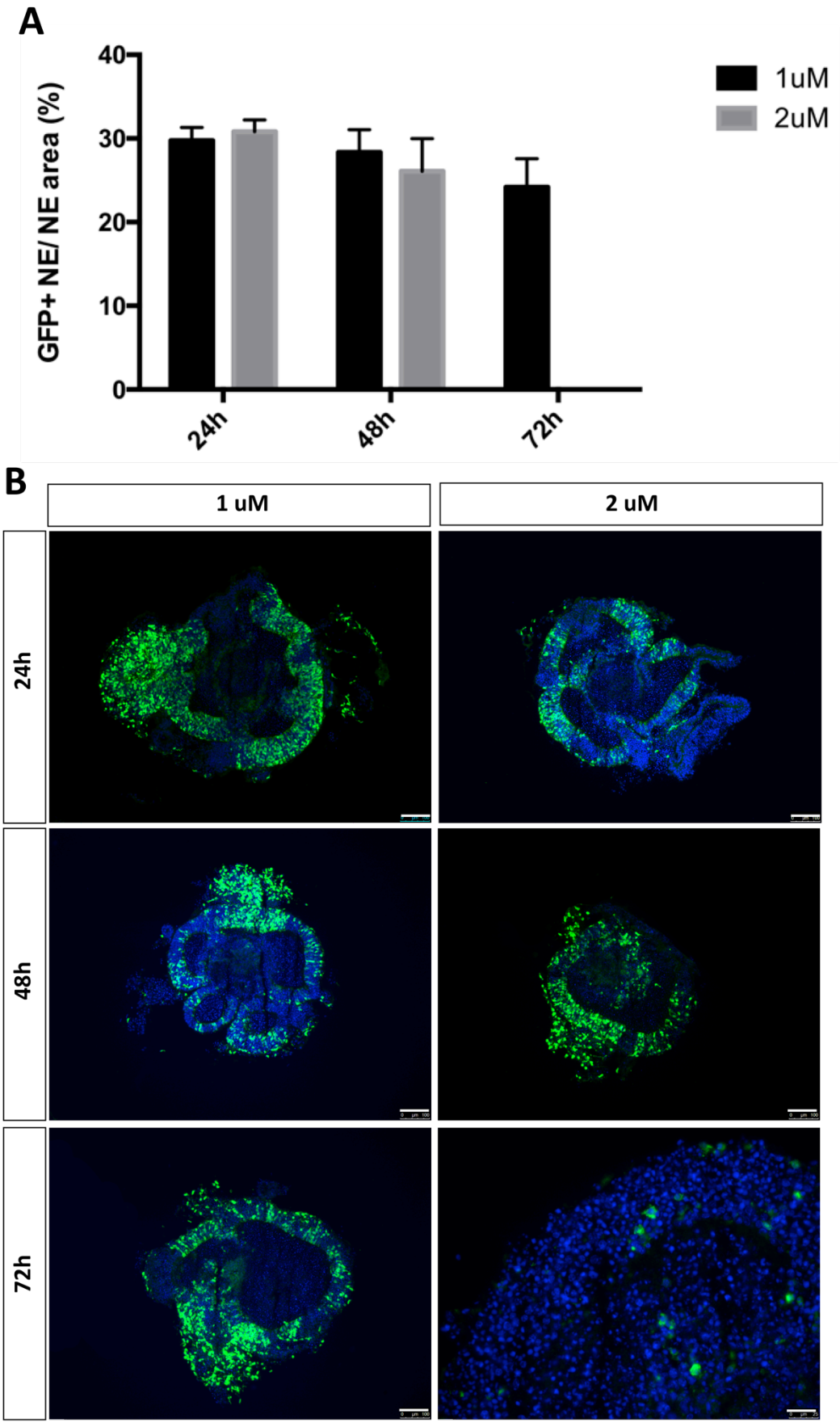
A
GFP+ NE/ NE area (%)
40
30
20
10
0
24h
48h
72h
1uM
2uM
B
1 uM
2 uM
24h
48h
72h

Figure 5.2 Comparison between 1 µM and 2 µM 4-OHT treatment at 24, 48, and 72 hours, on the activation of *Cre* (GFP) in cerebral organoids. (A) Quantitative analysis of GFP+ NE area of cKOhom1 cerebral organoids shows no significant difference between 1 µM and 2 µM 4-OHT treatment, with 24 hours of treatment sufficient to activate *Cre*. Data presented as means ± SEM. (B) Representative images of cKOhom1 cerebral organoids in the three different 4-OHT treatments, with 2 µM 4-OHT for 72 hours show damaged tissue. Scale bar: all 100 µM, except 2 µM,72h: 25 µM.

Although there was no significant difference between these conditions (ANOVA, $p>0.05$, n.s), it is evident that prolonged 4-OHT treatment did not significantly increase *Cre* activation, with some indication of 4-OHT toxicity at a higher dose (2 μM). Therefore, 1 μM 4-OHT for 24 hours was used in subsequent experiments.

Interestingly, despite the presence of a *Cre* reporter allele (Figure 4.5) and the expression of *Emx1* in both sets of cerebral organoids, activation of Cre can only be detected in cKOhom1 but not in cKOhet1 (Figure 5.3).

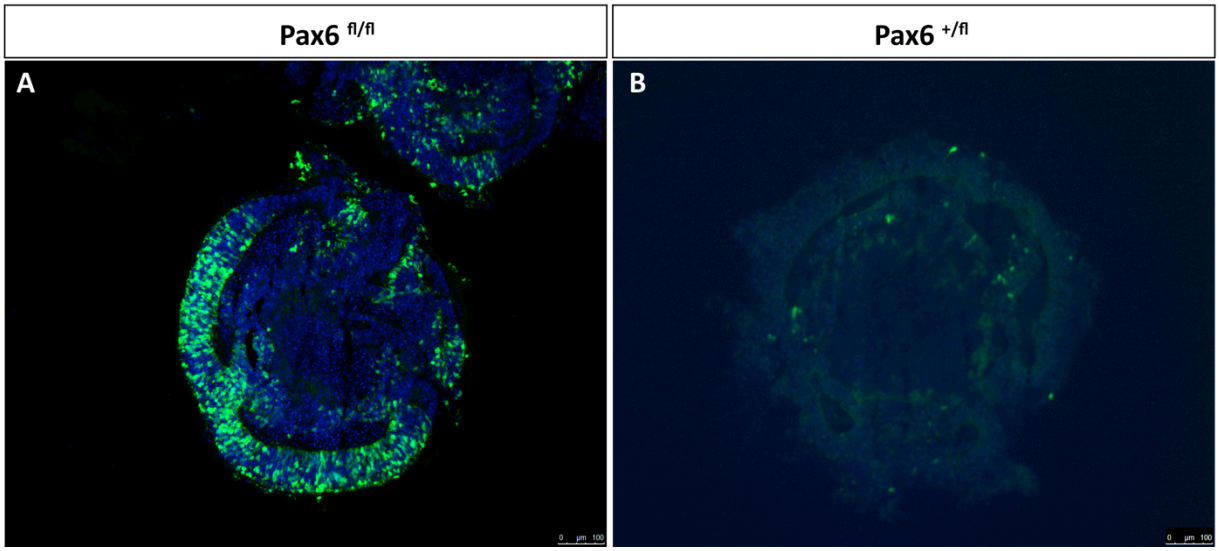

Figure 5.3 Activation of *Cre* (GFP+) in cKOhom1 and cKOhet1 cerebral organoids. (A) Representative image of cKOhom1 organoids (*Pax6*$^{fl/fl}$) showing the presence of GFP+ cells and (B) cKOhet1 organoids (*Pax6*$^{+/fl}$) with no GFP+ cells detected (n=3). Scale bar: 100 µm.

5.2.2 Effect of 4-OHT on cell proliferation in *Pax6* cKO organoids

To ensure that the observed effects were due to acute loss of *Pax6*, and not due to other factors such as 4-OHT, the percentage of proliferating cells (Ki67+) in cerebral organoids treated with 4-OHT were compared to the untreated ones (Figure 5.4).

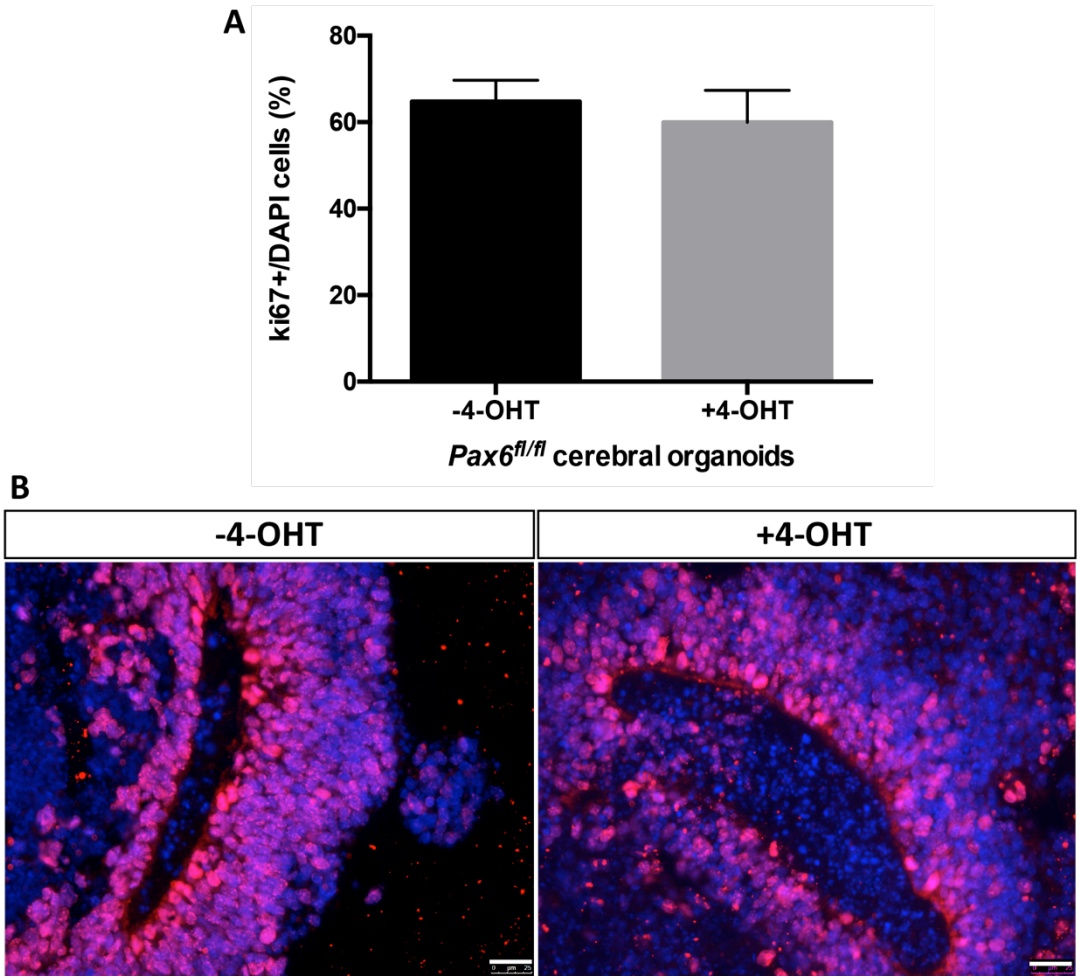

Figure 5.4 Percentage of proliferating cells in the cKOhom1 (*Pax6*$^{fl/fl}$) cerebral organoids. (A) Organoids with or without 4-OHT treatment show no significant difference in the percentage of proliferating cells (Ki67+). Data are mean±SEM of organoids from four independent experiments ($p<0.05$, unpaired t-test, not significant). (B) Representative image of organoids with and without 4-OHT, labelled with Ki67. Scalebar: 25 µm.

Quantitative analysis of Ki67+ cells showed that only 65% of cells in the NE of untreated organoids were proliferating (Figure 5.4A), which is 25% lower than the number of proliferating cells in the E12.5 embryonic cortex (Caviness et al., 1995; Estivill-Torrus et al., 2002). Interestingly, a similar percentage of proliferating cells was also found in human cerebral organoids (60%), suggesting a consistent percentage of proliferating cells in the organoid systems regardless of the species difference (Matsui et al., 2017). Therefore, the lower percentage of proliferating cells in the organoids may be due to a difference between the 3D in vitro and in vivo systems.

Nevertheless, proliferating cells in the 4-OHT-treated cerebral organoids were comparable to the untreated ones (control), indicating that no significant effect was observed in cerebral organoids treated with 1 μM 4-OHT for 24 hours (unpaired t-test, $p>0.05$, n.s). Taken together, this condition is suitable in the activation of *Cre* (Figure 5.2A) with no concomitant toxicity to the proliferating cells.

5.2.3 Characterisation of CreER^{T2} expressing (GFP+) cells

Following successful activation of *CreER*^{T2} as reported by GFP, the GFP+ cells of cKOhom1 and cKOhom2 cerebral organoids were further characterised. Both of these organoids are of *Pax6*$^{fl/fl}$*; Emx1-CreER*^{T2}*; RCE* genotype and were treated with 1 μM 4-OHT for 24 hours, and collected at day eight.

Consistent with previous observations, GFP immunolabelling showed cells expressing *Cre* (GFP+) in a mosaic pattern (Figure 5.5B). Quantification of GFP-expressing cells

in the GFP+ NE further demonstrated a low proportion of GFP+ cells in the NE (Figure 5.5A), thus further supporting the observed *Cre* mosaicism. *Cre* mosaicism resulted in two subpopulations of cells in the NE, the majority of which were GFP- cells (control), while the remaining was the GFP+ cell population.

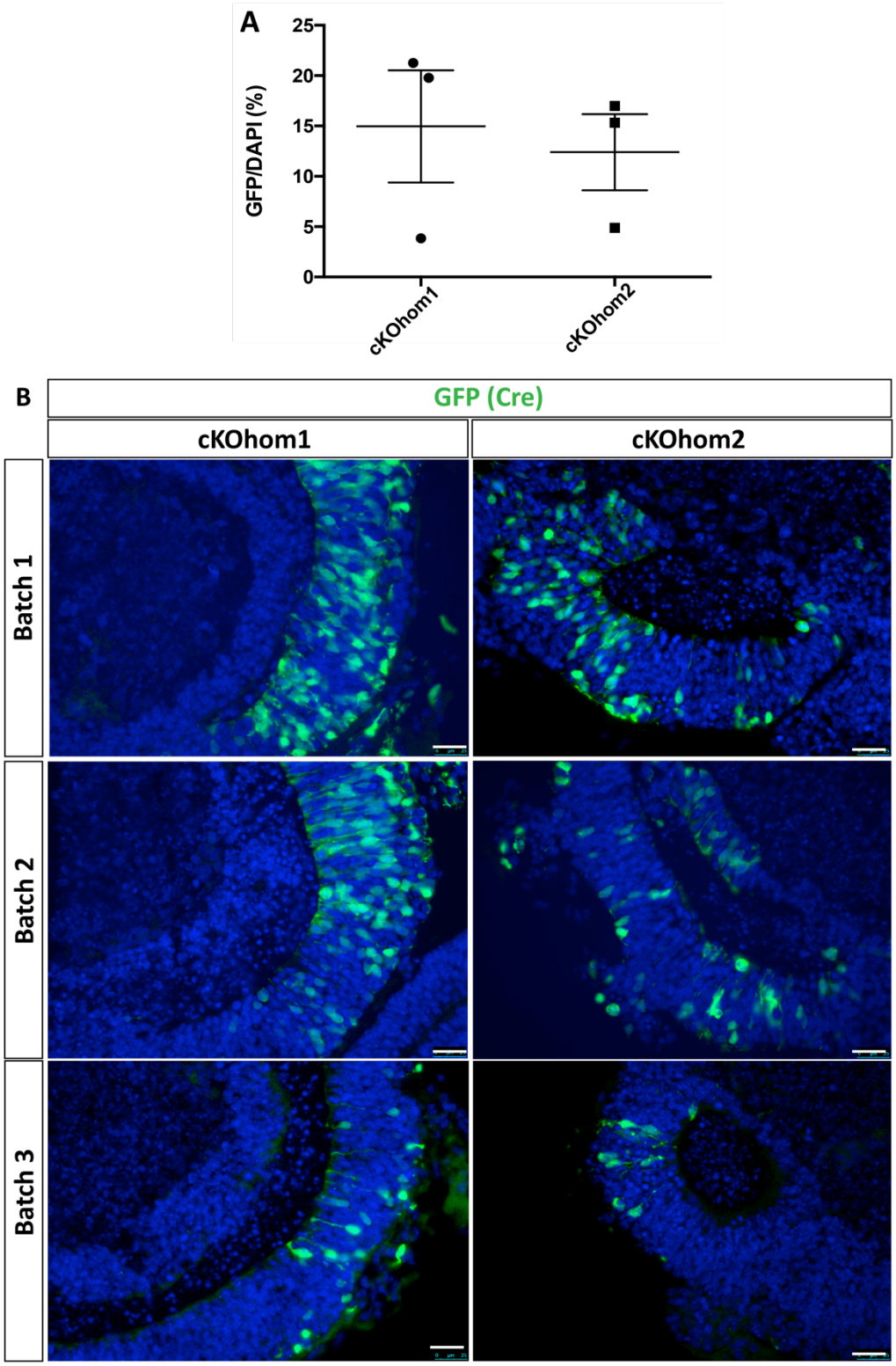

Figure 5.5 Quantitative analysis of GFP+ cells in cKOhom1 and cKOhom2 cerebral organoids. (A) NE of cKOhom1 and cKOhom2 organoids show comparable percentage of GFP+ cells. (B) Representative image of NE labelled with GFP from three different batches. Scalebar: 25 µm.

As *CreER*^{T2} is driven by the *Emx1* promoter, it is possible that *Cre* mosaicism was due to mosaic expression of *Emx1*. To confirm this and to validate whether these *Cre*-expressing cells (GFP+) accurately reflect the endogenous expression of *Emx1*, 4-OHT-treated cerebral organoids were double-labelled with *Emx1* in situ and GFP antibody. Quantitative analysis of the GFP+ cells of cKOhom1 showed 92% of these cells co-localised with *Emx1* (n=3 batches), suggesting the expression of GFP reflected the expression of endogenous *Emx1* (Figure 5.6A,B). However, due to the mosaic pattern of GFP+ cells, there were *Emx1*-expressing cells without the expression of GFP (arrowhead, Figure 5.6A'', B''). Therefore, *Emx1*+ NE consists of two cell populations, including GFP+ and GFP- cells.

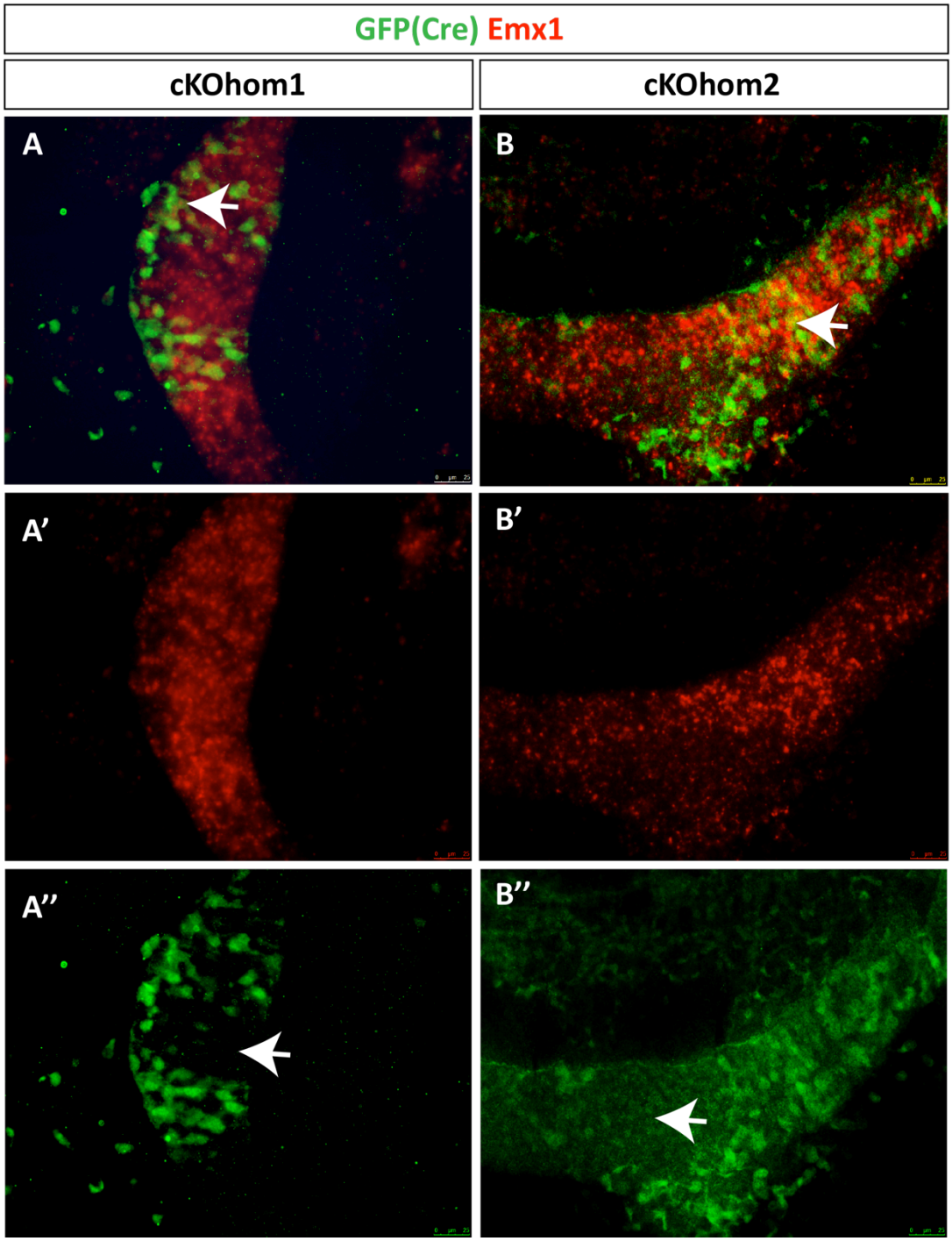

Figure 5.6 Expression of *Emx1* and GFP (Cre) in cKOhom1 and cKOhom2 cerebral organoids. (A, B) Representative images of cKOhom1 and cKOhom2 organoids labelled with *Emx1* and GFP show co-localisation between these two markers. (A'', B'') However, due to the mosaic expression of GFP, there are *Emx1*+ cells that do not activate Cre (GFP-, arrowhead). Scale bar: 25 µm.

Having established co-localisation between the expression of GFP and *Emx1*, we then determined whether the *Cre*-expressing cells (GFP+) successfully deleted *Pax6* by performing double labelling with GFP and Pax6 antibodies. Indeed, these two markers appeared to be exclusively expressed (arrowhead, Figure 5.7A-D). Quantitative analysis of cKOhom1 organoids confirmed that 98% of the GFP+ cells did not express *Pax6*, which suggests successful and efficient deletion of *Pax6* in the *Cre*-expressing cells.

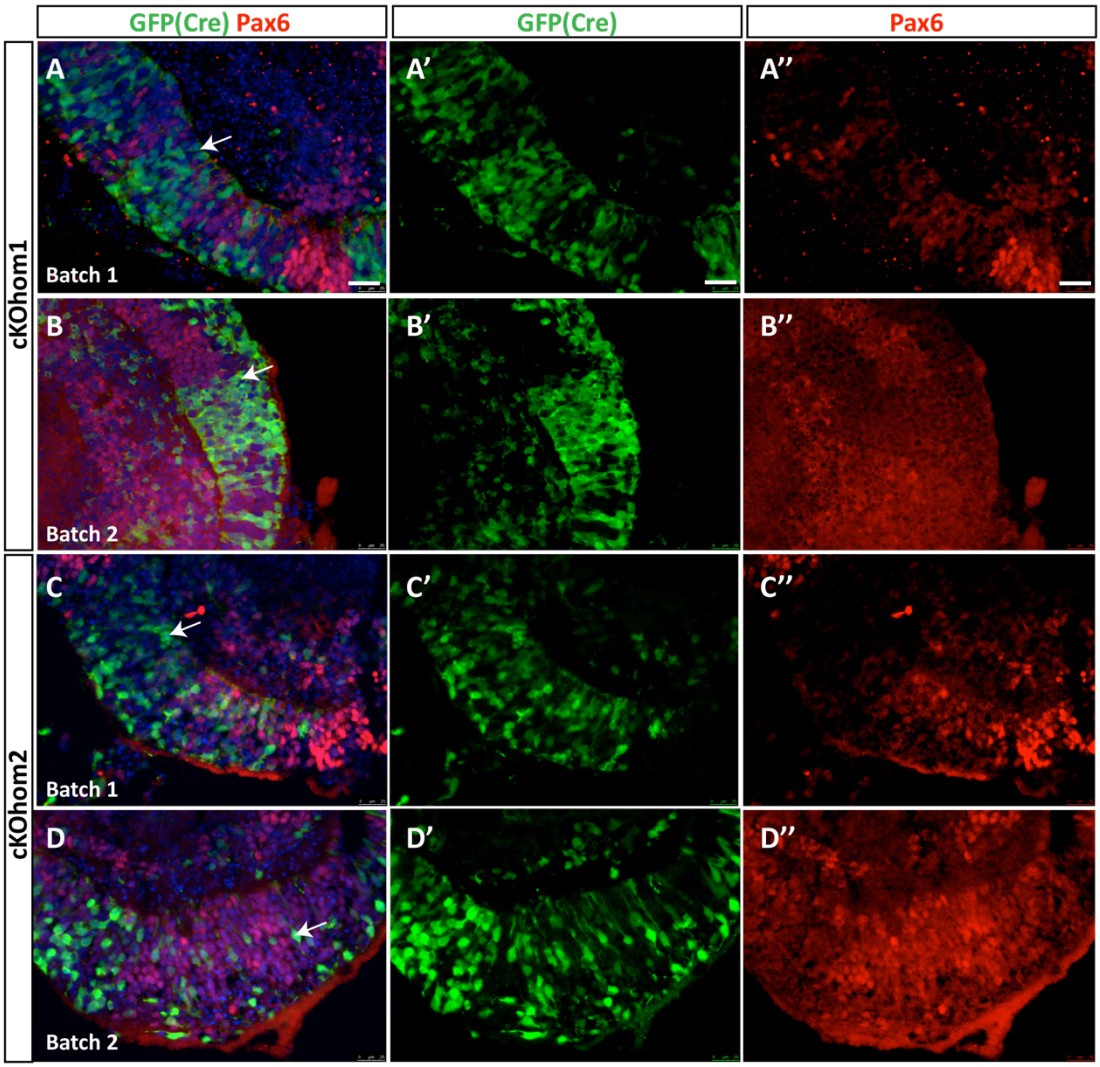

Figure 5.7 Deletion of *Pax6* in Cre-expressing cells (GFP+). (A, B) Representative images of cKOhom1 (C, D) and cKOhom2 organoids labelled with GFP and Pax6 show exclusive expression of these two markers (arrowhead). Scalebar: 25 µm.

Taken together, 4-OHT-treated *Pax6* cKO organoids resulted in two populations of cells in *Emx1*+ NE, with successful deletion of *Pax6* in the GFP+ cells. This allows comparison between GFP+ and GFP- cells in subsequent experiments.

5.2.4 Acute *Pax6* deletion does not alter the labelling index

To determine the effect of acute cortex-specific *Pax6* deletion on cortical progenitor proliferation of cerebral organoids, the proportion of cells in S-phase (EdU+) or labelling index (LI) of EdU+ cells of GFP+ and GFP- cells (control) in cKOhom1 and cKOhom2 organoids were examined. Quantitative analysis showed a non-significant decrease in the LI of GFP+ cells compared to the GFP- cell population (Figure 5.8A).

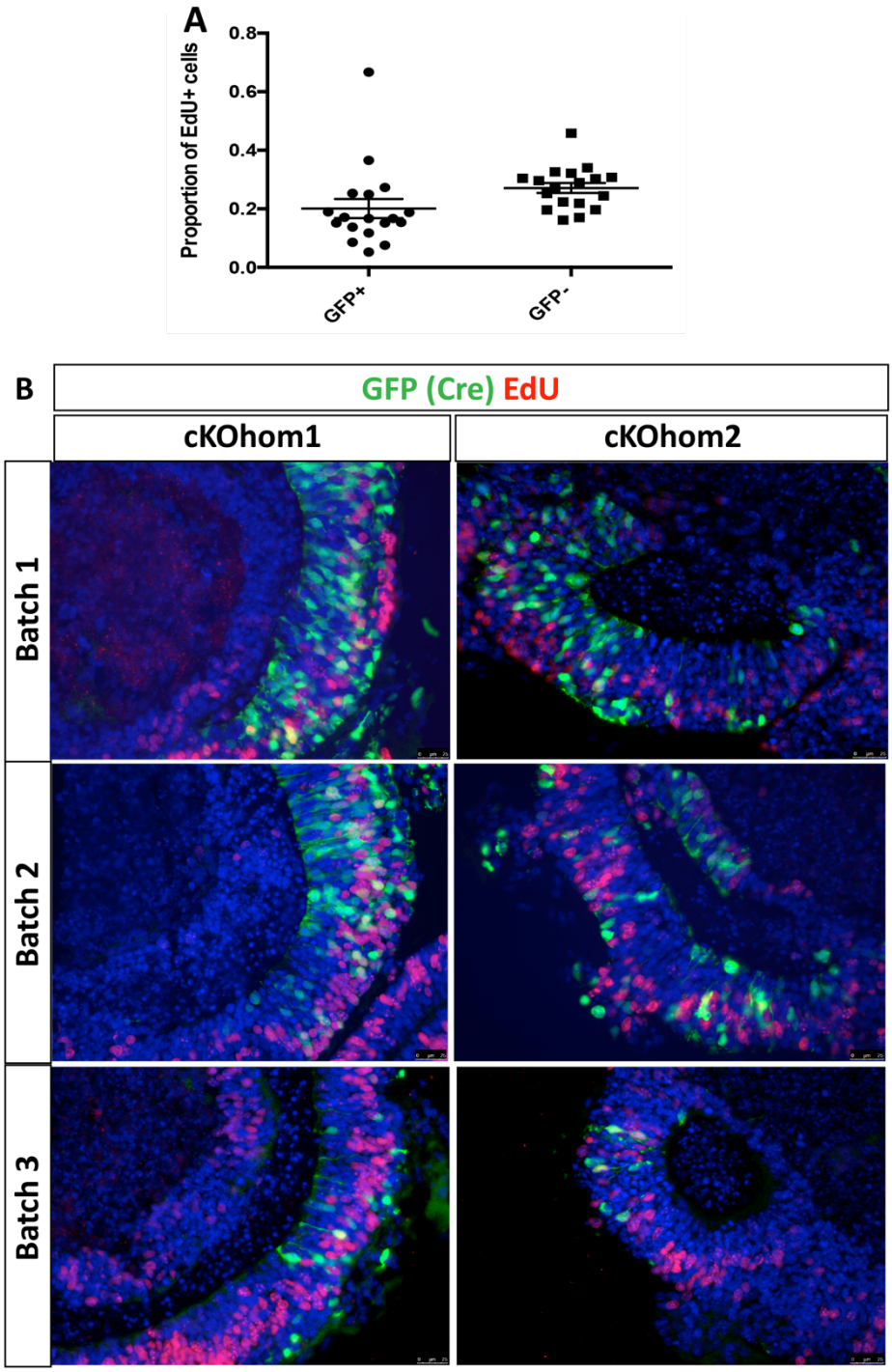

Figure 5.8 Labelling index (LI) of GFP+ and GFP- cells of both cKOhom1 and cKOhom2 cerebral organoids. (A) GFP+ cells showed a non-significant decrease in LI compared to control (GFP-) cell. Means are presented as SEM ($p>0.05$, t-test, n.s). (B). Representative images of cKOhom1 and cKOhom2 cerebral organoids labelled with GFP and EdU. Scalebar: 25 µm.

Although the difference was not significant (t-test, p>0.05, n.s), the decreased LI was consistent with the LI observed in Pax6$^{-/-}$ cerebral organoids (chapter three). The subtle difference found in the *Pax6* cKO organoids might be due to the presence of control cells (GFP-) next to the mutant cells (GFP+) – which might influence cell proliferation of the mutant cells.

Nevertheless, both constitutive and acute loss of *Pax6* in cerebral organoids resulted in a decreased LI, in contrast to the increased LI of both *Pax6*$^{-/-}$ and *Pax6* cKO mutant embryos (Mi et al., 2013; Warren et al., 1999). LI analysis estimates the proportion of cells in S-phase, without information on the cell cycle kinetics such as the cell cycle length. Therefore, to address whether this discrepancy is due to changes in the cell cycle kinetics, we then determined the total cell cycle time (Tc) and the length of S phase (Ts) of the GFP+ and GFP- cells.

5.2.5 Acute *Pax6* deletion does not alter cell cycle length

To calculate cell cycle time (Tc), cumulative EdU labelling was performed on both cKOhom1 and cKOhom2 cerebral organoids every two hours in a total of five time points (Figure 5.9).

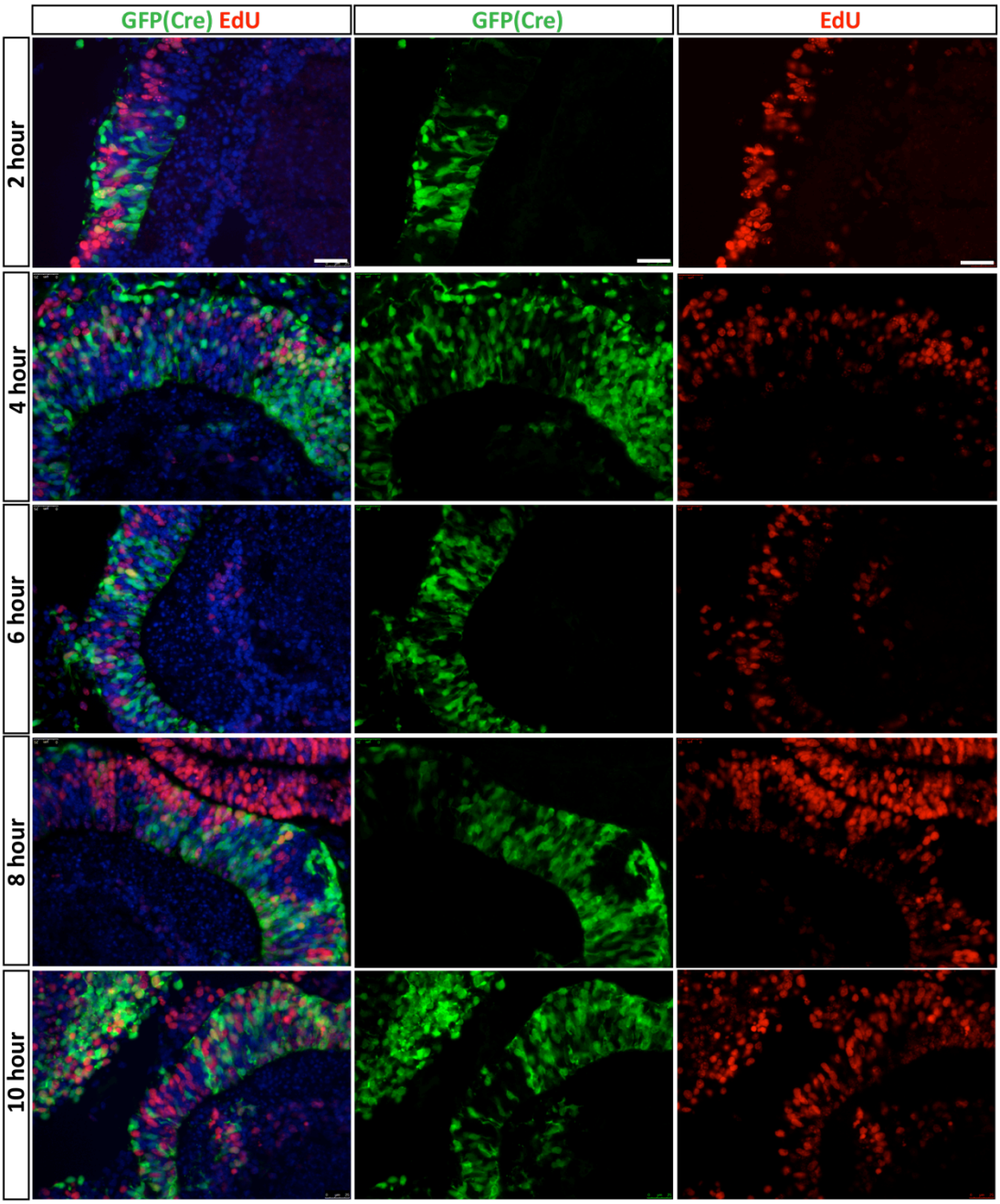

Figure 5.9 Representative images of cerebral organoids taken every two hours of cumulative EdU labeling, labelled with GFP and EdU. Scalebar: 25 µm.

The organoids were collected at day 8, labelled with GFP and EdU and the proportion of EdU+ cells of both GFP+ and GFP- cells was calculated (Appendix B) and plotted (Figure 5.10).

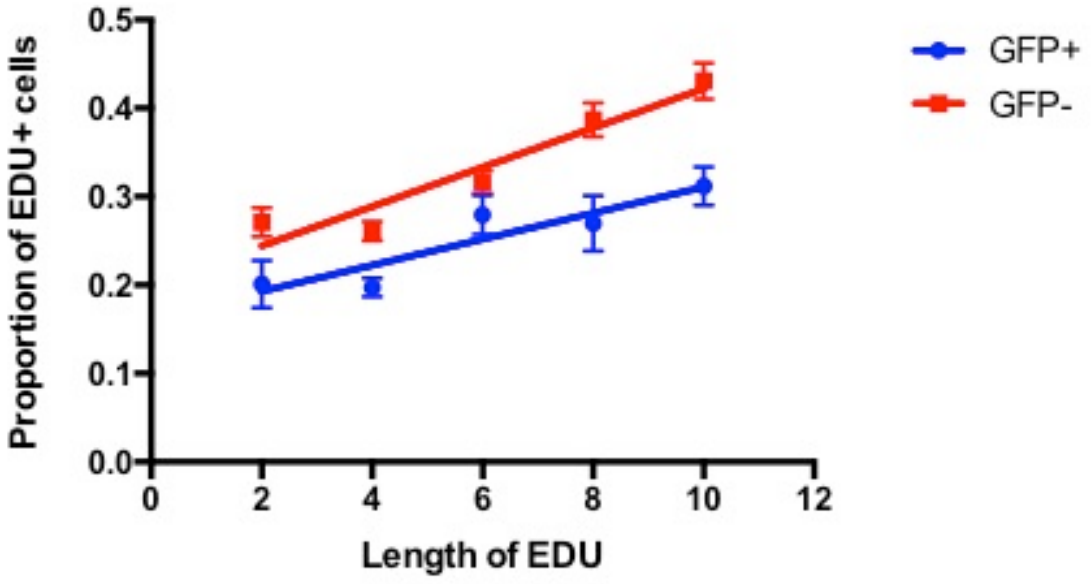

Figure 5.10 Graph of the cumulative EdU labelling in cKOhom1 and cKOhom2 cerebral organoids. Proportions of EdU+ cells in both GFP+ and GFP- cells increased over time and data were presented as means±SEM (n=6). Cell cycle parameters were extrapolated from the trendline and equation obtained from the least square fit analysis; y= 0.0147x + 0.1634 (GFP+) and y= 0.0222x + 0.1998 (GFP-).

The graph plotted follows the protocol described in (Nowakowski et al., 1989), which allows determination of the proportion of proliferating cells or growth fraction (GF), the total cell cycle time (Tc) and the length of S phase (Ts). Calculation of the Tc and Ts of GFP+, GFP-, as well as the established Tc and Ts of E12.5 cortical progenitors (Takahashi et al.,1995; Estivill-Torrus et al., 2002) is summarised in Table 5.2.1.

Table 5.2.1 Calculation of cell cycle kinetics of GFP+ and GFP- cells

	GFP- (control)	GFP+ (*Pax6*$^{fl/fl}$)	E12.5 cortex (wt)
GF	0.43	0.3	1.0
Tc (hour)	19	20	12
Ts (hour)	9	11	4.5

Interestingly, the GF of GFP- cells was lower than the GF of E12.5 cortical progenitors, which suggests that cerebral organoids have a lower proportion of proliferating cells compared to embryonic cortex.

On the other hand, GFP+ cells showed lower GF than the control (GFP- cells), suggesting a decrease in proliferating cells following acute *Pax6* deletion. In addition, the Tc of GFP+ cells was slightly longer by 10% than the Tc of control cells (t-test, $p>0.05$, n.s). This subtle effect might be due to the presence of both cell populations (GFP+ and GFP- cells) next to each other. Therefore, effects from the loss of *Pax6* in GFP+ cells might be compensated by the external cues from the control cells (GFP-), indicating a non-cell autonomous effect of *Pax6* in cell proliferation.

Although acute cortex-specific *Pax6* deletion in the organoids does not alter the cell cycle length, this phenotype is similar to the findings of Mi Da et al., 2013, which showed no significant changes in the Tc of regions expressing low levels of *Pax6* (caudo-medially), following acute *Pax6* deletion. However, due to the heterogenous expression of *Pax6* in the untreated organoids, it is not possible to determine whether the GFP+ cells were also expressing low levels of *Pax6* prior to treatment with 4-OHT (Figure 5.2). Furthermore, it was difficult to determine the regional identity of the organoids, due to the lack of developmental axes.

In addition, there was also no significant change in the length of S-phase between GFP+ and GFP- cell populations. Therefore, acute deletion of *Pax6* does not alter the cell cycle length of cortical progenitors in cerebral organoids. As *Pax6* control is very complex and context-dependent, this finding will be discussed further in the following section.

5.3 DISCUSSION

Results presented in this chapter provided insights into the effects of acute *Pax6* deletion in cerebral organoids, particularly into the effects on cell cycle kinetics.

5.3.1 Optimum conditions for *CreER^{T2}* activation in cerebral organoids

Our *Pax6*cKO cerebral organoids has enabled spatio-temporal control of *Pax6* deletion, which circumvents the limitations of constitutive loss of *Pax6* – thus the roles of *Pax6* can be more accurately determined (Georgala et al., 2011; Mi et al., 2018). This control requires optimisation of 4-OHT treatment, in order to induce *CreER^{T2}* activation, as well as *Pax6* deletion. This inducible system has been successfully used in mouse, with efficient activation of *CreER^{T2}* after 48 hours, followed by loss of detectable Pax6 protein after 72 hours (Mi et al., 2013).

We found that *CreER^{T2}* activation in cerebral organoids occurs at a relatively faster rate, which is 24 hours earlier than *CreER^{T2}* activation in vivo (Figure 5.2). This is consistent with the activation of *Cre* another in vitro study that used the same system in ES cells (Vallier et al., 2001). This rapid activation is due to the use of 4-OHT, a tamoxifen metabolite; which eliminates the intermediate stage of tamoxifen conversion to 4-OHT, that caused the lag in CreER^{T2} activation in vivo (Felker et al., 2016).

Furthermore, prolonged treatment with 4-OHT appears to have no significant effect on *CreER^{T2}* activation in vitro (except at high higher dosage i.e. 2 μM, Figure 5.2),

suggesting the direct action of 4-OHT in vitro at 24 hours, which further supports rapid activation of *CreER*^{T2}. This direct and rapid effect in vitro may be due to the instability of 4-OHT, as its potency is reduced in prolonged cell culture (after 48 hours) due to isomerisation into cis-4-OHT, an isoform with lower affinity to *CreER*^{T2} (Katzenellenbogen et al., 1984).

Although activation of *Cre* with 1uM 4-OHT is comparable to 2 μM, without concomitant toxicity, we found that 2 μM 4-OHT at 72 hours was detrimental to the organoids, evident from the damaged organoid tissue in this condition (Figure 5.2B). This could be due to 4-OHT toxicity leading to a high level of *Cre* expression, which has been shown to induce apoptosis, DNA damage and aneuploidy (Gauduchon et al., 2005; Loonstra et al., 2001; Schmidt-Supprian and Rajewsky, 2007). Therefore, it may also be informative in future studies to determine possible toxicity effects of 4-OHT by determining the percentage of apoptosis in the organoids.

The safe use of 1 μM 4-OHT is further supported by the comparable percentage of proliferating cells between organoids treated with 1 μM 4-OHT and untreated organoids (Figure 5.4). Interestingly, it appears that there are fewer proliferating cells in (untreated) cerebral organoids (60%) than in the embryonic cortex (90-100%). Our finding is also consistent with the percentage of proliferating cells reported in human cerebral organoids, despite the species difference (Matsui et al., 2017). Considering the simple set up of the in vitro system, it is possible that the reduced proliferating cells in cerebral organoids could be due to the use of minimal medium that may lack the required factors pertinent to cell proliferation. For example, cerebrospinal fluid (CSF) has been shown to influence the growth of cortical progenitors in the cerebral

cortex (Lehtinen et al., 2011). This fluid is rich with signalling molecules that play significant roles in the proliferation and survival of cortical progenitors, which may be absent in the minimal medium used in vitro.

5.3.2 *CreER^{T2}* activation in cerebral organoids is mosaic

One of the caveats of Cre-Loxp technology observed in this study is *Cre* mosaicism, which is evident from the low proportion of *Cre*-expressing cells (GFP+) in the organoids NE, in a sporadic fashion (Figure 5.6). Furthermore, although these GFP+ cells reflected the endogenous expression of *Emx1*, Emx1/GFP double labelling showed that there were *Emx1*+ cells without co-expression with GFP (Figure 5.6 A'', B'').

Cre mosaicism suggests that *Cre* activation may be incomplete, due to its inconsistent and variable activity between tissues in a single litter (Eckardt et al., 2004; Heffner et al., 2012). In the context of a 3D in vitro culture, it is possible that the inconsistent *Cre* expression may be due to the influence of mass transfer diffusion. Established studies have shown that the concentrations of oxygen and cytokines are lower at the core centre of 3D in vitro structures, which subsequently influences the niche and differentiation efficiency, resulting in heterogeneity (Van Winkle et al., 2012). Thus, the 3D structure of organoids and their lack of vasculature could result in heterogenous uptake of 4-OHT, as the diffusion of 4-OHT at the surface may differ from the centre of organoids, forming a concentration gradient within the 3D structure. Agitation has been shown to improve mass transfer within the 3D in vitro structure, therefore it may be necessary to use agitation to ensure a more homogenous

uptake of 4-OHT in the organoids, which may impact the expression of *Cre* (Carpenedo et al., 2007).

Inconsistent *Cre* activity is also evident between littermates (Heffner et al., 2012), which might explain the undetected *Cre* activity in the cKOhet1 organoids (Figure 5.3). cKOhet1 is a littermate to cKOhom1, as they were derived from the same dam in batch 115 (table 4.1). Although there is another cell line with $Pax6^{+/fl}$ genotype from batch 115 (Figure 4.5B), the cell line does not express *Cre*, thus hampers its utility.

In another note, a study has shown that genomic PCR is able to detect inactivated *Cre,* which could be a consequence of multiple recombination events after consecutive generations (Schulz et al., 2007). Therefore, it is plausible that the undetectable activation of *Cre* in cKOhet1 organoids could be due to a false positive genotype, detected by genomic PCR (Figure 4.5). It would therefore be necessary in future studies to re-assess the result by checking the *Cre* mRNA transcripts by RT-PCR.

Nevertheless, this confounding result would complicate subsequent experiments. Therefore, an alternative method is to take advantage of the *Cre* mosaicism and use the neighbouring *Cre* negative cells (GFP-) in the NE as an isogenic control.

5.3.3 Effect of acute *Pax6* deletion on cortical progenitor proliferation

One of the important roles of *Pax6* in cortical development is in cell proliferation, demonstrated by the altered labelling index (LI) in both $Pax6^{-/-}$ and *Pax6* cKO mouse models (Mi et al., 2013; Warren et al., 1999). LI measures the proportion of DNA-

synthesising cells through incorporation of a thymidine analogue such as EdU, therefore it is an estimate of cells undergoing S-phase, indicative of proliferative activity.

Here we present the effect of acute, cortex-specific *Pax6* deletion on the organoids' cortical proliferation. We showed that cortex-specific *Pax6* deletion resulted in a decreased LI compared to control (Figure 5.8), consistent with the effect seen in the LI of $Pax6^{-/-}$ cerebral organoids (chapter three). However, despite the consistent trend in both constitutive and conditional *Pax6* mutant cerebral organoids, it is important to note that the decreased LI in the latter is not significant. This subtle effect might be due to the observed *Cre*-mosaicism, as the mutant cells (GFP+) are surrounded by control cells (GFP-), which may influence cell proliferation.

This consequently may indicate a non-autonomous (indirect) requirement of *Pax6* in cortical proliferation of organoids, which is important in distinguishing between the primary and secondary defects of *Pax6* (Talamillo et al., 2003). For instance, the cell autonomous requirement of *Pax6* has been demonstrated in chimera studies, which show that *Pax6* is required autonomously for several cellular processes, such as production of cortical progenitors in the correct number, expression of the basal progenitor marker, *Tbr2*, neuronal migration, and the correct level of *Pax6* in cell proliferation (Manuel et al., 2006; Quinn et al., 2007; Talamillo et al., 2003). Chimeras consist of cells of two different genotypes; for example, normal ($Pax6^{+/+}$) and $Pax6^{-/-}$ mutant cells, which allows the analysis of $Pax6^{-/-}$ cells in a normal niche. If the abnormal characteristics of $Pax6^{-/-}$ cells persist despite the normal environment, and the presence of neighbouring normal cells could not influence the abnormalities

of *Pax6*$^{-/-}$ cells, this indicates a cell autonomous requirement of *Pax6*. On the contrary, non-significant defects in the mutant cells in the presence of *Pax6*$^{+/+}$ cells (normal niche) indicates that *Pax6* is required non-autonomously in cell proliferation.

Therefore, as there is no significant change in the LI of GFP+ cells, this suggests that *Pax6* may be cell non-autonomously required in cortical proliferation of organoids, and that the proliferation defect is secondary. In addition, the non-altered LI in the *Pax6* cKO organoids also corresponds to the LI of caudo-medial region of *Pax6* cKO mice (Mi et al., 2013). It is well established that *Pax6* control in cortical proliferation is regional, as acute deletion of *Pax6* only affects the rostro-lateral region where *Pax6* is highly expressed, whereas there is no significant change in the LI of caudo-medial region where *Pax6* expression is relatively low (Mi et al., 2013). Therefore, it is possible that *Pax6* expression in the organoids is relatively low, prior to acute deletion of *Pax6*. Unfortunately, due to the lack of axes and heterogenous nature of the organoids, this would be difficult to demonstrate.

Another possible explanation underlying the abnormal LI would be a difference in cell cycle kinetics between the two systems, which will be discussed in the following section.

5.3.4 Cortical progenitors of cerebral organoids cycle longer with comparable S-phase length to embryonic cerebral cortex

Despite rapid developments in the field of organoids, little is known about their cell cycle kinetics. Cell cycle regulation is fundamental to tissue morphogenesis, and any errors in the kinetics could lead to abnormalities and diseases such as, cancer (Cecchini et al., 2012).

Due to the established role of *Pax6*'s in cell proliferation, it is plausible that cell cycle kinetics can account for the differences observed between organoids and their matched in vivo counterparts. For example, we know there is an altered LI in constitutive and conditional *Pax6* mutant cortical progenitors, which indicates a change in the proportion of cells in S-phase. However, there is insufficient information to address why or how this change occurs.

In vivo findings have confirmed that the altered LI following acute loss of *Pax6* is due to a decrease in cell cycle time (Tc) as well as in G1 phase, which results in rapid cell proliferation (Mi et al., 2018; Mi et al., 2013). However, it is important to note that *Pax6* exerts its effect in a regional fashion, and this change is specific to the rostro-lateral region, where *Pax6* is highly expressed, but not in caudo-medial region, where *Pax6* expression is low (Mi et al., 2013). Therefore, as there is no significant change in the LI of GFP+ cells in *Pax6* cKO cerebral organoids, which is similar to the acute loss of *Pax6* in the caudo-medial region, we anticipate that their cell cycle time is not affected.

Cumulative EdU labelling was used to calculate the total cell cycle time (Tc) and the length of S-phase (Ts) of both *Pax6* mutant (GFP+) and control cells (GFP-). Interestingly, the control cells (GFP-) show longer Tc (19h) than the matched E12.5 *Pax6* cKO mice control cells (12h), which suggests that cortical progenitors in organoids cycle at a slower rate than in vivo. As the length of S-phase between these two types of control cells are remarkably similar (i.e. 4h in GFP- cells and 4.5h in *Pax6* cKO control cells), the lengthening of Tc in cerebral organoids could be due to the lengthening of other cell cycle parameters, such as G1 phase.

It is well established that G1 phase is associated with cell fate decisions and differentiation (Julian et al., 2016). Studies using pluripotent stem cells show that these cells have characteristically truncated G1 and G2 phases, suggesting that they proliferate rapidly. However, as they differentiate into other types of cells, G1 and G2 phase become longer and recent studies have shown that the expression of developmental genes is highest/most concentrated at G1 phase, suggesting that stem cells are more susceptible to signals promoting differentiation/commitment in this phase (Singh et al., 2013). This is consistent with the studies in cerebral cortical cells, which consist of two types of progenitors with distinct length of G1 phase. The apical progenitors are the primary progenitors that maintain the progenitor pool by symmetrical division, as well as giving rise to the secondary progenitor pool (basal progenitors) by asymmetrical division. On the other hand, basal progenitors have a relatively longer G1 phase and mainly give rise into neuronal cells (Calegari et al., 2005). Therefore G1 is a critical window for the balance between cell proliferation/differentiation, as cells are more responsive to specification cues in this period.

Given that the proportion of non-proliferating cells in the organoids is higher than in the embryonic cortex (Figure 5.4), it is possible that most of cortical progenitors in organoids undergo neurogenic divisions, therefore spending more time in G1 phase, slowing down the proliferation rate. It would therefore be interesting to further confirm this by characterising the G1 phase of the cells, as well as comparing the proportion of apical progenitors (*Pax6+)* and basal progenitors (*Tbr2+)*.

5.3.5 *Pax6* does not regulate cell cycle length of cortical progenitors in cerebral organoids

Interestingly, we found that *Pax6* mutant cells (GFP+) have slightly longer Tc than control (GFP-) cells, though the change is not significant (Figure 5.10). This suggests that cell cycle kinetics in the cerebral organoids are not regulated by *Pax6*, and this is consistent with our previous finding, which demonstrated no significant change in the LI of GFP+ cells (Figure 5.8).

Given the regional effect of *Pax6* in early corticogenesis, this finding is consistent with the acute loss of *Pax6* in the caudo-medial region of the cortex (low expression of *Pax6*), which also shows no significant difference in the Tc (Mi et al., 2013). Therefore, it is possible that cerebral organoids have relatively low *Pax6* expression, which may be insufficient to repress *Cdk6*, a cell cycle regulator that is directly regulated by *Pax6* in the rostro-lateral region (Mi et al., 2018). However, due to the lack of developmental axes and inherent heterogeneity of the organoids, this would be difficult to address, which highlights some of the shortcomings of this complex and heterogenous 3D model.

One of the caveats of the mosaic analysis in this study is that *Pax6* expression in the GFP- cells (control) is also mosaic, resulting in the presence of GFP-*Pax6*- cells in the cortical, Emx1-expressing NE (Figure 5.7). Thus the estimation of cell cycle length in the organoids may be overestimated due to the inclusion of *Pax6*- cells as part of the control.

In addition, a recent finding discovered opposite roles for *Pax6* in the cell cycle of telencephalic and diencephalic progenitors (Quintana-Urzainqui et al., 2018). Acute deletion of *Pax6* in the thalamus showed a decreased LI in the *Pax6*- progenitors, with a corresponding decrease in Tc, compared to control. The contrasting role of *Pax6* between telencephalic and diencephalic tissues is due to the presence of *Foxg1*, a transcription factor expressed in telencephalic progenitors but not in the diencephalic progenitors. Therefore, it would be interesting to examine the expression of *Foxg1* in these organoids in future studies.

Essentially, our findings further highlight the context-specific and dynamic role of *Pax6* in cell proliferation, which is dependent on its level of expression as well as the specific region of expression. Given this complexity, it is possible that *Pax6* control in cerebral organoids cell proliferation is highly dependent on the types of tissues that exist in this 3D in vitro model, which is heterogenous and requires more detailed characterisation than we previously anticipated.

Taken together, we provide a comparison of the cell cycle kinetics between cerebral organoids and their matched in vivo counterpart. We found that organoids have a longer cell cycle time, which is possibly due to the lengthening in G1 phase – as the

length of S-phase between cerebral organoids and embryonic cortex is remarkably similar. Although it is evident that *Pax6* controls cell proliferation in both of these systems, its role in the cell cycle kinetics of cortical progenitors in organoids seems unclear due to the complication and caveats of the analysis, in addition to *Pax6* function that is highly complex and context-dependent.

CHAPTER 6: DISCUSSION

Previous studies have demonstrated the resemblance of mouse cerebral organoids to mouse embryonic cerebral cortex in many aspects, such as cellular composition, lamination and organisation (Eiraku et al., 2008; Nasu et al., 2012). Furthermore, cerebral organoids can also be established from human pluripotent cells, which allows investigation on human cortical-like tissues that would be otherwise difficult to access. Indeed, most reported studies use human cerebral organoids, which has been extensively optimised and characterised (Lancaster et al., 2017; Renner et al., 2017). These studies show that human cerebral organoids follow human-specific cortical development, including the presence of outer radial glia (oRG) cells, a type of cortical progenitor unique to human (Qian et al., 2016). Furthermore, transcriptomic and epigenomic data reported the resemblance of human cerebral organoids to human mid-trimester embryonic development (Camp et al., 2015; Luo et al., 2016; Quadrato et al., 2017b).

Despite rapid progress in this field, mechanisms underlying cerebral organoid development are much less understood. This is important in order to understand the accuracy and utility of this 3D in vitro model. To address whether cerebral organoids can be used as a tool for studying forebrain development, it is important to ensure that the phenotypes of cerebral organoids in a normal and mutant conditions matched with the phenotypes of their in vivo counterparts. To test this, mouse cerebral organoids provide a good model, as we understand much more of mouse forebrain development, in addition to readily available genetically modified (GM) mice. Both of these factors are important as a basis to probe the cerebral organoid system, identify their

phenotypes and subsequently compare them to the matched GM mouse embryonic cerebral cortex. Furthermore, engineering and manipulation of the 3D in vitro system is more feasible and practical using mouse cerebral organoids, as their developmental time is shorter than humans.

Firstly, we established a robust 3D culture protocol, which demonstrates reproducible formation of NE structures expressing *Foxg1*, an early marker of telencephalic tissues (Figure 3.1). A robust protocol is essential to produce consistent and reproducible results, in order to identify phenotypes in *Pax6*$^{-/-}$ cerebral organoids. Despite the robust formation of NE, characteristics of each organoids are unique. This is due to the absence of developmental axes in organoids and their random orientation during cryosectioning. Furthermore, organoids appear to be more variable between batches – and this is consistent with limitations reported by other studies (Lancaster et al., 2017; Renner et al., 2017). This heterogeneity leads to the difficulty to determine specific region of interest (ROI). Although heterogeneity is inevitable in organoids culture, ROI can be addressed by using specific molecular markers. For example, to understand the roles of *Pax6* in cortical structures of cerebral organoids in this study, analysis and quantification was limited to NE structures within *Pax6*$^{-/-}$ cerebral organoids that expressed cortex-specific markers, such as *Tbr2*.

We discovered that *Pax6*$^{-/-}$ cerebral organoids reproduce the main cellular phenotypes described in E12.5 *Pax6*$^{-/-}$ embryonic cortex (Estivill-Torrus et al., 2002; Quinn et al., 2007; Warren et al., 1999), such as an increase in abventricular mitoses (Figure 3.10), altered labelling index (Figure 3.11), and precocious differentiation (Figure 3.12). This suggests that cerebral organoids and cerebral cortex might share a similar *Pax6*

regulatory mechanism, thus making organoids a potential additional tool in studying corticogenesis, complementary to mouse models. This finding is significant, as this is the first comparative study, to our knowledge, which compares mutant cerebral organoids to the matched *in vivo* model.

However, it is important to note that although *Pax6*$^{-/-}$ cerebral organoids show proliferation defects based on the decreased labelling index (LI) of cells in S-phase, this is in contrast to the increased LI found in the *Pax6*$^{-/-}$ embryonic cerebral cortex (Mi et al., 2013; Warren et al., 1999). This discrepancy is addressed in the second part of the study, which aimed to assess cell cycle kinetics of cerebral organoids in both normal and *Pax6* mutant condition. Prior to cell cycle analysis, we demonstrated successful establishment of ES cell lines derived from blastocysts of *Pax6* conditional knock-out (cKO) mice, a conditional mutant model that allows cortex-specific and acute *Pax6* deletion (Figure 4.7). This mouse model has been used in a recent *Pax6* study, as acute *Pax6* deletion in a cortex-specific region eliminates the possibility of secondary effects due to constitutive loss of *Pax6* (Mi et al., 2013). In addition, the presence of a *Cre* reporter allele facilitates analysis of cerebral organoids, as it is driven by *Emx1* which illuminates a cortex-specific region (Kessaris et al., 2006).

Our successful establishment of *Pax6* cKO ES cells supports the efficiency of the chemically-defined medium known as 2i/LIF to derive ES cells from any mouse strain, including from CD1 background (Czechanski et al., 2014; Nichols et al., 2009). We showed that 62% of the derived blastocysts were successfully cultured and maintained as ES cells, with just four cell lines are karyotypically normal and carry the correct genotypes (Figure 4.7). These cell lines are also pluripotent, evident from

the expression of *Oct4* and *Nanog*, and are able to aggregate in a serum-free medium (Figure 4.8, 4.9).

Although these ES cell lines can aggregate in a serum-free medium, we found that the aggregation is suboptimal, as only a few of the cells aggregated, which resulted in smaller aggregates (Figure 4.9). Studies have shown that the size of aggregates eventually influences cell fate, possibly due to differences in cell interactions (Valamehr et al., 2008). We later found that the cell aggregation was dramatically improved when ES cells are maintained in ES medium supplemented with PD0325901, a MEK/Erk inhibitor, prior to differentiation. Although it is well established that supplementation with Leukemia inhibitory factor (LIF) is sufficient to maintain ES cells in an undifferentiated state, dependence on MEK/Erk inhibition seems to suggest additional mechanisms underlying the undifferentiated state in our ES cell lines. In fact, our finding is consistent with the work of Hanna et al., 2009, who reported similar findings: their pluripotent stem cell lines, which are derived from a non-obese diabetic (NOD) mouse strain (non-permissive), are dependent on MEK/Erk inhibitor to maintain an undifferentiated state. This may suggest that mouse genetic background (permissive/non-permissive strain) plays an important role in ES cell pluripotency, which can be regulated by exogenous factors, for example by a MEK/Erk inhibitor. In addition, future studies should also determine whether there is an increased cell death in the organoids by including apoptosis studies, such as TUNEL assay or expression of Caspase.

We then found that although all of the four ES cell lines successfully aggregate, one of them (cKOhet2) failed to form NE structures, suggesting the inability of the cells to

self-organise. Self-organisation stems from the ability of cells to sort themselves, based on the presence of cell adhesion molecules (Lancaster and Knoblich, 2014). These cell adhesion molecules interact with extracellular matrix (Matrigel) and activate downstream effector molecules such as extracellular regulated kinase (Erk), which promotes cell motility (Tanimura and Takeda, 2017). Therefore, it is conceivable that the inability of cKOhet2 to form NE structures may be due to the effect of MEK/Erk inhibition, as there is evidence that Erk promotes cell motility, which is part of self-organisation (Klemke et al., 1997). Indeed, recent reports found that prolonged treatment with MEK/Erk inhibitor can affect the stability and epigenome of ES cells (Choi et al., 2017; Di Stefano et al., 2018). However, as the effect appears to be dose-dependent, more recent study demonstrate that lower doses of PD0325901 supplementation do not induce epigenomic changes that lead to chromosomal abnormality, further supporting the safe conditions used in this study (Di Stefano et al., 2018). As each cell line is unique, thus subject to clonal variation, this might explain the susceptibility of cKOhet2 to MEK/Erk inhibition, despite the standard treatment with PD0325901 to all four ES cell lines. Taken together, only three ES cell lines successfully self-organise, forming cerebral organoids (Figure 4.10).

In chapter five, we demonstrated that *Cre* activation in cerebral organoids seems to be less efficient compared to in vivo. This is based on the activation of *Cre*, which can be observed only in cerebral organoids with homozygous floxed *Pax6* alleles (cKOhom1 and cKOhom2) upon treatment with 4-OHT, but cKOhet1 did not (Figure 5.3). Furthermore, *Cre* activation in both cKOhom1 and cKOhom2 appears to be mosaic (Figure 5.5), suggesting inconsistent *Cre* activation between cells in an

organoid, and between organoid littermates (Heffner et al., 2012). The inefficient *Cre* activation might be due to the 3D structure of cerebral organoids and the absence of vascularisation, which may affect the uptake of 4-OHT.

Studies have shown that the growth of 3D in vitro models is hampered by the access of nutrients, oxygen and growth factors to their core, resulting in concentration gradients and uneven diffusion of these factors to the cells, especially near to the centre (Lancaster and Knoblich, 2014; Van Winkle et al., 2012). This may include the uptake of 4-OHT, which could diffuse heterogeneously, causing heterogeneous *Cre* activation and mosaic expression. Furthermore, 4-OHT is given intravenously in vivo, which could also explain its efficient 4-OHT uptake, in contrast to cerebral organoids, which lack vascularisation.

Despite the *Cre* mosaicism, we found that treatment with 1uM 4-OHT for 24 hours is sufficient to activate *Cre* and remove *Pax6* in cerebral organoids (Figure 5.7). Although prolonged treatment had no significant effect on *Cre* activation, 2 μM 4-OHT treatment for 72 hours was detrimental to the tissues. Therefore, *Cre* activation is more rapid in vitro, with activation evident by 24 hours compared to 48 hours in vivo (Figure 5.2). This finding supports the observations of Felker et al., 2016 who systematically assessed 4-OHT action in vitro, and found that the trans isoform of this molecule (the more potent isoform) is stable for 24 hours in vitro. However, 4-OHT undergoes isomerization after 48 hours, forming the cis-isoform, which has lower affinity to the estrogen receptor. Therefore, this may justify the rapid action of 4-OHT, and the insignificant effect of prolonged treatment, in vitro (Figure 5.2A). Furthermore, direct addition of 4-OHT into organoids cultures eliminates the

intermediate step that converts tamoxifen to 4-OHT, which cause the lag in *Cre* activation in vivo (Felker et al., 2016). Due to the previously mentioned complications of both cKOhet1 and cKOhet2, these two cell lines were not used in the subsequent cell cycle analysis.

Cre mosaicism has enabled cells in the cKOhom1 and cKOhom2 organoids to either activate *Cre* (GFP+) in the *Emx1*+ region, thus acutely removing *Pax6* (*Pax6*-), or remain *Cre*- (*GFP*-), providing an isogenic control (Figure 5.7). Therefore, taking advantage of *Cre* mosaicism, which generates both experimental (GFP+) and control (GFP-) cells, we report cell cycle analysis in both cKOhom1 and cKOhom2 cerebral organoids.

First we showed that there is a non-significant decrease in the LI of GFP+ cells compared to the control (Figure 5.8), suggesting that there are no proliferation defects following acute deletion of *Pax6* in the cortical progenitors of cerebral organoids. Interestingly, both conditional and constitutive loss of *Pax6* in cerebral organoids show a consistent trend in the LI, as it decreased compared to the control (Figure 3.11). This is in contrast to the increased LI of $Pax6^{-/-}$ embryonic cortex, suggesting a gap between these two systems.

This gap may be due to the artificial environment of the in vitro system, as cerebral organoids were cultured in a minimal medium that only consists of basal medium and KSR. The use of minimal medium is based on the principle of neural default model; whereby in the absence of external factors, ES cells will acquire a default neural identity, which suggests intrinsic control of neural fate acquisition (Levine and

Brivanlou, 2007). However, compared to the embryonic cortex, the minimal medium may be lacking of many factors important for cortical progenitor proliferation. For example, the cerebral cortex is located next to ventricles containing cerebrospinal fluid (CSF), which contains extrinsic signaling molecules such as FGF, Shh, IGF-1 and IGF-2 that may influence cortical cell proliferation (Lehtinen et al., 2011). These exogenous factors are transduced to apical progenitors via their primary cilia, which are extended and immersed in CSF (Louvi and Grove, 2011; Lun et al., 2015). Furthermore, a recent study found that cortical explants and neurosphere cultures could be maintained in a primary cerebrospinal fluid (CSF) used as a culture medium, without any additional factors (Lehtinen et al., 2011). Indeed, there are growing evidence of the importance of CSF in normal cortical development (Lehtinen et al., 2011; Pothayee et al., 2018; Shen, 2018).

Nevertheless, the subtle, yet non-significant, change in the LI of *Pax6* cKO organoids might be due to the use of isogenic control (GFP- cells), present among the *Pax6*$^{-/-}$ cell population (GFP+). This could imply that the control cells (Pax6$^{+/+}$) may have influence or rescue the effect of acute loss of *Pax6* on cortical progenitor proliferation, suggesting that *Pax6* has a cell non-autonomous effect in cerebral organoids. Therefore, cell proliferation could be a secondary defect in the absence of *Pax6* in cerebral organoids. This could further explain the discrepancies in the LI data between cerebral organoids and E12.5 embryonic cortex, described in chapter three.

Alternatively, the cell cycle kinetics data could also explain the non-significant decrease in LI of *Pax6* cKO organoids. To date, cell cycle analysis of cerebral organoids has been limited to quantifying the proportion of cells in the cell cycle

phase (Matsui et al., 2017), and measuring the proportion of cells exiting the cell cycle (Li et al., 2016). Therefore, there is a lack of information on the cell cycle kinetics of cerebral organoids, such as the length of the cell cycle (Mason and Price, 2016). Hence, we report a novel cell cycle kinetics data, which includes the total cell cycle time (Tc) and S–phase length (Ts) of cerebral organoids, following acute deletion of *Pax6*.

First we calculated the Tc of the control cortical progenitors (GFP-) as a baseline, and compare it to the Tc of matched in vivo counterpart, which is the control *Pax6* cKO embryonic cortex. Interestingly, the Tc of GFP- cortical progenitors was slightly longer than the Tc of control *Pax6* cKO embryonic cortex. This is possibly due to the lengthening of the G1 phase. Studies have shown that G1 phase is an important window for cell fate determination, as cells are susceptible to differentiation signals in this period (Dalton, 2015). For example, a truncated G1 phase is characteristic of pluripotent stem cells, and as the cells differentiate, the G1 phase lengthens with overall lengthening of Tc (Singh et al., 2013). In addition, G1 phase also distinguishes the apical and basal progenitors of embryonic cortex, as it is longer in the latter, which is associated with their neurogenic cell division (Calegari et al., 2005). Therefore, if the G1 phase is longer in the cortical progenitors of organoids, it is also plausible that they are undergoing neurogenic division, which would result in more post-mitotic neurons. Indeed, the proportion of non-proliferating cells (Ki67-) is higher in cerebral organoids than in embryonic cortex, which supports the possibility of a longer G1 phase, thus a longer Tc in cerebral organoid cortical progenitors. To further confirm this, future studies should characterise these non-proliferating cells with basal progenitor marker (*Tbr2*) or post-mitotic marker (*Tuj1*).

We then showed that there was no significant change in the Tc of mutant cells (GFP+) compared to control cells (GFP-), which supports our previous finding that revealed no significant changes in the LI of GFP+ cells. Interestingly, this phenotype is similar to the Tc of cortical progenitors in the caudo-medial region of *Pax6* cKO embryonic cortex, which correlates with low *Pax6* expression (Manuel et al., 2015). It is well established that *Pax6* action is region-specific. For example, acute *Pax6* deletion accelerates cell proliferation and shortens the Tc of cortical progenitors only in the rostro-lateral region, where *Pax6* expression is the highest, and no significant effect was observed in caudo-medial cortex, where *Pax6* expression is relatively low (Mi et al. 2013). Therefore, it is conceivable that the level of *Pax6* expression in cerebral organoids is low, thus no alteration is observed in their Tc upon acute *Pax6* deletion. However, due to the absence of developmental axes and organoid heterogeneity, it is impossible to determine the regions associated with the level of *Pax6* expression in cerebral organoids prior to acute deletion of *Pax6*. Furthermore, considering the use mosaic analysis in the calculation of cell cycle kinetics, it cannot be ruled out that this could also be due to a cell non-autonomous requirement of *Pax6* in cerebral organoids.

Despite these encouraging results, it is worth noting the limitations encountered in this study. Firstly, cerebral organoids is a heterogenous model lacking of developmental axes. To address this, it is important to specify the region of interest (in this case, cortex) by using a cortex-specific marker such as *Tbr2* or *Emx1*. Quantitative analysis is also essential to address batch-to-batch variation and to reveal phenotypes of mutant organoids. As cerebral organoids are valuable for their spatial information, this study examines the organoids using a conventional technique used in

the embryo; by immunohistochemistry and manual cell counting on cryosections – which is laborious and time consuming. Therefore, future studies should incorporate more high-throughput techniques to take full advantage of the potential of cerebral organoids.

Secondly, unexpected findings in the *Pax6* cKO cerebral organoids such as *Cre* mosaicism and undetectable *Cre* in the control ($Pax6^{+/fl}$) organoids, makes it challenging to perform the subsequent experiment, which is to calculate the cell cycle kinetics of the organoids. We then took advantage of *Cre* mosaicism, which provides GFP+ and GFP- cell population within a cortical-like NE (*Emx1*+). GFP+ cells are the experimental cells as *Pax6* was successfully deleted in these cells (Figure 5.7) and GFP- cells were used as controls.

Mosaic analysis is a classic tool to examine cell autonomous functions of several transcription factors, including *Pax6*, by using *Pax6* chimaeric embryos (Manuel et al., 2010, 2006; Quinn et al., 2007). Therefore, the cell autonomous requirement of *Pax6* in the cerebral organoids can also be determined, which allows us to distinguish whether the phenotypes observed is due to the requirement of *Pax6* or otherwise, illuminating any weaknesses in the 3D in vitro system that may require further improvement. Indeed, we found that *Pax6* is cell non-autonomously required in cortical proliferation of cerebral organoids. Although this in contrast to the findings in vivo (Manuel et al., 2006), it could be a consequence of the in vitro artificial environment, which may lack some of the exogenous factors important in cortical proliferation, as discussed previously.

However, it is important to note that although 98% of the GFP+ cells show successful deletion of *Pax6*, the GFP- cell population, which was used as control, appears to have a more heterogenous expression of *Pax6.* Therefore, calculation of the Tc might be overestimated. Due to time constraint, further analysis including Pax6 staining could not be performed; therefore, future studies should include this step and include GFP-/Pax6+ cells as controls.

Taken together, despite the caveats outlined above, our findings are promising. Compared to a 2D in vitro system that lacks complexity and organisation, cerebral organoids are particularly suitable for addressing questions that require spatial information; such as cortical lamination, interkinetic nuclear migration (IKNM), neuronal migration, and phenotypes with positional information. Though the lack of developmental axes would complicate studies on cortical patterning and regionalisation, this could be circumvented by using specific molecular markers that specify caudal and rostral axes, such as COUPTF-I and Sp8, respectively (Sansom and Livesey, 2009).

Future work should also include more detailed characterisation and optimisation of the mouse cerebral organoids. For example, as this study has focused on characterisation with several key cortical markers, other types of cells present in the organoids should be further discerned, such as ventral telencephalic cells, Cajal Retzius cells and signalling centres. The presence of these cells should also be systematically quantified, to determine whether the presence of these cells is random or consistent. A previous study in human cerebral organoids detects the presence of

signaling centres, although their presence is random and infrequent compared to tissues with cortical characteristics (Renner et al., 2017).

As discussed previously, the artificial in vitro environment might lack external signaling molecules important for cell proliferation in cerebral organoids. Therefore, further optimisation of the culture condition should also be addressed. For example, more signaling molecules described in the CSF can be added to the minimal medium, following a developmental timeline. For example, these signaling molecules should be added after the neural and telencephalic induction stage, which takes places on day one of cerebral organoid differentiation. The readout of this optimisation step could be through the assessment of fundamental aspect of tissue morphogenesis, such as cell proliferation and cell death (apoptosis). Alternatively, following aggregation of ES cells, cerebral organoids could also be transplanted into lateral ventricles containing CSF. This transplantation approach has been demonstrated to be successful in the survival of neurospheres, as they consist of all major types of neuronal cells such as neurons, microglia, astrocytes, oligodendrocytes, as well as forming mature synapse and axonal projections (Pothayee et al., 2018).

In summary, our results show that *Pax6*$^{-/-}$ cerebral organoids are able to reproduce phenotypes of their matched in vivo counterparts. However, due to the complex and pleiotropic actions of *Pax6* in cortical progenitor proliferation, the roles of *Pax6* in the cell cycle of cortical progenitors in cerebral organoids remain unclear. It seems *Pax6* is either cell non-autonomously required, or that the expression of *Pax6* in organoids is low, corresponding to caudo-medial region of embryonic cortex. These interesting findings warrant further investigation as well as optimisation of the system. In

addition, this study also revealed the extent of genetic manipulation tools such as Cre-recombinase system in cerebral organoids, which was used to acutely remove *Pax6* from the system, albeit with lower efficiency than in the mouse. Overall, cerebral organoids are a highly prospective tool for investigating forebrain development, though further optimisation of the system might be necessary. For example, microfluidics system or air-liquid interface culture could improve diffusion of nutrients into the organoids, ultimately reducing cell death (Bhatia and Ingber, 2014; Giandomenico et al., 2019). Furthermore, limitations in analysing this system could also be improved by using alternative techniques such as high throughput quantification, such as machine learning quantification software, as well as advanced microscopy techniques, such as light sheet microscopy (Rios and Clevers, 2018).

APPENDIX A: Result of mycoplasma test

	Sample	A	B	B/A	Result
1		1299	498	0.38	Negative
2		1106	392	0.35	Negative
3		1144	390	0.34	Negative
4		931	336	0.36	Negative
5		1209	378	0.31	Negative
6		831	265	0.32	Negative
7	113.1	1485	894	0.60	Negative
8	113.2	2388	1340	0.56	Negative
9	114.1	1509	856	0.57	Negative
10	114.3	1432	885	0.62	Negative
11	115.7	1413	837	0.59	Negative
12	115.9	1472	926	0.63	Negative
13	Positive C	3344	195711	58.53	Positive
14	Negative C	3242	416	0.13	Negative

APPENDIX B: Cumulative EdU cell counts

Sample: cKOhom1

Batch	EDU	DAPI	Total GFP	Total GFP-	Total EDU	GFP+EDU+	GFP-EDU+	GFP+EDU+/GFP	GFP-EDU+/Total GFP-
Batch 1	2hr	402	66	336	118	10	108	0.151515152	0.321428571
		533	66	467	119	5	114	0.075757576	0.244111349
		632	178	454	134	45	89	0.252808989	0.196035242
	4hr	538	89	449	113	17	96	0.191011236	0.213808463
		454	175	279	110	38	72	0.217142857	0.258064516
		239	63	176	53	7	46	0.111111111	0.261363636
	6hr	455	105	350	119	23	96	0.219047619	0.274285714
		473	121	352	131	33	98	0.272727273	0.278409091
		239	72	167	65	12	53	0.166666667	0.317365269
	8h	480	145	335	143	44	99	0.303448276	0.295522388
		379	122	257	112	21	91	0.172131148	0.354085603
		482	110	372	168	29	139	0.263636364	0.373655914
	10h	430	92	338	172	35	137	0.380434783	0.405325444
		465	112	353	239	46	193	0.410714286	0.546742 21
		324	100	224	111	27	84	0.27	0.375

Batch	EDU	DAPI	Total GFP	Total GFP-	Total EDU	GFP+EDU+	GFP-EDU+	GFP+EDU+/GFP	GFP-EDU+/Total GFP-
Batch 2	2hr	223	48	175	62	9	53	0.1875	0.302857143
		318	68	250	71	8	63	0.117647059	0.252
		362	76	286	77	13	64	0.171052632	0.223776224
	4hr	438	153	285	110	30	80	0.196078431	0.280701754
		307	67	240	71	10	61	0.149253731	0.254166667
		410	78	332	108	12	96	0.153846154	0.289156627
	6hr	393	168	225	127	48	79	0.285714286	0.351111111
		303	118	185	94	31	63	0.262711864	0.340540541
		359	146	213	137	69	68	0.47260274	0.319248826
	8hr	340	72	268	112	28	84	0.388888889	0.313432836
		312	73	239	114	13	101	0.178082192	0.422594142
		270	32	238	100	3	97	0.09375	0.407563025
	10hr	401	52	349	149	10	139	0.192307692	0.398280802
		291	24	267	137	8	129	0.333333333	0.483146067
		302	19	283	93	4	89	0.210526316	0.314487633

Batch	EDU	DAPI	Total GFP	Total GFP-	Total EDU	GFP+EDU+	GFP-EDU+	GFP+EDU+/GFP	GFP-EDU+/Total GFP-
Batch 3	2hr	350	19	331	109	1	108	0.052631579	0.326283988
		439	13	426	117	2	115	0.153846154	0.269953052
		252	8	244	85	2	83	0.25	0.340163934
	4hr	336	7	329	89	1	88	0.142857143	0.267477204
		265	19	246	64	4	60	0.210526316	0.243902439
		284	42	242	79	12	67	0.285714286	0.276859504
	6hr	306	61	245	102	17	85	0.278688525	0.346938776
		253	21	232	87	3	84	0.142857143	0.362068966
		534	49	485	131	16	115	0.326530612	0.237113402
	8hr	382	56	326	96	8	88	0.142857143	0.26993865
		435	18	417	141	0	141	0	0.338129496
		355	61	294	145	19	126	0.31147541	0.428571429
	10hr	249	48	201	85	13	72	0.270833333	0.358208955
		361	81	280	175	30	145	0.37037037	0.517857143
		292	33	259	108	9	99	0.272727273	0.382239382

Sample: cKOhom2

Batch	EDU	DAPI	Total GFP	Total GFP-	Total EDU	GFP+EDU+	GFP-EDU+	GFP+EDU+/GFP	GFP-EDU+/GFP-
Batch 1	2hr	335	82	253	146	30	116	0.365853659	0.458498024
		460	80	380	121	11	110	0.1375	0.289473684
		353	33	320	79	9	70	0.272727273	0.21875
	4hr	297	21	276	62	4	58	0.19047619	0.210144928
		271	54	217	80	15	65	0.277777778	0.299539171
		315	50	265	111	11	100	0.22	0.377358491
	6h	325	49	276	104	9	95	0.183673469	0.344202899
		610	159	451	227	55	172	0.34591195	0.381374723
		464	72	392	130	24	106	0.333333333	0.270408163
	8h	288	90	198	155	30	125	0.333333333	0.631313131
		451	65	386	182	18	164	0.276923077	0.424870466
		300	94	206	111	36	75	0.382978723	0.36407767
	10h	326	99	227	114	28	86	0.282828283	0.378854626
		421	89	332	192	24	168	0.269662921	0.506024096
		554	30	524	195	9	186	0.3	0.354961832

Batch	EDU	DAPI	Total GFP	Total GFP-	Total EDU	GFP+EDU+	GFP-EDU+	GFP+EDU+/GFP	GFP-EDU+/GFP-
Batch 2	2hr	323	33	290	91	5	86	0.151515152	0.296551724
		337	48	289	97	8	89	0.166666667	0.307958478
		384	79	305	75	15	60	0.189873418	0.196721311
	4hr	344	42	302	70	7	63	0.166666667	0.208609272
		351	56	295	84	15	69	0.267857143	0.233898305
		348	38	310	75	8	67	0.210526316	0.216129032
	6hr	386	158	228	135	46	89	0.291139241	0.390350877
		423	49	374	140	22	118	0.448979592	0.315508021
		343	78	265	117	23	94	0.294871795	0.354716981
	8hr	324	117	207	166	45	121	0.384615385	0.584541063
		478	48	430	163	20	143	0.416666667	0.33255814
		430	92	338	96	16	80	0.173913043	0.236686391
	10hr	346	115	231	132	44	88	0.382608696	0.380952381
		375	46	329	121	18	103	0.391304348	0.313069909
		444	94	350	199	38	161	0.404255319	0.46

Batch	EDU	DAPI	Total GFP	Total GFP-	Total EDU	GFP+EDU+	GFP-EDU+	GFP+EDU+/GFP	GFP-EDU+/GFP-
Batch 3	2hr	393	12	381	118	2	116	0.166666667	0.304461942
		443	35	408	69	3	66	0.085714286	0.161764706
		247	6	241	45	4	41	0.666666667	0.170124481
	4hr	120	18	102	33	3	30	0.166666667	0.294117647
		241	28	213	77	11	66	0.392857143	0.309859155
		561	8	553	112	0	112	0	0.202531646
	6hr	445	29	416	109	5	104	0.172413793	0.25
		279	27	252	88	8	80	0.296296296	0.317460317
		286	30	256	69	7	62	0.233333333	0.2421875
	8hr	438	69	369	186	25	161	0.362318841	0.436314363
		312	103	209	138	35	103	0.339805825	0.492822967
		284	12	272	73	4	69	0.333333333	0.253676471
	10hr	383	122	261	144	31	113	0.254098361	0.432950192
		243	27	216	103	9	94	0.333333333	0.435185185
		171	35	136	106	10	96	0.285714286	0.705882353

BIBLIOGRAPHY

Andersson-Rolf, A., Mustata, R.C., Merenda, A., Kim, J., Perera, S., Grego, T., Andrews, K., Tremble, K., Silva, J.C.R., Fink, J., Skarnes, W.C., Koo, B.-K., 2017. One-step generation of conditional and reversible gene knockouts. Nat. Methods 14, 287–289.

Antón-Bolaños, N., Espinosa, A., López-Bendito, G., 2018. Developmental interactions between thalamus and cortex: a true love reciprocal story. Curr. Opin. Neurobiol. 52:33-41.

Azzarelli, R., Hardwick, L.J.A., Philpott, A., 2015. Emergence of neuronal diversity from patterning of telencephalic progenitors. Wiley Interdiscip. Rev. Dev. Biol. 4, 197–214.

Bain, G., Kitchens, D., Yao, M., Huettner, J.E., Gottlieb, D.I., 1995. Embryonic stem cells express neuronal properties in vitro. Dev Biol. 168(2):342-57.

Bhatia, S.N., Ingber, D.E., 2014. Microfluidic organs-on-chips. Nat. Biotechnol. 32(8):760-72.

Bibel, M., Richter, J., Schrenk, K., Tucker, K.L., Staiger, V., Korte, M., Goetz, M., Barde, Y.-A., 2004. Differentiation of mouse embryonic stem cells into a defined neuronal lineage. Nat. Neurosci. 7, 1003–1009.

Boroviak, T., Loos, R., Bertone, P., Smith, A., Nichols, J., 2014. The ability of inner-cell-mass cells to self-renew as embryonic stem cells is acquired following epiblast specification. Nat. Cell Biol. 16(6):516-28.

Bredenoord, A.L., Clevers, H., Knoblich, J.A., 2017. Human tissues in a dish: The research and ethical implications of organoid technology. Science (80-.). 355, 1–7.

Buehr, M., Meek, S., Blair, K., Yang, J., Ure, J., Silva, J., McLay, R., Hall, J., Ying, Q.L., Smith, A., 2008. Capture of Authentic Embryonic Stem Cells from Rat Blastocysts. Cell. 135 (7):1287-98.

Caballero, I.M., Manuel, M.N., Molinek, M., Quintana-Urzainqui, I., Mi, D., Shimogori, T., Price, D.J., 2014. Cell-autonomous repression of Shh by transcription factor Pax6 regulates diencephalic patterning by controlling the central diencephalic organizer. Cell Rep. 8, 1405–18.

Calegari, F., 2005. Selective Lengthening of the Cell Cycle in the Neurogenic Subpopulation of Neural Progenitor Cells during Mouse Brain Development. J. Neurosci. 25(28): 6533-8.

Camp, J.G., Badsha, F., Florio, M., Kanton, S., Gerber, T., Wilsch-Bräuninger, M., Lewitus, E., Sykes, A., Hevers, W., Lancaster, M., Knoblich, J.A., Lachmann, R., Pääbo, S., Huttner, W.B., Treutlein, B., 2015. Human cerebral organoids recapitulate gene expression programs of fetal neocortex development. Proc. Natl. Acad. Sci. U. S. A. 112, 15672–7.

Carpenedo, R.L., Sargent, C.Y., McDevitt, T.C., 2007. Rotary Suspension Culture Enhances the Efficiency, Yield, and Homogeneity of Embryoid Body Differentiation. Stem Cells 25, 2224–2234.

Caviness, V.S., Takahashi, T., Nowakowski, R.S., 1995. Numbers, time and neocortical neuronogenesis: a general developmental and evolutionary model. Trends Neurosci. 18, 379–383.

Cecchini, M.J., Amiri, M., Dick, F., 2012. Analysis of Cell Cycle Position in Mammalian Cells. J. Vis. Exp. 7, 1–7.

Chambers, I., Silva, J., Colby, D., Nichols, J., Nijmeijer, B., Robertson, M., Vrana, J., Jones, K., Grotewold, L., Smith, A., 2007. Nanog safeguards pluripotency and mediates germline development. Nature 450, 1230–1234.

Chan, C.-H., 2001. Emx1 is a Marker for Pyramidal Neurons of the Cerebral Cortex. Cereb. Cortex 11, 1191–1198.

Chen, B., Dodge, M.E., Tang, W., Lu, J., Ma, Z., Fan, C.-W., Wei, S., Hao, W., Kilgore, J., Williams, N.S., Roth, M.G., Amatruda, J.F., Chen, C., Lum, L., 2009. Small molecule-mediated disruption of Wnt-dependent signaling in tissue regeneration and cancer. Nat. Chem. Biol. 5, 100–7.

Chen, H., Guo, R., Zhang, Q., Guo, H., Yang, M., Wu, Z., Gao, S., Liu, L., Chen, L., 2015a. Erk signaling is indispensable for genomic stability and self-renewal of mouse embryonic stem cells. Proc. Natl. Acad. Sci. U. S. A. 112, E5936-43.

Chen, H., Guo, R., Zhang, Q., Guo, H., Yang, M., Wu, Z., Gao, S., Liu, L., Chen, L., 2015b. Erk signaling is indispensable for genomic stability and self-renewal of mouse embryonic stem cells. Proc. Natl. Acad. Sci. 112, E5936-43.

Choi, H., Song, J., Park, G., Kim, J., 2016. Modeling of Autism Using Organoid Technology. Mol. Neurobiol. 1–7.

Choi, J., Huebner, A.J., Clement, K., Walsh, R.M., Savol, A., Lin, K., Gu, H., Di Stefano, B., Brumbaugh, J., Kim, S.Y., Sharif, J., Rose, C.M., Mohammad, A., Odajima, J., Charron, J., Shioda, T., Gnirke, A., Gygi, S., Koseki, H., Sadreyev, R.I., Xiao, A., Meissner, A., Hochedlinger, K., 2017. Prolonged Mek1/2 suppression impairs the developmental potential of embryonic stem cells. Nature 548, 219–223.

Czechanski, A., Byers, C., Greenstein, I., Schrode, N., Donahue, L.R., Hadjantonakis, A.-K., Reinholdt, L.G., 2014. Derivation and characterization of mouse embryonic stem cells from permissive and nonpermissive strains. Nat. Protoc. 9, 559–574.

Dalton, S., 2015. Linking the Cell Cycle to Cell Fate Decisions. Trends Cell Biol. 25, 592–600.

Danesin, C., Houart, C., 2012. A Fox stops the Wnt: implications for forebrain development and diseases. Curr. Opin. Genet. Dev. 22, 323–30.

Dehay, C., Kennedy, H., 2007. Cell-cycle control and cortical development. Nat. Rev. Neurosci. 8, 438–450.

Descalzo, S.M., Rué, P., Garcia-Ojalvo, J., Arias, A.M., 2012. Correlations between the levels of Oct4 and Nanog as a signature for naïve pluripotency in mouse embryonic stem cells. Stem Cells 30, 2683–2691.

Detrick, R.J., Dickey, D., Kintner, C.R., 1990. The effects of N-cadherin misexpression on morphogenesis in xenopus embryos. Neuron 4, 493–506.

Di Lullo, E., Kriegstein, A.R., 2017. The use of brain organoids to investigate neural development and disease. Nat. Rev. Neurosci. 18(10):573-84.

Di Stefano, B., Ueda, M., Sabri, S., Brumbaugh, J., Huebner, A.J., Sahakyan, A., Clement, K., Clowers, K.J., Erickson, A.R., Shioda, K., Gygi, S.P., Gu, H., Shioda, T., Meissner, A., Takashima, Y., Plath, K., Hochedlinger, K., 2018. Reduced MEK inhibition preserves genomic stability in naive human embryonic stem cells. Nat. Methods 15, 732–740.

Eckardt, D., Theis, M., Döring, B., Speidel, D., Willecke, K., Ott, T., 2004. Spontaneous Ectopic Recombination in Cell-Type-Specific Cre Mice Removes loxP-Flanked Marker Cassettes In Vivo. Genesis 38, 159–165.

Eiraku, M., Sasai, Y., 2012. Mouse embryonic stem cell culture for generation of three-dimensional retinal and cortical tissues. Nat. Protoc. 7, 69–79.

Eiraku, M., Watanabe, K., Matsuo-Takasaki, M., Kawada, M., Yonemura, S., Matsumura, M., Wataya, T., Nishiyama, A., Muguruma, K., Sasai, Y., 2008. Self-organized formation of polarized cortical tissues from ESCs and its active manipulation by extrinsic signals. Cell Stem Cell 3, 519–532.

Englund, C., Fink, A., Lau, C., Pham, D., Daza, R. a M., Bulfone, A., Kowalczyk, T., Hevner, R.F., 2005. Pax6, Tbr2, and Tbr1 are expressed sequentially by radial glia, intermediate progenitor cells, and postmitotic neurons in developing neocortex. J. Neurosci. 25, 247–51.

Estivill-Torrus, G., Pearson, H., van Heyningen, V., Price, D.J., Rashbass, P., 2002. Pax6 is required to regulate the cell cycle and the rate of progression from symmetrical to asymmetrical division in mammalian cortical progenitors. Development 129, 455–66.

Felker, A., Nieuwenhuize, S., Dolbois, A., Blazkova, K., Hess, C., Low, L.W.L., Burger, S., Samson, N., Carney, T.J., Bartunek, P., Nevado, C., Mosimann, C., 2016. In vivo performance and properties of Tamoxifen metabolites for CreERT2 control. PLoS One 11, e0152989.

Fujimori, T., Miyatani, S., Takeichi, M., 1990. Ectopic expression of N-cadherin perturbs histogenesis in Xenopus embryos. Development 110, 97–104.

Gaspard, N., Bouschet, T., Hourez, R., Dimidschstein, J., Naeije, G., van Den Ameele, J., Espuny-Camacho, I., Passante, L., Herpoel, A., Schiffmann, S.N., others, 2008. An intrinsic mechanism of corticogenesis from embryonic stem cells. Nature 455, 351–357.

Gaspard, N., Vanderhaeghen, P., 2011. Laminar fate specification in the cerebral cortex. F1000 Biol. Rep. 3, 6.

Gauduchon, J., Gouilleux, F., Maillard, S., Marsaud, V., Renoir, J.M., Sola, B., 2005. 4-Hydroxytamoxifen inhibits proliferation of multiple myeloma cells in vitro through down-regulation of c-Myc, up-regulation of p27Kip1, and modulation of Bcl-2 family members. Clin. Cancer Res. 11, 2345–2354.

Gelman, D.M., Marín, O., 2010. Generation of interneuron diversity in the mouse cerebral cortex. Eur. J. Neurosci. 31(12):2136-41.

Georgala, P.A., Carr, C.B., Price, D.J., 2011a. The role of Pax6 in forebrain development. Dev. Neurobiol. 71, 690–709.

Georgala, P.A., Manuel, M., Price, D.J., 2011b. The generation of superficial cortical layers is regulated by levels of the transcription factor Pax6. Cereb. Cortex 21, 81–94.

Geschwind, D.H., Levitt, P., 2007. Autism spectrum disorders: developmental disconnection syndromes. Curr. Opin. Neurobiol. 17(1):103-11.

Giandomenico, S.L., Mierau, S.B., Gibbons, G.M., Wenger, L.M., Masullo, L., Sit, T., Sutcliffe, M., Boulanger, J., Tripodi, M., Derivery, E., Paulsen, O., Lakatos, A., Lancaster, M., 2019. Cerebral organoids at the air-liquid interface generate diverse nerve tracts with functional output. Nat Neurosci. 22(4):669-79.

Greig, L.C., Woodworth, M.B., Galazo, M.J., Padmanabhan, H., Macklis, J.D., 2013. Molecular logic of neocortical projection neuron specification, development and diversity. Nat. Rev. Neurosci. 14, 755–69.

Hanna, J., Markoulaki, S., Mitalipova, M., Cheng, A.W., Cassady, J.P., Staerk, J., Carey, B.W., Lengner, C.J., Foreman, R., Love, J., Gao, Q., Kim, J., Jaenisch, R., 2009. Metastable Pluripotent States in NOD-Mouse-Derived ESCs. Cell Stem Cell 4, 513–524.

Hayashi, S., McMahon, A.P., 2002. Efficient recombination in diverse tissues by a tamoxifen-inducible form of Cre: a tool for temporally regulated gene activation/inactivation in the mouse. Dev Biol 244, 305–318.

Heemskerk, I., Warmflash, A., 2016. Pluripotent stem cells as a model for embryonic patterning: From signaling dynamics to spatial organization in a dish. Dev. Dyn. 245, 976–990.

Heffner, C.S., Herbert Pratt, C., Babiuk, R.P., Sharma, Y., Rockwood, S.F., Donahue, L.R., Eppig, J.T., Murray, S.A., 2012. Supporting conditional mouse mutagenesis with a comprehensive cre characterization resource. Nat. Commun. 3, 1–9.

Hill, R.E., Favor, J., Hogan, B.L.M., Ton, C.C.T., Saunders, G.F., Hanson, I.M., Prosser, J., Jordan, T., Hastie, N.D., Heyningen, V. van, 1991. Mouse Small eye results from mutations in a paired-like homeobox-containing gene. Nature 354, 522–525.

Hindley, C., Philpott, A., 2012. Co-ordination of cell cycle and differentiation in the developing nervous system. Biochem. J. 444, 375–382.

Hwang, N.S., Varghese, S., Elisseeff, J., 2008. Controlled differentiation of stem cells. Adv. Drug Deliv. Rev. 60(2): 199-214.

Julian, L.M., Carpenedo, R.L., Rothberg, J.L.M., Stanford, W.L., 2016. Formula G1: Cell cycle in the driver's seat of stem cell fate determination. BioEssays 38, 325–332.

Kadowaki, M., Nakamura, S., Machon, O., Krauss, S., Radice, G.L., Takeichi, M., 2007. N-cadherin mediates cortical organization in the mouse brain. Dev. Biol. 304, 22–33.

Kalmar, T., Lim, C., Hayward, P., Muñoz-Descalzo, S., Nichols, J., Garcia-Ojalvo, J., Arias, A.M., 2009. Regulated fluctuations in Nanog expression

mediate cell fate decisions in embryonic stem cells. PLoS Biol. 7, e1000149.

Katzenellenbogen, B.S., Norman, M.J., Eckert, R.L., Peltz, S.W., Mangel, W.F., 1984. Bioactivities, Estrogen Receptor Interactions, and Plasminogen Activator-inducing Activities of Tamoxifen and Hydroxy-tamoxifen Isomers in MCF-7 Human Breast Cancer Cells. Cancer Res. 44, 112–9.

Kessaris, N., Fogarty, M., Iannarelli, P., Grist, M., Wegner, M., Richardson, W.D., 2006. Competing waves of oligodendrocytes in the forebrain and postnatal elimination of an embryonic lineage. Nat. Neurosci. 9, 173–179.

Klemke, R.L., Cai, S., Giannini, A.L., Gallagher, P.J., De Lanerolle, P., Cheresh, D.A., 1997. Regulation of cell motility by mitogen-activated protein kinase. J. Cell Biol. 137, 481–492.

Kosodo, Y., Suetsugu, T., Suda, M., Mimori-Kiyosue, Y., Toida, K., Baba, S.A., Kimura, A., Matsuzaki, F., 2011. Regulation of interkinetic nuclear migration by cell cycle-coupled active and passive mechanisms in the developing brain. EMBO J. 30, 1690–1704.

Kunath, T., Saba-El-Leil, M.K., Almousailleakh, M., Wray, J., Meloche, S., Smith, A., 2007. FGF stimulation of the Erk1/2 signalling cascade triggers transition of pluripotent embryonic stem cells from self-renewal to lineage commitment. Development 134, 2895–902.

Lancaster, M. a., Knoblich, J. a., 2014. Organogenesis in a dish: modeling development and disease using organoid technologies. Science 345, 1247125.

Lancaster, M. a, Renner, M., Martin, C., Wenzel, D., Bicknell, L.S., Hurles, M.E., Homfray, T., Penninger, J.M., Jackson, A.P., Knoblich, J. a, 2013. Cerebral organoids model human brain development and microcephaly.

Nature 501, 373–9.

Lancaster, M.A., Corsini, N.S., Wolfinger, S., Gustafson, E.H., Phillips, A.W., Burkard, T.R., Otani, T., Livesey, F.J., Knoblich, J.A., 2017. Guided self-organization and cortical plate formation in human brain organoids. Nat. Biotechnol. 35, 659–666.

Lancaster, M.A., Knoblich, J.A., 2014. Generation of cerebral organoids from human pluripotent stem cells. Nat. Protoc. 9, 2329–2340.

Lee, H.O., Norden, C., 2013. Mechanisms controlling arrangements and movements of nuclei in pseudostratified epithelia. Trends Cell Biol. 23(3):141-50.

Lehtinen, M.K., Zappaterra, M.W., Chen, X., Yang, Y.J., Hill, A.D., Lun, M., Maynard, T., Gonzalez, D., Kim, S., Ye, P., D'Ercole, A.J., Wong, E.T., LaMantia, A.S., Walsh, C.A., 2011. The cerebrospinal fluid provides a proliferative niche for neural progenitor cells. Neuron 69, 893–905.

Levine, A.J., Brivanlou, A.H., 2007. Proposal of a model of mammalian neural induction. Dev. Biol. 308(2):247-56.

Li, Y., Muffat, J., Omer, A., Bosch, I., Lancaster, M.A., Sur, M., Gehrke, L., Knoblich, J.A., Jaenisch, R., 2016. Induction of Expansion and Folding in Human Cerebral Organoids. Cell Stem Cell 20, 385–396.

Loonstra, A., Vooijs, M., Beverloo, H.B., Allak, B.A., van Drunen, E., Kanaar, R., Berns, A., Jonkers, J., 2001. Growth inhibition and DNA damage induced by Cre recombinase in mammalian cells. Proc. Natl. Acad. Sci. 98, 9209–14.

Louvi, A., Grove, E.A., 2011. Cilia in the CNS: The quiet organelle claims center stage. Neuron. 69(6):1046-60.

Lun, M.P., Monuki, E.S., Lehtinen, M.K., 2015. Development and functions of the choroid plexus-cerebrospinal fluid system. Nat. Rev. Neurosci. 16(8):445-57.

Luo, C., Lancaster, M.A., Castanon, R., Nery, J.R., Knoblich, J.A., Ecker, J.R., 2016. Cerebral Organoids Recapitulate Epigenomic Signatures of the Human Fetal Brain. Cell Rep. 17: 3369–3384.

Manuel, M., Georgala, P.A., Carr, C.B., Chanas, S., Kleinjan, D.A., Martynoga, B., Mason, J.O., Molinek, M., Pinson, J., Pratt, T., Quinn, J.C., Simpson, T.I., Tyas, D.A., van Heyningen, V., West, J.D., Price, D.J., 2006. Controlled overexpression of Pax6 in vivo negatively autoregulates the Pax6 locus, causing cell-autonomous defects of late cortical progenitor proliferation with little effect on cortical arealization. Development 134, 545–555.

Manuel, M., Martynoga, B., Yu, T., West, J.D., Mason, J.O., Price, D.J., 2010. The transcription factor Foxg1 regulates the competence of telencephalic cells to adopt subpallial fates in mice. Development 137, 487–97.

Manuel, M.N., Mi, D., Mason, J.O., Price, D.J., 2015. Regulation of cerebral cortical neurogenesis by the Pax6 transcription factor. Front. Cell. Neurosci. 9, 70.

Martello, G., Smith, A., 2014. The Nature of Embryonic Stem Cells. Annu. Rev. Cell Dev. Biol. 30, 647–675.

Martin Gonzalez, J., Morgani, S.M., Bone, R.A., Bonderup, K., Abelchian, S., Brakebusch, C., Brickman, J.M., 2016. Embryonic Stem Cell Culture Conditions Support Distinct States Associated with Different Developmental Stages and Potency. Stem cell reports 7, 177–91.

Martynoga, B., Morrison, H., Price, D.J., Mason, J.O., 2005. Foxg1 is required for specification of ventral telencephalon and region-specific regulation of

dorsal telencephalic precursor proliferation and apoptosis. Dev. Biol. 283, 113–127.

Mason, J.O., Price, D.J., 2016. Building brains in a dish: Prospects for growing cerebral organoids from stem cells. Neuroscience 334, 105–118.

Matsui, T., Nieto-Estévez, V., Kyrychenko, S., Schneider, J.W., Hsieh, J., 2017. Retinoblastoma protein controls growth, survival and neuronal migration in human cerebral organoids. Development 144, 1025–1034.

Mi, D., Carr, C., Georgala, P.A., Huang, Y.T., Manuel, M.N., Jeanes, E., Niisato, E., Sansom, S.N., Livesey, F.J., Theil, T., Hasenpusch-Theil, K., Simpson, T.I., Mason, J.O., Price, D.J., 2013. Pax6 Exerts regional control of cortical progenitor proliferation via direct repression of Cdk6 and Hypophosphorylation of pRb. Neuron 78, 269–84.

Mi, D., Manuel, M., Huang, Y.-T., Mason, J.O., Price, D.J., 2018. Pax6 Lengthens G1 Phase and Decreases Oscillating Cdk6 Levels in Murine Embryonic Cortical Progenitors. Front. Cell. Neurosci. 12, 1–10.

Morgani, S., Nichols, J., Hadjantonakis, A.-K., 2017. The many faces of Pluripotency: in vitro adaptations of a continuum of in vivo states. BMC Dev. Biol. 17, 7.

Muñoz-Sanjuán, I., Brivanlou, A.H., 2002. Neural induction, the default model and embryonic stem cells. Nat. Rev. Neurosci. 3, 271–280.

Nair, G., Abranches, E., Guedes, A.M. V., Henrique, D., Raj, A., 2015. Heterogeneous lineage marker expression in naive embryonic stem cells is mostly due to spontaneous differentiation. Sci. Rep. 5, 13339.

Nasu, M., Takata, N., Danjo, T., Sakaguchi, H., Kadoshima, T., Futaki, S., Sekiguchi, K., Eiraku, M., Sasai, Y., 2012. Robust Formation and Maintenance of Continuous Stratified Cortical Neuroepithelium by

Laminin-Containing Matrix in Mouse ES Cell Culture. PLoS One 7, 13–14.

Nichols, J., Jones, K., Phillips, J.M., Newland, S.A., Roode, M., Mansfield, W., Smith, A., Cooke, A., 2009. Validated germline-competent embryonic stem cell lines from nonobese diabetic mice. Nat. Med. 15, 814–8.

Nichols, J., Smith, A., 2012. Pluripotency in the embryo and in culture. Cold Spring Harb. Perspect. Biol. 4(8):a008128.

Nichols, J., Ying, Q.-L., 2006. Derivation and propagation of embryonic stem cells in serum- and feeder-free culture. Methods Mol. Biol. 329, 91–8.

Noctor, S.C., Martinez-Cerdeño, V., Ivic, L., Kriegstein, A.R., 2004. Cortical neurons arise in symmetric and asymmetric division zones and migrate through specific phases. Nat. Neurosci. 7, 136–44.

Nowakowski, R.S., Lewin, S.B., Miller, M.W., 1989. Bromodeoxyuridine immunohistochemical determination of the lengths of the cell cycle and the DNA-synthetic phase for an anatomically defined population. J. Neurocytol. 18, 311–318.

Osumi, N., Shinohara, H., Numayama-Tsuruta, K., Maekawa, M., 2008. Concise Review: Pax6 Transcription Factor Contributes to both Embryonic and Adult Neurogenesis as a Multifunctional Regulator. Stem Cells 26, 1663–1672.

Petros, T.J., Tyson, J.A., Anderson, S.A., 2011. Pluripotent Stem Cells for the Study of CNS Development. Front. Mol. Neurosci. 4, 1–12.

Pothayee, N., Maric, D., Sharer, K., Tao-Cheng, J.-H., Calac, A., Bouraoud, N., Pickel, J., Dodd, S., Koretsky, A., 2018. Neural precursor cells form integrated brain-like tissue when implanted into rat cerebrospinal fluid. Commun. Biol. 1:114.

Qian, X., Nguyen, H.N., Song, M.M., Hadiono, C., Ogden, S.C., Hammack, C., Yao, B., Hamersky, G.R., Jacob, F., Zhong, C., Yoon, K.-J., Jeang, W., Lin, L., Li, Y., Thakor, J., Berg, D.A., Zhang, C., Kang, E., Chickering, M., Nauen, D., Ho, C.-Y., Wen, Z., Christian, K.M., Shi, P.-Y., Maher, B.J., Wu, H., Jin, P., Tang, H., Song, H., Ming, G.-L., 2016. Brain-Region-Specific Organoids Using Mini-bioreactors for Modeling ZIKV Exposure. Cell 1–17.

Quadrato, G., Nguyen, T., Macosko, E.Z., Sherwood, J.L., Min Yang, S., Berger, D.R., Maria, N., Scholvin, J., Goldman, M., Kinney, J.P., Boyden, E.S., Lichtman, J.W., Williams, Z.M., McCarroll, S.A., Arlotta, P., 2017a. Cell diversity and network dynamics in photosensitive human brain organoids. Nature 545, 48–53.

Quinn, J.C., Molinek, M., Martynoga, B.S., Zaki, P.A., Faedo, A., Bulfone, A., Hevner, R.F., West, J.D., Price, D.J., 2007. Pax6 controls cerebral cortical cell number by regulating exit from the cell cycle and specifies cortical cell identity by a cell autonomous mechanism. Dev. Biol. 302, 50–65.

Quinn, J.C., Molinek, M., Nowakowski, T.J., Mason, J.O., Price, D.J., 2010. Novel lines of Pax6-/- embryonic stem cells exhibit reduced neurogenic capacity without loss of viability. BMC Neurosci. 11, 26.

Quintana-Urzainqui, I., Kozić Zrinko, Mitra, S., Tian, T., Manuel, M., Mason, J.O., Price, D.J., 2018. Tissue-specific actions of Pax6 on proliferation-differentiation balance in the developing forebrain are Foxg1-dependent. iScience 171–191.

Reiner, O., Karzbrun, E., Kshirsagar, A., Kaibuchi, K., 2016. Regulation of neuronal migration, an emerging topic in autism spectrum disorders. J. Neurochem. 136, 440–456.

Reinholdt, L.G., Howell, G.R., Czechanski, A.M., Macalinao, D.G., MacNicoll, K.H., Lin, C.S., Donahue, L.R., John, S.W.M., 2012. Generating Embryonic Stem Cells from the Inbred Mouse Strain DBA/2J, a Model of Glaucoma and Other Complex Diseases. PLoS One 7, e50081.

Renner, M., Lancaster, M.A., Bian, S., Choi, H., Ku, T., Peer, A., Chung, K., Knoblich, J.A., 2017. Self-organized developmental patterning and differentiation in cerebral organoids. EMBO J. e201694700.

Rios, A.C., Clevers, H., 2018. Imaging organoids: A bright future ahead. Nat. Methods. 15(1):24-26.

Romero, D.M., Bahi-Buisson, N., Francis, F., 2018. Genetics and mechanisms leading to human cortical malformations. Semin. Cell Dev. Biol. 76, 33–75.

Sansom, S.N., Griffiths, D.S., Faedo, A., Kleinjan, D.-J., Ruan, Y., Smith, J., van Heyningen, V., Rubenstein, J.L., Livesey, F.J., 2009. The Level of the Transcription Factor Pax6 Is Essential for Controlling the Balance between Neural Stem Cell Self-Renewal and Neurogenesis. PLoS Genet. 5, e1000511.

Sansom, S.N., Livesey, F.J., 2009. Gradients in the brain: the control of the development of form and function in the cerebral cortex. Cold Spring Harb. Perspect. Biol. 1, a002519.

Sauer, M.E., Walker, B.E., 1959. Radioautographic Study of Interkinetic Nuclear Migration in the Neural Tube. Exp. Biol. Med. 101, 557–60.

Schmidt-Supprian, M., Rajewsky, K., 2007. Vagaries of conditional gene targeting. Nat. Immunol. 8, 665–8.

Schulz, T.J., Glaubitz, M., Kuhlow, D., Thierbach, R., Birringer, M., Steinberg, P., Pfeiffer, A.F.H., Ristow, M., 2007. Variable expression of Cre recombinase transgenes precludes reliable prediction of tissue-specific gene disruption by tail-biopsy genotyping. PLoS One 2, e1013.

Seto, Y., Eiraku, M., 2018. Human brain development and its in vitro recapitulation. Neurosci. Res. 138, 33–42.

Shen, M.D., 2018. Cerebrospinal fluid and the early brain development of autism. J. Neurodev. Disord. 7, 1–10.

Silva, J., Smith, A., 2008. Capturing pluripotency. Cell 132, 532–6.

Simeone, A., Gulisano, M., Acampora, D., Stornaiuolo, A., Rambaldi, M., Boncinelli, E., 1992. Two vertebrate homeobox genes related to the Drosophila empty spiracles gene are expressed in the embryonic cerebral cortex. EMBO J. 11, 2541–50.

Simpson, T.I., Pratt, T., Mason, J.O., Price, D.J., 2009a. Normal ventral telencephalic expression of Pax6 is required for normal development of thalamocortical axons in embryonic mice. Neural Dev. 4, 19.

Simunovic, M., Brivanlou, A.H., 2017. Embryoids, organoids and gastruloids: new approaches to understanding embryogenesis. Development 144, 976–985.

Singh, A.M., Chappell, J., Trost, R., Lin, L., Wang, T., Tang, J., Wu, H., Zhao, S., Jin, P., Dalton, S., 2013. Cell-cycle control of developmentally regulated transcription factors accounts for heterogeneity in human pluripotent cells. Stem Cell Reports 2, 398.

Smukler, S.R., Runciman, S.B., Xu, S., Van Der Kooy, D., 2006. Embryonic stem cells assume a primitive neural stem cell fate in the absence of extrinsic influences. J. Cell Biol. 172, 79–90.

Sousa, V.H., Miyoshi, G., Hjerling-Leffler, J., Karayannis, T., Fishell, G., 2009. Characterization of Nkx6-2-derived neocortical interneuron lineages. Cereb. Cortex 19, 1–10.

Stoykova, A., Treichel, D., Hallonet, M., Gruss, P., 2000. Pax6 modulates the dorsoventral patterning of the mammalian telencephalon. J. Neurosci. 20, 8042–50.

Suzuki, I.K., Vanderhaeghen, P., 2015. Is this a brain which I see before me? Modeling human neural development with pluripotent stem cells. Development 142, 3138–3150.

Takahashi, T., Nowakowski, R.S., Caviness, V.S., 1995. The cell cycle of the pseudostratified ventricular epithelium of the embryonic murine cerebral wall. J Neurosci 15, 6046–57.

Talamillo, A., Quinn, J.C., Collinson, J.M., Caric, D., Price, D.J., West, J.D., Hill, R.E., 2003. Pax6 regulates regional development and neuronal migration in the cerebral cortex. Dev. Biol. 255, 151–163.

Tamm, C., Pijuan Galito, S., Anneren, C., 2013. A comparative study of protocols for mouse embryonic stem cell culturing. PLoS One 8, e81156.

Tan, X., Shi, S.H., 2013. Neocortical neurogenesis and neuronal migration. Wiley Interdiscip. Rev. Dev. Biol. 2(4), 443-59.

Tanimura, S., Takeda, K., 2017. ERK signalling as a regulator of cell motility. J. Biochem. 162(3), 145-154.

Taverna, E., Götz, M., Huttner, W.B., 2014a. The Cell Biology of Neurogenesis: Toward an Understanding of the Development and Evolution of the Neocortex. Annu. Rev. Cell Dev. Biol. 30, 465–502.

Taverna, E., Götz, M., Huttner, W.B., 2014b. The cell biology of neurogenesis: toward an understanding of the development and evolution of the neocortex. Annu. Rev. Cell Dev. Biol. 30, 465–502.

Torres-Padilla, M.-E., Chambers, I., 2014. Transcription factor heterogeneity in pluripotent stem cells: a stochastic advantage. Development 141, 2173–81.

Tropepe, V., Hitoshi, S., Sirard, C., Mak, T.W., Rossant, J., van der Kooy, D., 2001. Direct neural fate specification from embryonic stem cells: a primitive mammalian neural stem cell stage acquired through a default mechanism. Neuron 30, 65–78.

Valamehr, B., Jonas, S.J., Polleux, J., Qiao, R., Guo, S., Gschweng, E.H., Stiles, B., Kam, K., Luo, T.M., Witte, O.N., Liu, X., Dunn, B., Wu, H., 2008. Hydrophobic surfaces for enhanced differentiation of embryonic stem cell-derived embryoid bodies Results. Pnas 105, 14459–14464.

Vallier, L., Mancip, J., Markossian, S., Lukaszewicz, A., Dehay, C., Metzger, D., Chambon, P., Samarut, J., Savatier, P., 2001. An efficient system for conditional gene expression in embryonic stem cells and in their in vitro and in vivo differentiated derivatives. Proc. Natl. Acad. Sci. 98, 2467–72.

Van den Ameele, J., Tiberi, L., Vanderhaeghen, P., Espuny-Camacho, I., 2014. Thinking out of the dish: What to learn about cortical development using pluripotent stem cells. Trends Neurosci. 37, 334–342.

Van Winkle, A.P., Gates, I.D., Kallos, M.S., 2012. Mass transfer limitations in embryoid bodies during human embryonic stem cell differentiation. Cells Tissues Organs 196, 34–47.

Warren, N., Caric, D., Pratt, T., Clausen, J.A., Asavaritikrai, P., Mason, J.O., Hill, R.E., Price, D.J., 1999. The transcription factor, Pax6, is required for cell proliferation and differentiation in the developing cerebral cortex.

Cereb. Cortex 9, 627–35.

Watanabe, K., Kamiya, D., Nishiyama, A., Katayama, T., Nozaki, S., Kawasaki, H., Watanabe, Y., Mizuseki, K., Sasai, Y., 2005. Directed differentiation of telencephalic precursors from embryonic stem cells. Nat. Neurosci. 8, 288–296.

Weinberger, L., Ayyash, M., Novershtern, N., Hanna, J.H., 2016. Dynamic stem cell states: naive to primed pluripotency in rodents and humans. Nat. Rev. Mol. Cell Biol. 17, 155–169.

Wilson, S.W., Houart, C., 2004. Early steps in the development of the forebrain. Dev. Cell 6, 167–81.

Wu, J., Izpisua Belmonte, J.C., 2015. Dynamic Pluripotent Stem Cell States and Their Applications. Cell Stem Cell 17, 509–25.

Ying, Q.-L., Stavridis, M., Griffiths, D., Li, M., Smith, A., 2003a. Conversion of embryonic stem cells into neuroectodermal precursors in adherent monoculture. Nat. Biotechnol. 21, 183–186.

Ying, Q.-L., Stavridis, M., Griffiths, D., Li, M., Smith, A., 2003b. Conversion of embryonic stem cells into neuroectodermal precursors in adherent monoculture. Nat. Biotechnol. 21, 183–186.

Ying, Q.-L., Wray, J., Nichols, J., Batlle-Morera, L., Doble, B., Woodgett, J., Cohen, P., Smith, A., 2008. The ground state of embryonic stem cell self-renewal. Nature 453, 519–523.

Ypsilanti, A.R., Rubenstein, J.L.R., 2016. Transcriptional and epigenetic mechanisms of early cortical development: An examination of how Pax6 coordinates cortical development. J. Comp. Neurol. 524, 609–629.

Zaki, P.A., Quinn, J.C., Price, D.J., 2003. Mouse models of telencephalic development. Curr. Opin. Genet. Dev. 13(4), 423-37.